TESIS DE LA UNIVERSIDAD DE ZARAGOZA

2017

4

Raquel Simón Allué

Towards the *in vivo* mechanical characterization of abdominal wall in animal model: application to hernia repair

Departamento
Ingeniería Mecánica

Director/es
Calvo Calzada, Begoña
Martínez Montiel, José María

ISSN 2254-7606

Prensas de la Universidad
Universidad Zaragoza

ISSN 2254-7606

Universidad Zaragoza
1542

Tesis Doctoral

TOWARDS THE *IN VIVO* MECHANICAL CHARACTERIZATION OF ABDOMINAL WALL IN ANIMAL MODEL: APPLICATION TO HERNIA REPAIR

Autor

Raquel Simón Allué

Director/es

Calvo Calzada, Begoña
Martínez Montiel, José María

UNIVERSIDAD DE ZARAGOZA

Ingeniería Mecánica

2016

Escuela de
Ingeniería y Arquitectura
Universidad Zaragoza

Universidad
Zaragoza
1542

Towards the *in vivo* mechanical characterization of abdominal wall in animal model
Application to hernia repair

Thesis by

Raquel Simón Allué

Faculty Advisors

Dra. Begoña Calvo Calzada

Dr. José María Martínez Montiel

Doctoral Degree in *Mechanical Engineering*

Escuela de Ingeniería y Arquitectura (EINA)

Universidad de Zaragoza

Zaragoza, October 2016

A mi madre

El genio es 1% inspiración y 99% transpiración.

Thomas Alva Edison

Agradecimientos

Cualquier persona que dedique 4 años de su vida a un proyecto sabe que se pasan momentos buenos, malos, horribles y geniales. Cualquier persona que sea tan afortunada como yo, no los pasará sola. A todos aquellos que me han acompañado en este largo, tortuoso y emocionante camino va dedicado este apartado, procuraré no dejarme a muchos.

En primer lugar me gustaría agradecer a mis dos directores de tesis, Begoña Calvo Calzada y José María Martínez Montiel, el brindarme la oportunidad de realizar esta tesis, apostando por mí cuando ninguno de los tres sabíamos si iba a ser capaz. Especialmente, gracias a Begoña por su apoyo, consejo y paciencia cuando mis nervios y agobios venían a incordiar. Gracias también a Fany, por ver en mí algo que otros no vieron, y por abrirme la puerta a este mundo tan frustrante a veces como fascinante.

No puedo ni quiero olvidar a los estupendos compañeros de sala que han hecho que venir a trabajar cada mañana fuese más fácil. Gracias por llenar mis días de risas, fricadas y café. Por los viernes de bombero, las sobremesas al sol y los viajes inesperados. Gracias sobre todo a mis PhD VIP: Marina, Sara, Enrique y ya en la última etapa Andrea y Mar: vuestra alegría y ganas de vivir son impagables y sin vosotros, ni esta tesis ni yo seríamos las mismas.

Siguiendo a nivel becario, agradecer también a los veterinarios Angel y Marta su inestimable ayuda técnica y sobre todo moral en esta última etapa de doctorado. Siempre es un gusto reconocerse en otra gente y llorar las penas en compañía. Gracias también a Paúl, que apostó su voluntad y varias horas de sueño en ayudarme a mejorar la parte experimental de esta tesis. No salió, pero gracias por intentarlo.

No muy lejos de esta sala se encuentra otro grupo de amigos que han ido huyendo del CPS para acabar volviendo, alegrándome así los últimos años de doctorado. Fer, Waldo, Raúl y Cube son los *Researchers & CO* a los que debo abrazos, ánimos y risas sin fin, tanto dentro como fuera de esta Universidad. Futuros doctores (y adyacentes), os debo más de lo que creéis.

Fuera ya del mundo ingenieril e investigador, quisiera agradecer a mis amigas Luisa, Carla y Berta el seguir escuchándome con cara de interés aun sin entender a veces la mitad de lo que digo. A Blanca, que aunque quizá no se acuerde fue la que me hizo dar el paso de lanzarme a este mundo. A Bichu, pionera y compañera del mundo científico, por ser una persona genial que se merece más estrellas de las que observa. A Lauri, por ser mi otro yo, el yin de mi yang, la *follower* de mi *leader*. Compi de risas, lloros y bailes, solo confío en poder disfrutarte todavía muchos años para poder devolverte el cariño y fuerza que me aportas. Por último, a José Luis, fiel compañero de fatigas desde hace tiempo, que se las ha arreglado para estar 10.000Km de distancia y seguir oyendo cada uno de mis silbiditos. No he disfrutado un muffin y un café como contigo.

A Adrián, encargado de recoger mis pedazos al final del día. Gracias por alimentarme por dentro y por fuera, por recordarme que hay vida más allá del doctorado y por ayudarme a relativizar. Por cuidarme y apoyarme en esta última fase y gracias, sobre todo, por hacerme parar y disfrutar de los pequeños placeres del día a día.

Por último, a mi familia. A los que están y a los que ya no, pero siempre estarán. Por ser atípicos pero geniales, por enseñarme a pelear y celebrar cada una de las alegrías de esta vida. A Carmen, por animarme a aspirar a lo mejor y ofrecerme siempre todo lo que está a su alcance para lograrlo. A Isábena, por superar hace tiempo la frontera de hermana para convertirse en una amiga que disfrutar y admirar. Y por supuesto a mi madre Maite, por la que soy todo lo que soy. Por enseñarme que las vallas nunca son tan altas como parecen y menos para nosotras, y que con genio, esfuerzo, cabeza y corazón se puede conseguir todo aquello que nos propongamos.

A todos aquellos que han formado parte de este camino. Gracias.

Zaragoza, 13 de Octubre de 2016.

Abstract

The work presented in this Thesis focuses on the design and implementation of a methodology able to characterize *in vivo* the passive mechanical behavior of abdominal wall. The main aim of this work is to provide surgeons with patient specific mechanical information, which may contribute to improve the surgical mesh hernia repair.

The surgical treatment for hernia pathology goes through closing the defect in an operation, either directly by merging the edges with sutures or by the implantation of a surgical mesh that covers the weak spot. This surgical mesh or prosthesis is responsible for bearing the physical loading present on the wall during the time the muscle is healing. In order to avoid postoperative pain and reduce the tear risk or possible recurrences, the mesh should mimic the mechanical response of the muscle that is replacing, which may vary from one person to another with regards to several physical features, such as age, gender of body mass index among others. The understanding of the patient-specific mechanics on the abdominal wall becomes necessary to assess which one is the *ideal* mesh, mechanically speaking, for a determine patient.

To that end, an *in vivo* approach of the passive mechanical behavior on an animal model and its implementation to the hernia repair is presented here. In a first step, an initial biomechanical study of a wound closure in abdominal wall was performed to understand the relation between mechanics and biological processes present on the wound healing at short and long-term. Then, an experimental approach was developed in conjunction with imaging methods so that spatial and strain information could be obtained from the abdominal tissue in a non-invasive way. This experimental procedure was carried out on healthy and herniated specimen, where the defect was previously repaired with several surgical meshes, and their results were used to assess the *in vivo* response of these prosthesis on an animal model. Based on the experimental data, a numerical analysis was performed to numerically characterize the passive mechanical response found on each specific case of the abdominal wall. To that effect, the mechanical characterization was

considered as an inverse problem, solved first by means of the Response Surface Methodology and afterwards through the use of a home-made algorithm applied to hyperelastic models. Finally, this characterization was used to recreate a finite element model where the effect of different surgical meshes used in the hernia repair field was tested and evaluated.

Keywords: Biomechanics; Abdominal wall; *In vivo* testing; Mechanical properties; Finite element method; Computational simulation; Hyperelastic material models; Imaging techniques; Photogrammetry; Inverse analysis; Hernia; Surgical meshes.

Resumen

El trabajo presentado en esta tesis se centra en el diseño e implementación de una metodología que permita caracterizar *in vivo* el comportamiento mecánico pasivo de la pared abdominal. Esta metodología permitiría a los cirujanos disponer de información mecánica relevante sobre un paciente específico, lo que podría contribuir a mejorar el tratamiento quirúrgico de hernias mediante malla protésica.

El tratamiento quirúrgico de hernias consiste en cerrar la debilidad creada en el músculo, ya sea directamente con puntos de sutura o mediante la implantación de una malla protésica. En el caso de la malla, ésta es la responsable de absorber las tensiones a las que el músculo se ve sometido durante el tiempo en el que se produce la regeneración de tejido. Para reducir el riego de aparición de dolor postoperatorio, rotura o rasgadura de tejido o incluso una recidiva, la malla debe mimetizar la respuesta mecánica de la zona de la pared donde vaya a ser colocada, que a su vez puede variar de un paciente a otro en función de su edad, género, índice de masa corporal u otras características físicas. Un mejor conocimiento de las propiedades mecánicas del abdomen en paciente específico ayudaría al cirujano a determinar qué malla protésica se puede considerar la *ideal*, mecánicamente hablando.

Por todo ello, el trabajo que aquí se presenta plantea una aproximación *in vivo* para caracterizar la pared abdominal sobre un modelo animal y su posterior implementación en casos de patologías herniarias. En un primer paso, se ha realizado un estudio biomecánico del cierre en línea alba, que ayudase a entender los aspectos mecánicos y biológicos que tienen lugar durante la curación de la herida a corto y largo plazo. A continuación, se han llevado a cabo ensayos mecánicos de inflado sobre la pared, que combinados con el uso de cámaras y técnicas de adquisición de imagen han permitido extraer la respuesta del tejido de una manera no invasiva. Este estudio experimental, se ha llevado a cabo sobre especímenes sanos y otro herniados y reparados con distintas mallas quirúrgicas, lo que ha permitido extrapolar el efecto *in vivo* que provocan estas mallas. A partir de los datos experimentales también se ha desarrollado un análisis numérico que

permitiese caracterizar la respuesta mecánica específica de cada espécimen. A este efecto, dicha caracterización se ha tratado como un problema inverso y resuelto primeramente mediante un análisis de superficies de respuesta y después con un algoritmo propio aplicado a modelos hiperelásticos. Finalmente, también se ha reconstruido un modelo de elementos finitos de la cavidad abdominal que permite simular el efecto producido por distintas mallas protésicas así como su alteración respecto al tejido sano.

Palabras clave: Biomecánica; Pared abdominal; Estudios *in vivo*; Propiedades mecánicas; Método de los elementos finitos: Simulaciones numéricas; Modelos hiperelásticos; Técnicas de adquisición de imagen; Fotogrametría; Análisis inverso; Hernia; Ma- llas protésicas.

Contents

List of Figures

List of Tables

Towards the *in vivo* mechanical characterization of abdominal wall in animal model
Application to hernia repair

1

Introduction

This Thesis falls within the scope of the biomechanical area, which pursues the objective of applying mechanical and numerical methods to approach common problems on the biomedical field. Specifically, this work tries to define a methodology that provides information of passive mechanical behavior of abdominal wall that may contribute to the mesh hernia repair treatment. To fully understand the implications of this Thesis a general vision of the biological aspects involved is required, as well as a description of past and current works developed on this area, commonly known as the state of art. This Chapter includes this information, together with a brief description of the techniques and numerical methods used throughout the fulfillment of this Thesis.

1.1 Anatomy of the abdomen

In the case of humans and most of vertebrates, the term abdomen refers to the part of the body comprised between the thorax and the pelvis. The region enclosed by the abdomen is known as the abdominal cavity, which contains inside several vital organs essential for the normal human body function. This zone is mainly devoid of an osseous structure, with the exception of the spinal column at the back, so it is of the utmost importance for the muscle layer that covers the cavity to be correctly formed and defined. This external muscle layer takes the name of abdominal wall.

The abdominal wall labor is present in daily common motions, but this layer is specially important since it is the main responsible of normal activities needed for the body maintenance. Some of its functions include body mobility (bending, rotation and lateral movements, standing, walking, etc.), contribution to the inner pressure control (essential for breathing, coughing, vomiting, urinating, defecating, etc.) or protection of the abdominal inner organs (belonging to the digestive, urinary, reproductive or cardiovascular system among others).

Although the abdominal wall is sometimes considered as a muscle layer, the fact is that it is composed of multiple soft tissues which work in conjunction to provide integrity and stability to the whole. Its composition includes different structures such as skin, muscles, fascias, fat or ligaments. The development of this tissue is related to each individual, according to the fitness or surgical background. This thesis is going to be focused on the study of the anterolateral abdominal wall, which comprises the front and lateral area of the abdomen and encompasses different layers deeply detailed in next sections. In opposition to this, the posterior abdominal wall is found, formed by the lumbar vertebrae, pelvic girdle, posterior abdominal muscles and their associated fascia.

The anterolateral abdominal wall in mammals is mainly composed of four pairs of major muscles and associated fascias (Minn and Hutchings, 1982). These four muscles, shown in Fig. 1.1), are the rectus abdominis, the internal oblique muscle,

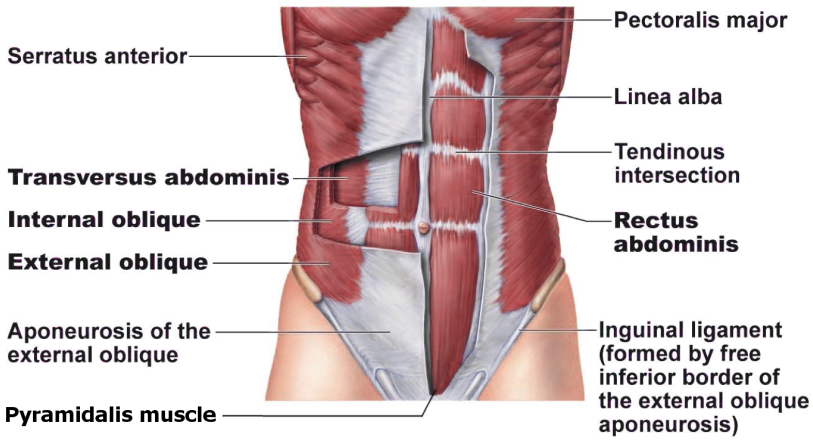

Figure 1.1: Main features of the anterolateral abdominal wall (Marieb, 2009).

the external oblique muscle y the transversus abdominis. They are situated in different layers along the wall thickness (see Fig. 1.2) and their aponeurosis join in a band of dense fibrous tissue called linea alba, located between the medial borders of the rectus abdominis. There is a fifth muscle in the anterolateral part called pyramidalis muscle, which is a small muscle located bellow the rectus abdominis with its base on the pubis and its apex attached superiorly and medially to the linea alba. Its mainly function is to tensor the linea alba and it is absent in 20% of people (Moore and Dalley, 1999). These muscles can be grouped into two categories: vertical and flat muscles.

1.1.1 Flat muscles

The three flat muscles of the anterolateral wall are the external oblique, the internal oblique and transversus abdominis. These muscle have muscular fibers that begin posterolaterally, pass anteriorly, and are replaced by an aponeurosis as the muscle continues toward the midline (Moore and Dalley, 1999; Drake et al., 2012).

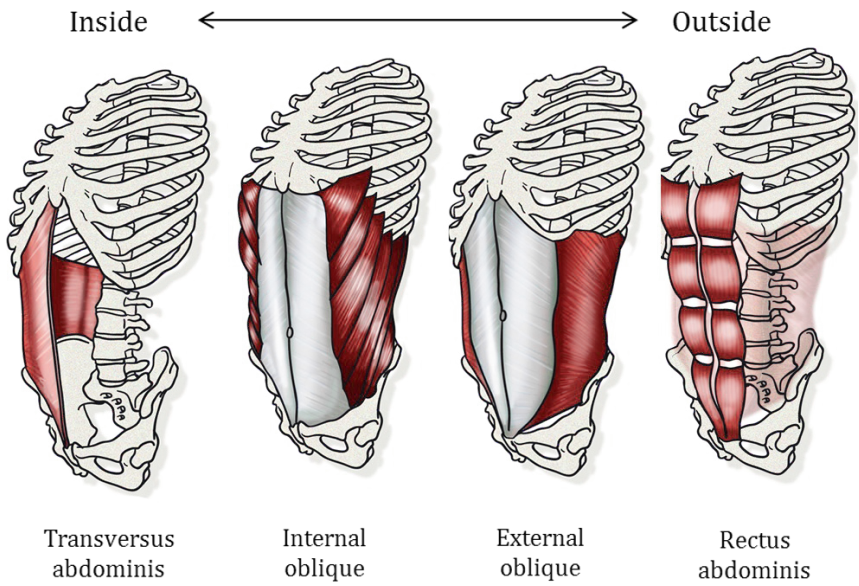

Figure 1.2: Situation of the main abdominal muscles in different layers, from the inside (left) to the outside (right) of the abdominal cavity.

The largest and most superficial of the three flat muscles is the external oblique, which is immediately deep to the superficial fascia. Its muscular part contributes to the anterolateral part and its aponeurosis contributes to the anterior part. Its laterally placed muscle fibers pass in an inferomedial direction, while its large aponeurotic component covers the anterior part of the abdominal wall to the midline. Medial to the pubic tubercle, the external oblique aponeurosis attaches to the pubic crest. Inferiorly, the inferior margin of this aponeurosis thickens and folds back on itself to form the inguinal ligament.

Each side of the obliques muscles can contract to create lateral flexion and contribute to both flexion and rotation of the vertebral column when both sides work together. The external oblique also functions to pull the chest downwards and compress the abdominal cavity, which increases the intra-abdominal pressure as in a valsalva maneuver.

Deep to the external oblique muscle is the internal oblique muscle, which is the second of the three flat muscles. This muscle is smaller and thinner than the external oblique, with most of its muscle fibers passing in a superomedial direction. Its lateral muscular components end anteriorly as an aponeurosis that blends into the linea alba at the midline. This layer has two major functions. On one side, it helps during breathing by controlling the pressure (and therefore the volume) in the lower wall of chest cavity. On the other side, it work together with the external oblique muscle of the opposite side to achieve the torsional movement of the trunk.

The innermost layer of the flat muscles is the transversus abdominis muscle, so named because of the direction of most of its muscle fibers (see Fig. 1.2). It ends in an anterior aponeurosis, which blends with the linea alba at the midline. It is also remarkable the presence of the transversalis fascia, which lines the abdominal cavity and continues into the pelvic cavity until become a continuous layer of deep fascia surrounding the abdominal cavity. The transverse abdominal muscle helps to compress the ribs and viscera, providing thoracic and pelvic stability. It also contributes during usual activities, such as vomiting or urinating, and participates directly during a childbirth.

1.1.2 Vertical muscles

The two vertical muscles in the anterolateral group of abdominal wall muscles are the large rectus abdominis and the small pyramidalis.

The rectus abdominis is the main vertical muscle and extends the length of the anterior abdominal wall. It is a paired muscle, separated by a midline band of connective tissue called the linea alba. It is broader and thinner superiorly but narrower and thicker inferiorly (see Fig. 1.2). Along its course, it is intersected by three or four transverse fibrous bands or tendinous intersections, which are easily visible on fit individuals. This long muscle is fundamental to the posture, providing stability to the pelvis and thorax. Besides that, it also contributes with

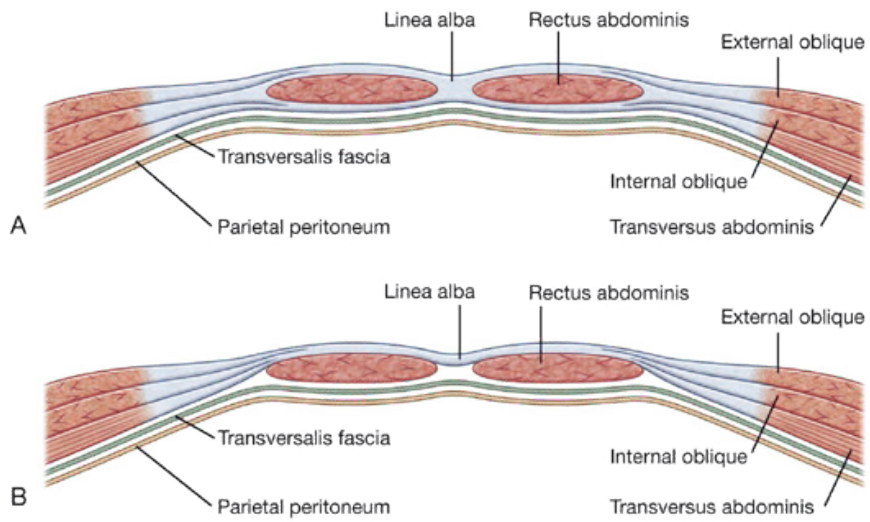

Figure 1.3: Organization of the rectus sheath. A. Transverse section through the upper three-quarters of the rectus sheath. B. Transverse section through the lower one-quarter of the rectus sheath (Drake et al., 2012).

the respiration, creating intra-abdominal pressure, and keeping internal organs intact.

The rectus abdominis and pyramidalis muscles are enclosed in an aponeurotic tendinous sheath called the rectus sheath, which is formed by a unique layering of the aponeuroses of the external and internal oblique, and transversus abdominis muscles. However, this sheath is slightly different depending on the rectus height. In the upper zone the aponeuroses of the flat muscles completely surround the rectus, forming anterior and posterior wall around this muscle. But in the lower zone, after an arch of fibers called the arcuate line, all of the aponeuroses move anterior to the rectus muscle leaving this layer in direct contact with the transversalis fascia in the absence of posterior wall. An scheme of both sections can be seen in Fig. 1.3.

1.1.3 Other anatomical structures

Besides the main muscles and fascias here commented, some additional anatomical structures are needed to be define in order to get a better understanding of the abdominal cavity.

- Linea alba: band of dense fibrous tissue that runs down the midline of the abdomen (see Fig. 1.1). It is formed by the fusion of the aponeuroses of the abdominal muscles (transversus, external and internal oblique muscles) and mostly composed of collagen connective tissue.
- Peritoneum: serous continuous membrane that lines the walls of the abdominal and pelvic cavities (see Fig. 1.3). It is composed of a layer of mesothelium supported by a thin layer of connective tissue. The peritoneum covers the abdominal organs and serves as a conduit for blood vessels and nerves.
- Thoracic diaphragm: it is a sheet of skeletal muscle located at the inferiormost aspect of the rib cage and separates the thoracic from the abdominal cavity (see Fig. 1.4 (a)). Composed of two domes, it is the primary muscle of respiration in humans: when the diaphragm contracts, it moves in the inferior direction enlarging the volume of the thoracic cavity and forcing air suction in the lungs. This is the inhalation. In the opposite phenomenon, when the diaphragm relaxes and other antagonist muscles contract, the pressure increases and the air is exhaled, provoking exhalation. The diaphragm is also present in other anatomical functions (urinate, defecate, vomiting) that imply intra abdominal pressure control.
- Inguinal ligament: this ligament is formed by the external abdominal oblique aponeurosis and is continuous with the fascia lata of the thigh. It is the base of the inguinal canal, through which an indirect inguinal hernia may develop.
- Pelvic floor: located in the lesser part of the pelvis, it separates the pelvic cavity from the inferior perineum (see Fig. 1.4 (b)). It is mainly composed by muscles and ligaments and has special relevance providing sup-

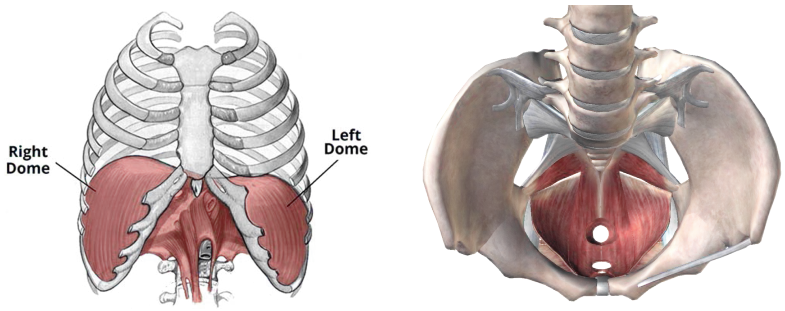

(a) Thoracic diaphragm (b) Pelvic floor

Figure 1.4: Other anatomical structures in the abdominal cavity (Tea, 2015; Yog, 2002).

port to pelvis viscera (bladder, intestines, uterus etc.) and controlling intra pelvic/abdominal pressure.

1.1.4 Mechanical behavior of the abdominal muscle

Abdominal muscles are generally regarded as part of the skeletal muscle, which forms the majority of the muscle tissue in the body together with the cardiac and smooth muscles. This type of muscle consists on parallel bundles of long, multinucleated fibers with transverse stripes (Drake et al., 2012), that moves bones or other structures and provides support to the body.

Muscles have an intricate support structure of connective tissue (see Fig. 1.5), where each muscle fibre is surrounded by a thin layer of connective tissue known as endomysium. These fibres are then grouped into bundles known as fascicles, which are surrounded by a layer of connective tissue known as perimysium. Many fascicles make up a muscle, which in turn is surrounded by a thick layer of connective tissue knows as the epimysium (Tea, 2015). On the whole, these three layers (endomysium, perimysium and epimysium) are mostly woven collagen fibers embedded in an amorphous ground substance.

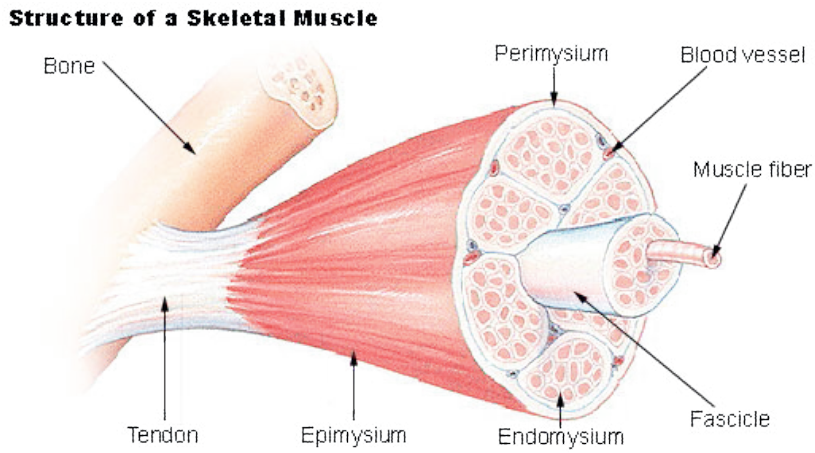

Figure 1.5: Structure of the skeletal muscle (U.S. National Cancer Institute, 2016).

When the mechanical behavior of the abdominal wall muscles is studied, the muscle structure is simplified and generally considered as an extracellular matrix mainly composed of muscular, collagen and elastin fibers. Collagen and elastin fibers are associated with the passive mechanical behavior of the tissue (Calvo et al., 2009; Hernández et al., 2011), which constitutes the muscle response to loads that only provoke tissue resistance, but do not contractions of the muscle. Muscular fibers, on the other hand, are the responsible of the active response of the tissue, i. e. when there is force generation in the tissue (Davis et al., 2003; Grasa et al., 2016). This Thesis is going to be mainly focused on assessing the passive mechanical behavior of abdominal wall.

The passive mechanical response is therefore strongly related with the collagen fibers of the tissue, that in case of abdominal wall muscle they present a wavy pattern. This fact implies a different response in the tissue when fibers are coiled in contrast to when they are completely stretched. Fig. 1.6 shows the typical response of a collagen fibred tissue. It is easily seen how in the beginning, when fibers are twined (state I), the material presents a compliance behavior that is getting more and more rigid while fibers are unrolled (state II). When fibers are completely stretched (state III) and load is increased, fibers may reach failure

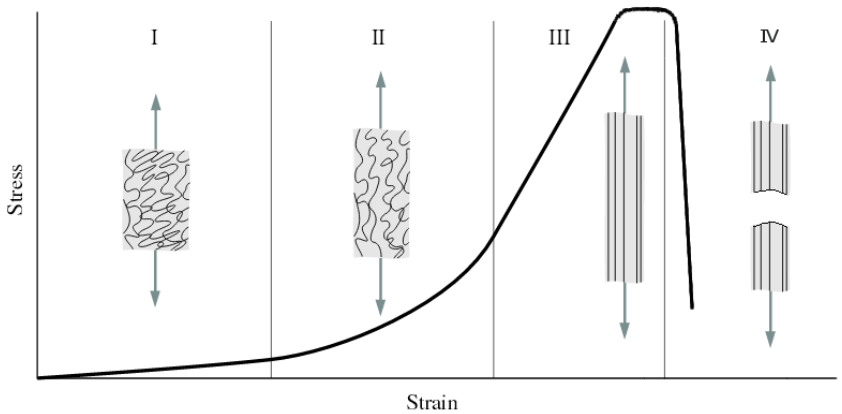

Figure 1.6: Schematic diagram of a typical (tensile) stress-strain curve associated to tissue showing collagen fiber morphology (Holzapfel, 2000).

(state IV). On account of this, abdominal muscles show a non linear response in large deformations to physiological loads.

1.2 Hernia: abdominal wall pathology

Hernia is a common disease that affects more than 20 million people per year around the world (Dabbas et al., 2011; Kingsnorth and LeBlanc, 2003) and is one of the most important surgical subject for all surgeons who operate on the abdomen (Park et al., 2006). It is more common in men than in women: about 27% of males and 3% of females develop a groin hernia at some time in their life (Fitzgibbons and Forse, 2015).

An hernia may be congenital and present at birth or it may develop over time in areas of weakness within the abdominal wall. Possible causes include bad nutrition, genetic disorders or damage in abdominal wall from previous injuries or surgery. Additionally, usual activities that entail an increase of intra abdominal pressure (pregnant, heavy lifting, chronic cough or obesity among others) can also raise the probability of suffering an hernia.

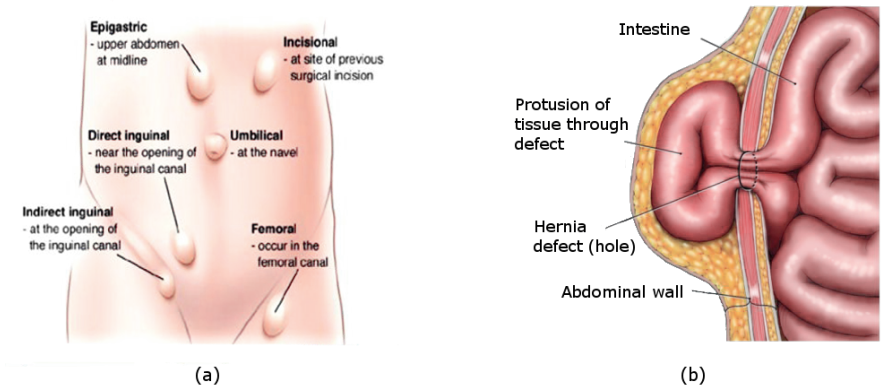

Figure 1.7: Types of hernias: (a) Main hernia types based on their emergence zone. (b) Example of hernia.

The term hernia is generally used to describe a bulge or protrusion of an organ through the structure or muscle that usually contains it (see Fig. 1.7 (b)). When this muscle is the abdominal wall, the complaint is considered abdominal hernia and may be subdivided into different types (inguinal, femoral, umbilical, etc.) mostly named according to its emergence zone (see Fig. 1.7 (a)). The most frequent is the inguinal hernia (70-75%) followed by femoral (6-17%), umbilical (3-8.5%) and other rarer forms (1-2%) (Bailey et al., 2000).

An abdominal hernia appears due to de presence of a defect in the abdominal wall. This defect can be a weakness in the muscle layer, or even a hole in severe cases, that usually provokes pain in the patient. Since the abdominal wall is subjected to a wide range of forces and internal pressures, as a result of common daily activities, the weakness can deteriorate to an opening and a peak of intra abdominal pressure may force the inner organs to go through the muscle causing an hernia.

In some cases this hernia is reducible, which means that the abdominal contents can be manually returned to their original compartment. This type of hernias may be in turn classified into easily reducible, incarcerated hernia or

strangulated hernia (Perrott, 2004). These last two are not easy to solved manually and they implies the use of anesthesia and a very carefully recovery in the patient, in order to avoid an obstruction or strangulation in the organ which may lead to an increased tissue edema, further complication with circulation or the arterial supply or even tissue necrosis.

However, in most of clinical cases the hernia is not reducible and the solution goes though the surgical treatment of the defect, i. e. hernia repair, frequently known as herniorrhaphy (Bendavid, Abrahamson, Arregui, Flament, and Phillips, Bendavid et al.).

1.2.1 Surgical hernia repair

There are two main different approaches in abdominal surgery:

- Open tension repair: it consists on an incision made in the abdomen to give surgeons direct access to the hernia. Once the protruding portion is placed back into the abdomen the edges of healthy tissue around the hernia are pulled together and sewn with sutures. This is the conventional and traditional method for hernia repair. Its use is associated to a faster procedure, but also a large scar, postoperative pain and high recurrence rates (Grant, 2000; Scott et al., 2002) is linked to this approach.
- Non-Tension or Tension-Free mesh repair: instead of pulling the tissue around the hernia together, this method consists on the insertion of a piece of mesh that covers the hernia defect. This mesh is positioned to reinforce the area and fixed to the edges of healthy tissue with sutures and/or staples (see Fig. 1.8). Also called the Lichtenstein technique, the use of prosthetic materials is related to several advantages, such as less postoperative pain, rapid recovery and low recurrence rates (Amid et al., 1995, 1996; Sakorafas et al., 2001). This procedure can be performed in two ways: open technique and the laparoscopic approach (see Fig. 1.9). The open technique uses the

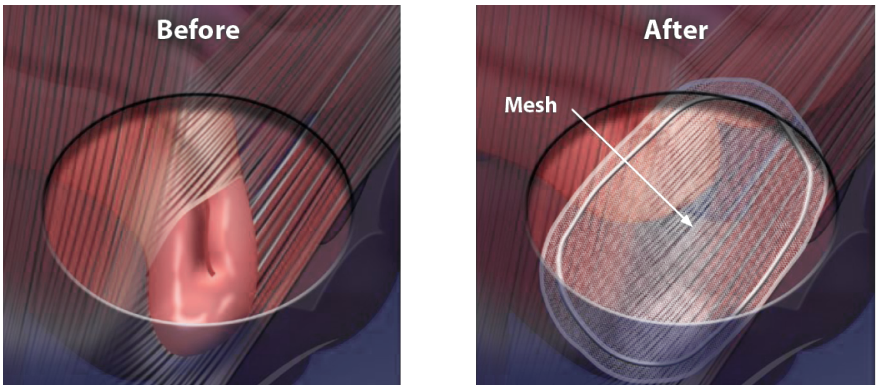

Figure 1.8: Scheme of the Non-Tension mesh repair of an inguinal hernia (Agency for Healthcare Research and Quality, 2013).

same method than the traditional open tension repair, but once the incision in the abdomen is done and the hernia is reduced, a mesh patch is inserted to cover weak spot of the muscle (where the hernia has appeared) and sutured to the healthy tissue. After that, the wound is closed. The laparoscopic approach on the contrary, does not need a big cut to access to the hernia, but only three or four small incisions where the surgical instruments are inserted. Besides them, an additional metal probe (laparoscope) is introduced with a light and a viewer connected to a screen, that allows surgeons to see the interior of the abdominal cavity and therefore, the hernia. This method is less invasive than the open techniques and consequently it is associated to less postoperative pain faster return to usual activities (Liem et al., 1997; Onofrio et al., 2004). However, among its drawbacks are a larger procedure, the use of general anesthesia and higher costs during the procedure (Park et al., 1998; McCormack et al., 2003), and the benefits in recurrence rate for primary hernias is unclear (Neumayer et al., 2004). Most of these authors also agreed in that more extensive studies are needed to confirm the advantages of the laparoscopic approach.

Although both approaches are nowadays used for the surgical treatment of the hernia pathology, the tension-free mesh repair seems to be the preferred option

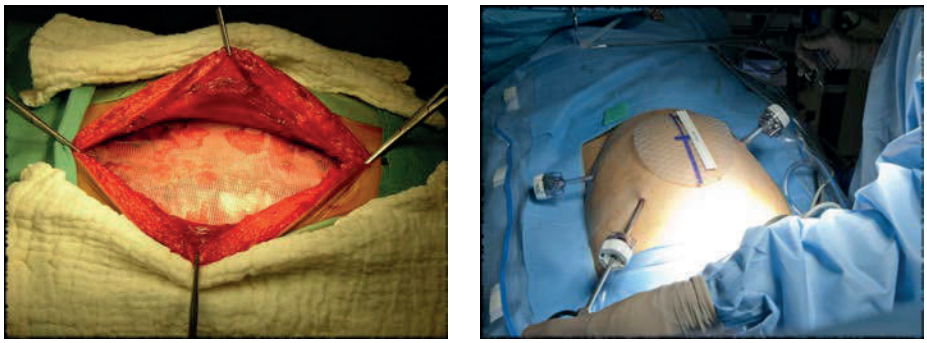

(a) Open hernia repair. (b) Laparoscopic hernia repair.

Figure 1.9: Two different approaches for the mesh repair.

to treat severe cases. However it appears to be needed of some optimization, since despite its wide use during last three decades there is not a generally accepted agreement about which material or mechanical features of the prothesis are more convenient for each patient. This is surprising considering that mesh characteristics, such as material, pore size, mesh density or tensile strength among others, may affect the compatibility between the mesh and tissue and condition the success or failure of the procedure.

The place to position the mesh with respect to the muscle layers can also affect to the posterior clinical result of the mesh. On this issue, the European Hernia Society defined five different ways to place the surgical prothesis for the case of ventral hernia repair (an scheme of this options can be observed in Fig. 1.10). The possible options are the following:

- Onlay: the mesh is positioned above the abdominal wall muscles and fascia, behind the subcutaneous fat.
- Inlay: the mesh is positioned in the hernia defect, without overlap, and fixed to the margins of the defect.
- Retromuscular: in medial hernias, the mesh is positioned behind the rectus abdominis muscle and in front of the posterior rectus fascia or in front of

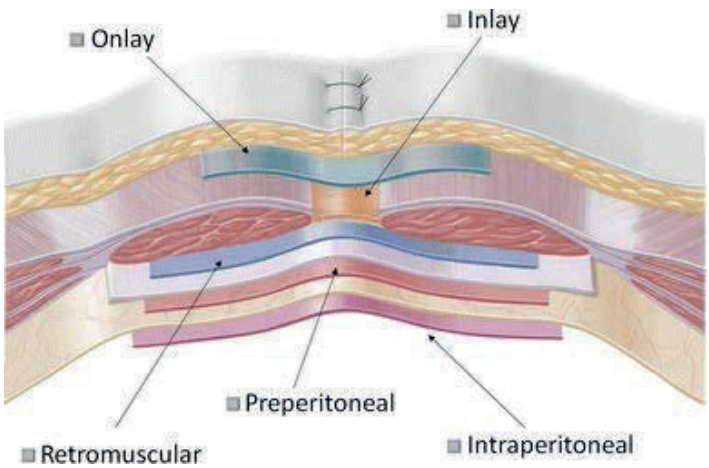

Figure 1.10: Different positions os the prothesis during ventral hernia repair (Muysoms et al., 2012).

the peritoneum. In lateral hernias, the mesh is placed in a plane between the lateral abdominal wall muscles.

- Preperitoneal: the mesh is placed in the plane behind all abdominal wall muscles in front of the peritoneum.
- Intraperitoneal: the mesh is placed behind all layers of the abdominal wall including the parietal peritoneum.

1.2.2 Types of prostheses

Nowadays, there are a lot of surgical prothesis on the medical market (see Fig. 1.11). Several classification can be stipulated based on material composition, geometrical structure, density or pore size.

According to the material composition, current prostheses can be classified into two main groups: biologic tissue and synthetic polymer meshes (Todros et al., 2015). Biological meshes were introduced in the 1990s and may be derived from

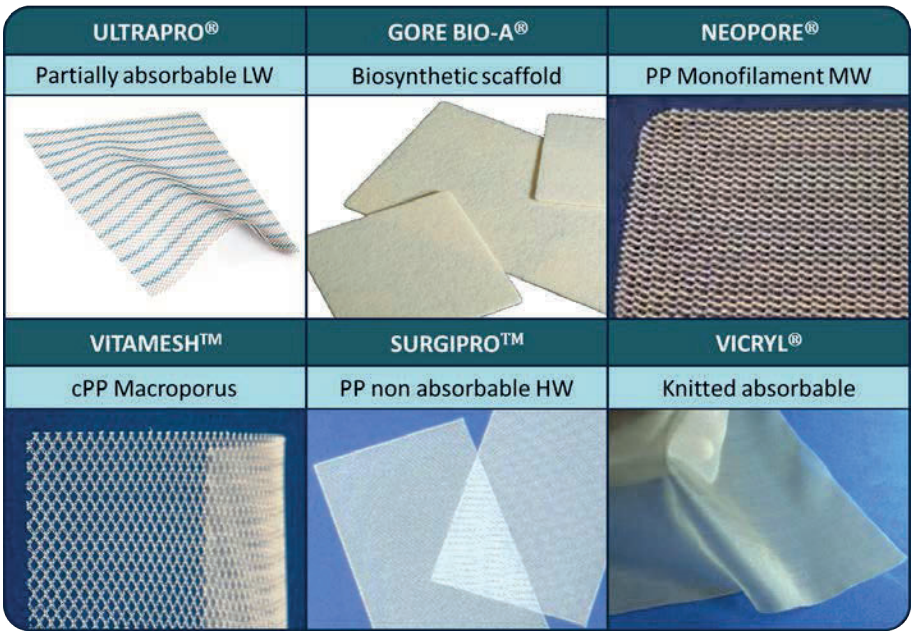

Figure 1.11: Some examples of commercial surgical meshes.

human or animal (porcine or bovine) tissues. They allow neovascularization and regeneration due to infiltration of native fibroblasts, which constitutes a theoretical advantage over synthetic meshes as they provide the extracellular scaffold necessary for the reconstruction of healthy tissue (Smart et al., 2012). Their use is specially indicated in the context of surgery in contaminated/infected fields, but they are not widely used in hernia reparations to their high cost. On the other hand, synthetical meshes can be in turn subdivide into absorbable or non–absorbable. Absorbable prostheses are mostly used for temporally repair or in contaminated cases where primary abdominal closure is not feasible, but their use is not recommended when prolonged tensile strength is required (Tyrell et al., 1989). The permanent synthetic prostheses are the most frequently applied in abdominal wall surgery due to their great mechanical characteristics and a reasonable good biocompatibility. The most widespread polymeric materials are polypropylene (PP), polyester and expended polytetrafluoroethylene (ePTFE).

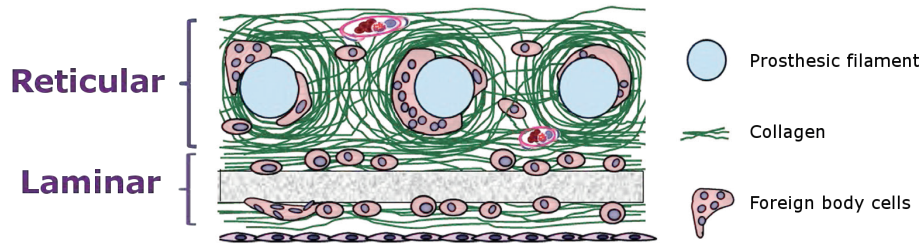

Figure 1.12: Transversal view of a composite mesh, where both the reticular and laminar part are visible (Bellón, 2014).

There is a third group, the partially absorbable meshes, that tries to join the advantages of both types. However, although the great development undergone by these prostheses, an *ideal* surgical mesh has not found yet, as the large branch of choices indicates (Bilsel and Abci, 2012).

An additional classification of the synthetic surgical meshes can be done attending to the structure. Based on the weaving of threads, polymeric meshes can be divided into reticular, laminar or composite prostheses (Bellón, 2014). Reticular meshes, composed of threads, are associated to an optimal tissue integration because the connective tissue tends to enclose the threads favoring the tissue regeneration. They can be in turn subdivide into monofilament and multifilament. Laminar meshes have a cell type integration, different from the reticular meshes, that does not assist that much to the regeneration but presents some advantages in cases of direct contact to the viscera. Finally, the composite meshes try to include the benefits of both prostheses types.

With regard to the weigh or density, prostheses are usually classified into three groups (Cobb et al., 2006): heavyweight (HW), with a density above 80 g/m^2; mediumweight (MW), between 80–50 g/m^2; and lightweight (LW), below 50 g/m^2. Some authors also consider a recent fourth group called ultralightweight (ULW) with a density lower than 35 g/m^2 (Earle and Mark, 2008). However, the boundaries of these categories are not completely defined and differ between authors (Coda et al., 2012). This classification was originally conceived for PP

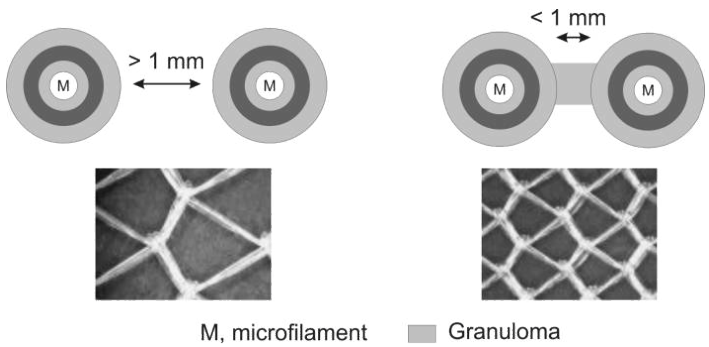

Figure 1.13: The bridging effect: granulomas form around individual fibres and bridging with each other, encapsulating the entire mesh (Brown and Finch, 2010).

meshes, but it is often use for other synthetic materials as an additional parameter to define them. In general terms, HW are associated to a greater amount of material and therefore higher foreign body reaction, while LW and ULW are related to larger pores and better to tissue regeneration. However, these considerations were made under the assumption that the density is totally related to the pore size (according to the German school (Schumpelick et al., 2004)), and this is not always fulfilled (Klinge, 2007).

Attending to the pore size, authors agree in considering 75 μm as the minimum diameter to allow infiltration by macrophages, fibroblasts, blood vessels and collagen. Meshes with larger pores allow increased soft tissue in-growth and are more flexible because of the avoidance of granuloma bridging (Brown and Finch, 2010). An additional effect related to the pore size is the 'bridging effect'. It occurs when pores are smaller than 1mm and the glaucoma surrounds the polymer fibers up to complete filling of the pores. This forms a rigid scar plate that contributes to the mesh shrinkage and to the loss of abdominal wall flexibility (Klinge et al., 2002; Todros et al., 2015). In order to avoid this effect, larger pores (and by association LW meshes) are more frequently used nowadays. The most accepted classification roughly established in literature is the Amid classification (Amid, 1997), that classified meshes into four types (type I-type IV) and defined biomaterial-related complications associated to each type.

Nowadays there is a large market of surgical meshes orientated to the hernia repair. However, although some specifications could be considered as established when choosing a mesh type, the fact is that there is no general agreement or accepted guide in surgery to determine the *ideal* mesh for each patient. Regarding the mechanical response, it is usually assumed that the *ideal* mesh should have a mechanical behavior similar than the tissue. Thereby, the risk of tear or excessive compliance in the mesh would decrease. Since the mechanical response of the tissue may differ from one abdomen to another, the possibility of characterize a specific patient would be very interesting to determine which mesh is the appropriate for this case. This idea constitutes one of this Thesis aims.

1.3 State of the art

In the literature there are many works related to the mechanical characterization of soft tissues. In this section we focus on those studies which deal with the characterization (partially or totally) of the abdominal wall. Likewise, this section includes some references to other numerical or experimental techniques used along this Thesis.

1.3.1 *In vitro* experimentation

Experimental procedures take the name of *in vitro* when the sample of interest is tested out of its usual environment. In the special case of soft tissues, *in vitro* characterization is associated to isolate the tissue from the whole to which it belongs (part of the body) and test it alone to obtain its particular properties. The most common *in vitro* tests to characterise the passive behavior of a muscle are uniaxial, biaxial, bulge or inflation tests. Most of them have been performed on animal models, due to the facility to obtain a high number of samples with a desirable repeatability, but some others were provided with human data.

Concerning the abdomen, Nilsson (1982) established mechanical differences between samples taken from distinct zones of the abdomen in a rabbit model and in Nilsson (1982), this author found that this differences might be influenced by fibre direction and amount of fibers in each sample. This conclusion may be related to the fact that abdomen is composed of distinct muscle layers, each one with their own muscle fiber direction, which work in conjunction with other components to withstand physiological stresses. Since then, many studies have been focused on the mechanical characterization of isolated tissues that compound the abdominal cavity, i.e. abdominal fascia, individual abdominal muscles or skin.

Regarding to the linea alba on human data, several authors analyzed the biological aspects of this tissue before mechanical tests were performed. Askar (1977) and Rizk (1980) proposed to consider the linea alba as the common area of decussation of intermediate aponeuroses of lateral abdominal muscles, i. e., where fibers ended. Based on that model, Axer et al. (2001a) deeply investigated the three-dimensional architecture of the collagen fibers in linea alba and rectus sheaths. Three fibril bundles were identified corresponding to the obliques and transversal muscles. In the following study, Axer et al. (2001b) analysed the biomechanics on linea alba and this author found gender differences regarding to the linea alba architecture, although the influence of pregnancy at this point remained to be proven. Considering this study, Grässel et al. (2005) performed uniaxial tests to human samples to determinate the anisotropy of the linea alba. This study showed a higher compliance in longitudinal and smallest in transverse direction, what contradicts the fiber model described by Askar (1977) where no fiber in transversal direction was found. As said before, all of this studies were performed on human samples. Other author focussed on the linea alba was Rath et al. (1996), who investigated its morphology and studied its mechanical parameters of resistance, deformation and elasticity. This work distinguished there levels (supra-umbilical, sub-umbilical and umbilical) and subjected the samples to burst tests. They found no significant difference in resistance between them. More recently, Cooney et al. (2015) also investigated properties of the linea alba through uniaxial and equibiaxial load testing on porcine linea alba samples. A finite element model with an hyperelastic material model was proposed following a

procedure similar to Lyons et al. (2014). Finally, Acosta Santamaría et al. (2015) tried to determine biomechanical properties of linea alba subjected to transverse planar tension and to compare its behavior at different locations of the abdominal wall. Porcine samples were used there, and contrary to Rath et al. (1996) significant differences between linea alba above and bellow the umbilicus were found.

Other authors focused the research in the rectus sheath, which contains the linea alba and the surrounding area. Förstemann et al. (2011) used uniaxial tests to determinate the force-elongation responses of the human abdominal wall in the linea alba region. They applied this data to a geometry of the abdominal wall, based on MRI images. The objective of this work was to use the properties of the fascia to model the mechanical responses of the abdominal wall under physiological stress. In this line, Martins et al. (2012) focused their work in characterizing and modelling the damage process in the anterior rectus abdominal. To do that, they performed uniaxial tests on female human samples, and both fiber directions were considered. Other interesting research was Ben Abdelounis et al. (2013), which studied the effect of loading rates on the elasticity of the rectus sheath. They concluded that loading rate effect was statistically significant and confirmed the viscoelastic behavior of these tissues. More recently, Lyons et al. (2014) performed uniaxial and biaxial tests on porcine rectus sheath in order to determine the stress-stretch responses of the tissue. They proposed a constitutive material model and validated it with the experimental data.

The literature on experimental characterization of abdominal tissues includes additional studies concerning other components of the abdomen. Kirilova et al. (2009, 2011) focused their work on the mechanical properties of the human fascia. Firstly through the study of the viscoelastic properties (Kirilova et al., 2009), and secondly determining the relation with the direction of loading and localization (Kirilova et al., 2011). Both studies were based on one-dimensional tensile tests on human fascia. Conversely, Hwang et al. (2005) performed uniaxial and biaxial tests to developed a comparative study between internal oblique and transversus abdominis. In this study, based on dog samples, the anisotropy of both layers

based on their fiber arrangement was assessed. However, they showed a less pronounced anisotropy when working as a composite, due to the presence of the extracellular connective tissue (Huijing, 1999). Hernández et al. (2011) developed a very interesting research in rabbits about the mechanical behavior of different layers in abdominal wall, performing uniaxial tests on rectus abdominis, external oblique and several composite layers. In this work directions of anisotropy were considered and the tissues were characterized with an hyperelastic anisotropic material model. Based on this work, in Hernández-Gascón et al. (2013) they reproduced the response of a complete abdominal wall under physiological stresses. To do that, the geometry of the abdomen was reconstructed from MRI images. This study also underlined the great importance of the the stiffest structures, aponeuroses and fascias, in terms of wall resistance.

Lately, further *in vitro* studies have been performed in order to determinate the effect of several mesh features on the abdominal wall after some time of regeneration. Thus, Greca et al. (2001) studied the influence of pore size on the biocompatibility between wall and mesh in an experimental study in dogs. On the other hand, Hernández-Gascón et al. (2012) compared the long-term behaviour of three commercial meshes measured at several dates after implantation. The analysis was made both mechanically and biologically on a rabbit model. Kureshi et al. (2008) worked on transversaly human fascia, and correlated mechanical properties of herniated and non-herniated specimen with fibrillar properties. No great differences were founded between groups after the study, which suggested that pre-existing mechanical weakness (herniated samples) may not be the primary cause of hernia progression. Lubowiecka et al. (2012) developed a mathematical modelling of a human fascia-implant system, based on in vitro tests performed on porcine tissue in a pressure chamber. Another noteworthy work was (Podwojewski et al., 2013), who performed a mechanical study of the abdominal wall under three configurations: intact, after simulating an incisional hernia and after the repair with a mesh. The experimentation was performed with a pressurized air cavity which reproduced the intra abdominal pressure.

All these works contribute to widen the knowledge of abdominal wall com-

ponents, providing useful mechanical data and interesting non-linear models that help to the understanding of abdomen mechanics. Nevertheless, these experiments are subjected to severe limitations (frozen samples, uniaxial tests, individual layers) and their mechanical information should be carefully analysed. The main constrain about *in vitro* studies lies in the fact that when one determined tissue is isolated from the whole, their mechanical properties may change due to the alteration on boundaries and the alteration of the composite. Besides, the original loading state of the tissue is lost and it is hard to retrieve. In order to avoid that, *ex vivo* and *in vivo* studies are needed.

1.3.2 *Ex vivo* and *In vivo* experimentation

Although the number of mechanical studies in *ex vivo* or *in vivo* conditions as regards abdominal wall are quite limited, some works in the literature need to be mentioned.

Particular highlights in this regard are Podwojewski et al. (2014) and Tran et al. (2014), who carried out *ex vivo* mechanical tests on human specimens considering the contribution of the different layers. Following the procedure started by Podwojewski et al. (2013) in a porcine model, Podwojewski et al. (2014) repeated experimental tests with a pressurized air cavity on human samples. Conclusions were similar to the prior work, when three configurations of abdominal wall (intact, herniated and repaired) were evaluated. Tran et al. (2014) on the contrary, analysed the contribution of the skin, rectus abdominis and the sheath. They conclude remarking the importance of the rectus sheath in the structural response of the anterior part of the abdominal wall *ex vivo*. Although these works provide very interesting information, the fact is that their condition of *ex vivo* tests could be called into question since all samples were remove from the whole and frozen and defrosted before testing.

On the other hand, some *in vivo* tests should be mentioned here. A very interesting study in abdominal wall was performed by Song et al. (2006), who

measured mechanical properties of a human abdomen during insufflation for laparoscopic surgery. This was a pioneering work in the mechanical characterization field, since they were the first in measuring *in vivo* properties, but the mechanical analysis was not really extend. The main conclusion was that the abdomen seemed to be stiffer in the transverse plane than in the sagittal plane. Other authors focused on *in vivo* abdominal response were Szymczak et al. (2012) and Śmietański et al. (2012), who studied strains in some points of the specimen. However, stress was originated from muscle contraction so active response of the muscle was studied there. In vivo data obtained in these works was subsequently used by Szepietowska and Lubowiecka (2013) and Lubowiecka et al. (2016) to determine the optimal orientation of several orthotropic meshes with regards to the hernia location on the abdomen. Tran et al. (2016) also evaluated the *in vivo* response of the abdomen when subjected to a external load. Specifically the local stiffness of the abdomen was calculated during 4 activities: rest, pullback loading, abdominal breathing and the Valsalva maneuver. In those cases (Szymczak et al., 2012; Śmietański et al., 2012; Tran et al., 2016), active behavior was also measured and the passive contribution of the muscles was unclear.

To the author´s knowledge there are no further *in vivo* studies focused on the passive response of the abdominal wall. Despite the high advance in non-invasive measurement techniques, *in vivo* mechanical behavior seems to be inaccessible for researchers, what prevent them from developing a proper numerical characterization. This Thesis addresses this issue, proposing a novel methodology to characterize the *in vivo* passive mechanical behavior of the anterolateral abdominal wall, based on an animal model.

1.3.3 Mechanical imaging in soft tissues

One of the main objections to *in vivo* tests lies in the difficulty of obtaining reliable mechanical data from a test without altering the tissue of interest. The solution of this problem seems to go through imaging methods, that allow to obtain certain information only by the use of images. This procedure means to

obtain information in a non-invasive way, which reduces the sample disturbance or the discomfort of the patient, improving the recovery period. In this respect, the great development undergone during the last decades by the elasticity imaging has represented a great step forward to measure mechanical features with non invasive measurement techniques. In this section, a brief review of these techniques applied to several tissues are expounded.

The most widely imaging techniques used thus far in mechanical imaging are magnetic resonance imaging (MRI) and ultrasound. Both of them are well known for their biomedical purposes, but thanks to the great advance undergone in effective algorithms to postprocess of the images, both techniques may provide useful mechanical data. Concerning to the MRI, it has been applied to predict biomechanical properties of articular cartilage (Nieminen et al., 2004), combined with indentation tests to characterize the mechanical behavior of the skin (Tran et al., 2007) or used to obtain aortic tissue characterization (Flamini et al., 2015) among others. Ultrasound has been also widely applied in literature. It can been found in works related to: the search of material parameters in human muscles (Hodges et al., 2003), imaging and treatment of liver tumors (Rivaz et al., 2013), constitutive modeling of porcine liver (Jordan and Howe, 2008) or the assessment of mechanical properties of human ribs (Mitton et al., 2014) among others.

Nevertheless, other imaging techniques have been used to obtain mechanical information, such as radiology (Kransdorf and Murphey, 2006), shear wave elastography (SWE) (Koo et al., 2013; Chauvet et al., 2015) or multi view stereo (MVS) (Buganza Tepole et al., 2015). This last method is slightly different from the others in terms of equipment needed for the procedure. While MRI, ultrasound or radiology requires big devices and really careful conditions to take the images, multi view vision only needs a calibrated camera and a minimum of two pictures from an object to reconstructed it. On the other hand, it is only able to image external faces rather than piercing the body to image internal tissue.

Depending on the requirements, one or another imaging technique should be considered. In the case of this Thesis, the target is visible and external so a system

similar to the multi view stereo was considered for the imaging.

1.3.4 Inverse analysis in soft tissues

None of these imaging techniques would have developed that much in terms of mechanical characterization without the parallel advance in efficient algorithms that facilitate the treatment of the data. However, the data acquired in the mechanical imaging is usually a displacement field and it may not be directly associated to the mechanical properties. Generally, to solve a *normal* problem a model and material properties are needed while the displacement field is considered as the solution of the problem. On the contrary, when the starting point is the displacement data and the unknown variables are the material parameters that cause it, it takes the name of inverse problem.

In science, inverse problem is known as the process of calculating from a set of observations the causal factors that produced them. This is exactly the problem to solve in biomechanical imaging, where the data comes from different types of images (resonances, radiographs, sonograms) and material parameters of the tissue are unknown. This kind of problems generally involves certain difficulties in the assessment of parameters since they are generally consider ill-posed (Kabanikhin, 2008; Oberai and Barbone, 2011).

To solve them, this method compares experimental data obtained from the biomedical images to results obtain from a numerical model that simulates the original experiment, and where initial unknown parameters have been supposed. Then, a function is defined to quantify the error committed between the numerical and the experimental data, called objective function. By minimizing this function, optimal value of the parameters is obtained. Still, this process is iterative, so it will be repeated until problem requirements were satisfied (Fig. 1.14).

Many works have availed of inverse analysis to solve biomechanical imaging problems. Some of these works are focused on the mathematics behind the

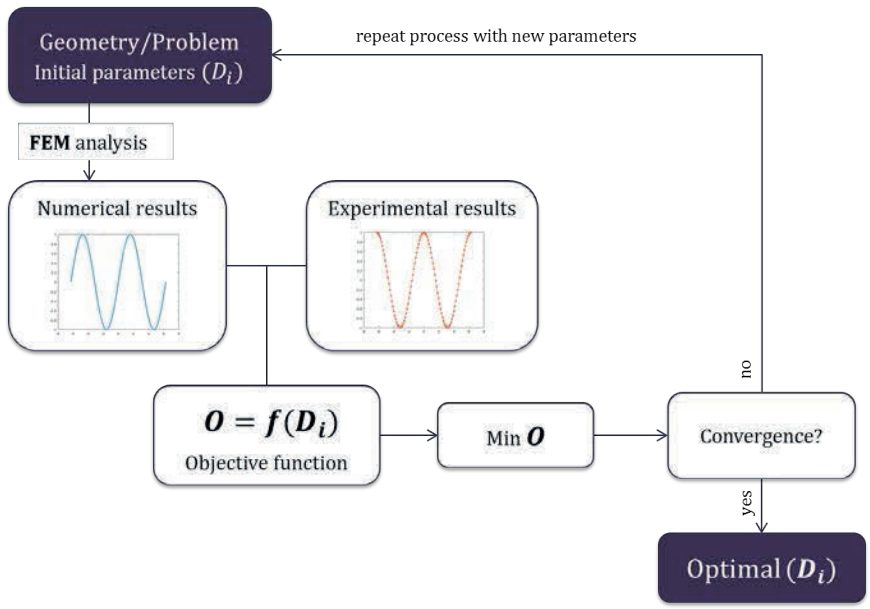

Figure 1.14: Scheme of an inverse finite element problem.

analysis (Raghavan et al., 1994; Kybic and Smutek, 2005; Barbone et al., 2009; Goenezen et al., 2011) and some others on the *in vivo* mechanical characterization of several soft tissues. In this aspect, a great variety of tissues were studied: human uteri (Kauer et al., 2002), organ of Corti (Zagadou et al., 2014), human liver Nava et al. (2008), porcine cornea (Nguyen and Boyce, 2011), soleus muscle (Böl et al., 2012), human skin (Delalleau et al., 2006) or among others.

Bearing in mind the great advance undergone by this method and the wide range of possibilities it can bring, inverse analysis is presented as a very useful tool for the *in vivo* mechanical characterization.

1.4 Motivation

The main motivation of this Thesis lies in the necessity of widen the knowledge about the *in vivo* mechanical behaviour of the abdominal wall.

Although hernia repair has been under research for the last three decades, the fact is that hernia surgery continues to draw the attention of surgeons, patients and the industry. The most widespread technique nowadays seems to be the laparoscopic tension free repair, which consists on the insertion by laparoscopy of a synthetic mesh that covers (partially or totally) the defect. The purpose of this mesh is to replace the tissue, both biologically and mechanically, during the time it is healing so the patient could revert to normal life as quickly and safely as possible. In order to avoid pain to the patient, the mesh has to mechanically behave as the muscle tissue where it is inserted. Otherwise the patient may suffer inflammation, discomfort, hernia relapse or even tissue tear. Nowadays there is a brunch of different surgical meshes for this purpose but the *ideal* mesh has yet to be found.

Additionally to the mesh, abdominal wall is not totally characterized yet. As explained in Section 1.3, some *in vitro* and *ex vivo* tests have been performed in order to assess the mechanical response of each layer, or the complete wall, but the mechanical behavior varies from the *in vitro* to the *in vivo* state. Whether due the complex structure of the tissues or the load states, to the author´s knowledge the *in vivo* mechanical properties of the abdominal wall have not so far been determined.

Furthermore, variations between specimens have to be taken into consideration. Even if an abdominal wall model was capable of reproducing the *in vivo* mechanical behavior, this would not be able to predict every clinical case, since abdomen changes from one person from another. Factors like age, gender, physical condition or medical background may affect to the mechanical behavior of the wall in a way impossible to foretell. So, determining mechanical information about the specific hernia patient seems to be indispensable to find the *suitable*

surgical mesh for this patient, i. e. the mesh that better mimic the mechanical behavior of this particular person abdomen.

Nowadays, surgeons do not have this information when they enter in an operating room but they guide their choices by experience and intuition. Despite many years of research in hernia repair, further investigations seem to be needed to provide surgeons with mechanical information about a specific patient. This is the main thought that motivates this Thesis.

1.5 Objectives

Based on the motivation previously explained, the main objective of this Thesis is to design a methodology able to characterize *in vivo* the passive mechanical behavior of the abdominal wall. The future idea is to apply this methodology in a surgical room during the initial pneumoperitoneum of the abdomen prior to a laparoscopy. The recording of this step and the postprocessing of the images, may be the key to provide biomechanical information about the abdomen of this specific patient. Thereby, surgeons would have individualized data that will help them to choose the most suitable surgical mesh in terms of mechanical behavior.

Nevertheless, before introducing any clinical novelty in a surgical room it must be previously tested and checked in depth. This is the sense of this Thesis: to design, develop and verify a methodology to mechanically characterize abdominal tissue from pneumoperitoneum tests. For this purpose, experimental procedures were performed on an animal model due to the increased availability of the specimen, lower costs and a greater ease to handle samples. Specifically, New Zealand rabbit were used used for this study.

To reach the main goal above exposed, the following partial objectives have also been achieved throughout the evolution of this Thesis.

- Study of the biological aspects of a abdominal wound closure. Short and

long-term biomechanical analysis of four suture materials on linea alba closure: *Surgipro*^{TM} (Covidien, USA) and *Assuplus*®, *Assufil*®, *Filbloc*® (Assut Europe, Italy) sutures.

- Search and adaptation of an imaging technique suitable for measuring displacement data in pneumoperitoneum tests.

- Fulfillment of pneumoperitoneum tests on the animal model. Understanding of the devices required for the test and the mechanics undergone on the abdominal wall during the development of the testing.

- Broadening of the experimental testing to new pneumoperitoneum tests performed on herniated specimen and repaired with different surgical meshes. Three polypropylene meshes were studied: *Surgipro*^{TM} (Covidien), *Neomesh Soft*® and *Neopore*® (DIMA S.L.). Differences with respect to the healthy tissue were established.

- Calculation of the displacement field of the anterolateral abdominal region. Based on the measured data, differences tracked by the cameras between healthy and repaired specimen were evaluated. Reconstruction of the abdominal geometries for several pressures in order to track the abdominal surface along the test. Pressure-displacement curves, radii of curvature and strain fields were also analysed.

- Creation of a FE model based on the experimental measurements and characterization of the abdominal wall through numerical simulation using three hyperelastic isotropic material models. Same material parameters for the whole tissue considered (homogeneous response). Optimal value of the parameters were obtained by the evaluation of response surfaces.

- Characterization of the abdominal wall through a hyperelastic isotropic material model, allowing parameters to vary along the surface (heterogeneous response). Optimal material parameters were obtained by inverse analysis, considering two different types of regularization: Total Variation Diminishing (TVD) and Tikhonov (H^1).

- *In vitro* experimental characterization of new surgical meshes in biaxial loading state and subsequent comparison between the *in vitro* and *in vivo* mechanical response.
- Construction of a FE abdominal wall model able to predict the mechanical response after being repaired with different surgical meshes.

1.6 Thesis outline

This Thesis is organized in 6 chapters (see scheme in Fig.1.15). In the beginning of each of them, a brief summary is included so that the reader could be correctly situated. Then, each chapter provides a short introduction with the basics needed to understand the findings presented in this part, the main body of this part and a last section where the main conclusions were highlighted and properly discussed. More specifically, the work is structured as follows:

- **Chapter 1** exposes a general view of the biomedical aspects addressed in this Thesis. This chapter includes a detailed description of the anatomy of the abdomen as well as the hernia procedure and the main current surgical treatments. A review of the state of art was also included, classifying the prior contributions in abdominal characterization with regards to its *in vitro* or *in vivo* character. It is completed with a general description of the techniques used throughout this Thesis (mechanical imaging and inverse analysis). Finally, the motivation, objectives and outline following in this work are itemized.
- **Chapter 2** presents an initial approach to the abdominal wound closure. Biological and mechanical aspects of the closure were analyzed at short and long-term for different suture materials. The amount of collagen was evaluated in order to assess the maturity of the wound while uniaxial tests were used to determine the mechanical response. The chapter was completed with a statistical analysis that determined the goodness of each type of

suture with respect to the healthy tissue. The contents of this Chapter were published in two original research papers, focussing on the biological (Bellón et al., 2014) and mechanical aspects (Simón-Allué et al., 2014).

- **Chapter 3** poses an initial methodology to *in vivo* characterize the passive mechanical response of abdominal wall on an animal model. The response was analysed in healthy and herniated specimen repaired with a $Surgipro^{TM}$ mesh. The whole experimental setup is properly detailed in this Chapter which constitutes the first round of the experimental burden of this Thesis, completed afterwards in Chapter 5. Geometry reconstructions, pressure-displacement relation, radii of curvature and strain fields were determined for both healthy and repaired specimen. The whole experimental procedure was partially introduced in Simón-Allué et al. (2013) and Simón-Allué et al. (2014) and entirety published in Simón-Allué et al. (2015).

- **Chapter 4** focusses on the numerical simulations performed on the model-specific abdominal wall obtained in Chapter 3. The numerical approach was based on the inverse analysis methodology, which uses the observed experimental data as an input to determine the material distribution that better reproduces this specific mechanical response. Two types of regularization were contrasted and results were correlated to anatomical features in abdominal wall. The initial idea of the inverse characterization was presented in Simón-Allué et al. (2015) and further extended in a research paper, currently under revision.

- **Chapter 5** develops an application to predict the alteration that a determine surgical mesh may provoke in a healthy abdominal wall. The *in vivo* experimentation performed in Chapter 3 was updated and expanded to other implant types. Besides, new synthetic prothesis with different mechanical properties were characterized from biaxial tests (*Neomesh Soft*®, *Neopore*® and *Neomesh SuperSoft*®, DIMA S.L.). Considering biaxial information and the mechanical characterization of healthy abdomen obtained in Chapter 4, FE simulations were performed to predict the effect that each mesh could cause in a healthy abdominal wall. Numerical model was also validated with the *in vivo* tests. The work presented in this Chapter defines

the main line of a research paper that is currently under preparation.

- **Chapter 6** summarizes the main conclusions arisen from the fulfillment of this Thesis and proposes some possible future lines to complement the research initiated in this study.

Additionally to the chapters, which define the main body of the Thesis, two appendices were added in the final part. **Appendix A** includes a summary of the Thesis redacted in Spanish, which constitutes a necessary requirement to apply for the International Doctor Degree. **Appendix B** remarks the original contributions of this study in form of publications and conferences.

Figure 1.15: Thesis outline.

2

Biomechanical study in abdominal wound closure

In this Chapter, a biomechanical study of the processes present after an abdominal wound closure is detailed. To do so, four different types of sutures were used to close a large incision performed on the linea alba in an animal model, specifically on New Zealand rabbits. The effects of each suture were analysed at 21 days (short-time) and 180 days (long-time) after surgery), in order to observe the influence of each suture type with regard to the healing process. After this time, sutured samples were subjected to uniaxial tests and stretched until failure. This results were compared to the healthy tissue and complemented with a

statistical analysis to determine the goodness of each suture type.

Additionally, a morphological evaluation was performed at both times in order to assess the type and amount of collagen as well as further biological tissue that were present in the sutured samples.

2.1 Introduction

An abdominal hernia is a disease associated to frequent post operative inconveniences such as pain, discomfort or mesh breakage. In some cases, these inconveniences may led in a new problem that requires further repair operations. It takes the name of hernia recurrence or relapse.

During last years, a general recurrence rate for hernia surgery was roughly established in $10-15\%$ (Neumayer et al., 2004; Granados, 2010). However, this rate widely varies depending on the hernia type or the surgical technique used during the procedure. Thus, the suture repair presents a recurrence rate between $30-50\%$ depending on the author while the use of a surgical mesh to repair the hernia seems to decrease this rate to $0-10\%$ (Cassar and Munro, 2002; Bellón, 2014). Minor differences have been observed between open and laparoscopic mesh repair, giving rise to contradictory conclusions (Beets et al., 1999; Neumayer et al., 2004; Lomanto et al., 2006).

Although the introduction of the prosthetic mesh to ensure abdominal wall strength without tension has decreased this recurrence rate, the fact is that this value still remains high and needed to be improved. Due to this, a study in depth of the processes that take place between the suture and the soft tissue after a wound closure becomes very interesting. To that end, this Chapter has been focused on midline laparotomy, one of the most commonly employed openings in the abdomen from a technical-surgical standpoint, to analyse the biomechanical and biological aspects of the suture-tissue integration.

The laparotomy can be performed rapidly and can also be easily widened in the proximal or distal direction. Moreover, it provides a good surgical field. Its execution requires the opening of the abdominal midline, also called the *linea alba*. This anatomical region is composed of a conjunction of fascia muscular fibers located on both sides of the abdomen. It behaves as a sinewy region and is considered a weak part of the abdominal wall, since this part can be damaged more easily than the rest of the abdominal wall. This weakness is emphasized when fibers are cut to reach the abdominal cavity during surgery.

The repair or linea alba closure can be reinforces by sutures. There are two sources of mechanical load present at the wound: the intra-abdominal pressure and the muscular forces, when fascias of the lateral muscles of the abdomen merge at the wound and try to split the incisional edges. These mechanical factors (Förstemann et al., 2011), together with other biological issues such as different types of collagen or certain enzymes present at the wound (Bellón, 2007), are responsible for a high percentage of postoperative incisional hernias. The incidence of this type of hernia after a medium laparotomy remains high, occurring in approximately a $16 - 20\%$ of cases (Diener et al., 2010). Several experimental and clinical studies (Israelsson and Jonsson, 1994; Israelsson and Millbourn, 2012; Höer et al., 2002; Weiland et al., 1998), have analyzed the influence of the suture type in laparotomy closure, irrespective of other technical approaches (i.e., continuous and discontinuous closure, distance between stitches, tissue edges included in the suture).

The suture types most commonly employed in laparotomy closure are polypropylene and polydioxanone. The first is a highly biocompatible non-absorbable material, whereas the second is an absorbable polymeric material with a medium/long duration in tissue of approximately $180 - 230$ days (Suzuki and Ikada, 2012). According to a recent clinical study (Bloemen et al., 2011), no differences have been observed between the restorative behavior of these materials with regard to the occurrence of incisional hernia. Recently new suture types with different properties have appeared; some are fully absorbable materials, and some are non-absorbable ones with greater compliance. These sutures have already been

tested in multicenter clinical studies (Albertsmeier et al., 2012) with short follow-up periods; therefore, the results related to their behavior remain preliminary. However, a more detailed mechanical analysis is still needed to understand their behavior. The same is true for another suture type that has recently appeared on the market, barbed sutures (Villa et al., 2008). This type of suture is not exactly a recent innovation, as the patent dates from 1964 (Alcamo, 1964), but its use has not been very widespread, and it has only lately become increasingly important. It has been used in diverse surgical applications, such as plastic surgery (Jandali et al., 2011), digestive surgery (Facy et al., 2013; Nemecek et al., 2013) and in recent experimental studies on fascia closure (Oni et al., 2012) and tendons (Nozaki et al., 2012), but this suture has only been mechanically studied from a theoretical viewpoint (Ingle et al., 2010).

In this work, two new sutures have been tested in an experimental model of laparotomy closure. The materials studied were non-absorbable sutures with elastic properties and absorbable barbed sutures. The aim of this work was to investigate whether these new sutures could provide any advantages in terms of mechanical behavior (e.g. less risk of tear or better adaptability with the healing tissue) compared with other more conventional materials that are currently used in the clinic, such as polypropylene and polydioxanone.

2.2 Material and Methods

2.2.1 Sutures

Four monofilament 3/0 sutures were tested: non-absorbable polypropylene ($Surgipro^{TM}$, Covidien, USA (PP)) and polyurethane ($Assuplus$®, Assut Europe, Italy (PUe)) sutures, absorbable polydioxanone ($Assufil$®, Assut Europe, Italy (PDX)) sutures and absorbable barbed polydioxanone ($Filbloc$®, Assut Europe, Italy (PDXb)) sutures. Diameters were measured using a scanning electron microscopy (SEM) as shown in Fig 2.1, and the software Quartz PCI 7. To obtain the diameter, 8 measures were performed for PP, PUe and PDXb while 12 were

performed for PDX. Table 2.1 lists the commercial name, material, absorbability and means and deviations in diameters for all four sutures used in this study. In the case of the barbed sutures, the average of the diameters of the barbed and non-barbed zones was considered.

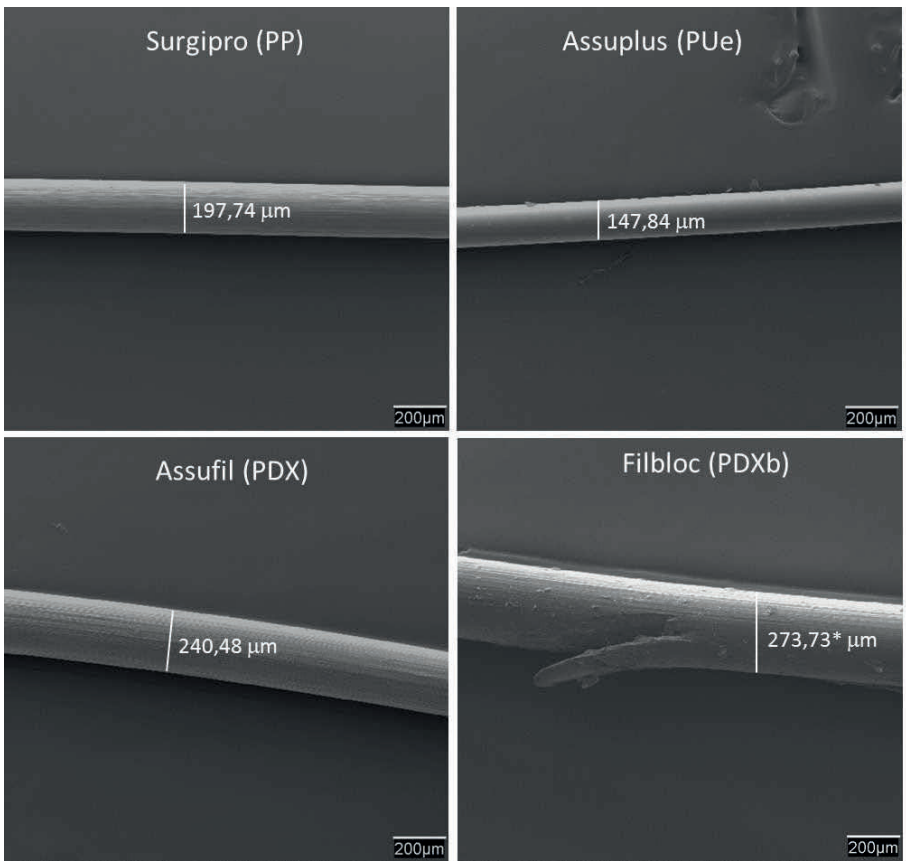

Figure 2.1: Diameters of the sutures used in this study, measured by scanning electron microscopy: $Surgipro^{TM}(PP)$, $Assuplus^{®}(PUe)$, $Assufil^{®}(PDX)$, $Filbloc^{®}(PDXb)$. *Average diameter of the barbed and non-barbed zones was considered in the case of barbed suture.

Commercial Name	Material	Abs./Non-Abs.	Diameter (μm)
$Surgipro^{TM}$ (PP)	Polypropylene	Non-Absorbable	197.74 ± 2.30
$Assuplus$® (PUe)	Polyurethane	Non-Absorbable	147.84 ± 1.70
$Assufil$® (PDX)	Polydioxanone	Absorbable	240.48 ± 2.12
$Filbloc$® (PDXb)	Polydioxanone	Absorbable	$273.73 \pm 11.94^*$

Table 2.1: Description of the monofilament sutures tested in this study. *Average diameter in the case of barbed suture.

2.2.2 Mechanical tests of individual sutures

Uniaxial tensile tests of each suture were performed under displacement control on an Instron E-1000 microtester with a 50-N full-scale load cell. A displacement rate of $v = 1mm \cdot min^{-1}$ was maintained throughout the tests, i.e. around 2.5% of stretch rate per minute, considering a quasi-static condition. Load and elongation were recorded until complete suture rupture. Stretching data was obtained from $\lambda = \frac{L_0 + \triangle L}{L_0}$, where L_0 was the initial length between clamps, set at 40 ± 5 mm depending on the test, and $\triangle L$ was the clamp displacement. Cauchy stress was obtained from $\sigma = \frac{N}{A} \cdot \lambda$, where N was the applied load and A the cross-section of the suture. For this study, 8 samples of each suture type were tested.

2.2.3 Animal model: experimental design

The study was performed on 60 male New Zealand white rabbits of approximately 3000 g. All of the animals were kept under stable conditions of light and temperature following the recommendations given by the Guide for the Care and Use of Laboratory Animals of the National and European Institutes of Health (Spanish law 32/2007, Spanish Royal Decree 1201/2005, European Directive 2010/63/UE and European Convention of the Council of Europe ETS123). All procedures were performed at the Animal Research Center of Alcala Univer-

sity. The study protocol was approved by the University Committee on the Ethics of Animal Experiments (CEI2012-016).

All animals were anesthetized using a combination of ketamine and xylazine (*Rompun*®, Bayer; 20 mg/mL/kg). Using a sterile surgical technique, three 2-cm midline laparotomies, 1 cm apart, were performed on each rabbit. The xiphoid process was used for reference, and the laparotomies were begun 3 cm away from this reference point (see Fig. 2.2.a). The surgical wound was then repaired with a running stitch using four different 3/0 sutures: non-absorbable polypropylene (*Surgipro*^{TM}, Covidien, USA); non-absorbable polyurethane (*Assuplus*®, Assut Europe, Italy), absorbable polydioxanone (*Assufil*®, Assut Europe, Italy) and absorbable barbed polydioxanone (*Filbloc*®, Assut Europe, Italy). The knot used to close the wound was formed with the surgeon'os knot method (two turn clock-wise, one anticlock-wise and one clock-wise (Kim et al., 2007)). All closures were performed by the same surgeon (J. M. Bellón), maintaining the 4:1 ratio.

During the 3 days after surgery, animals received *Meloxidyl*® (Esteve; 0.1 mg/kg) mixed with water. Throughout the study, the animals were visually inspected for signs of rupture of the closure, seroma formation and wound infection. Six animals from each group were euthanized in a CO_2 chamber at 21 and 180 days after surgery, and another six animals that were not subjected to surgery were used as controls for each time point. A total of 60 animals (48 sutured and 12 healthy) were used for this study. Specimens from each of the three midline laparotomies in the linea alba (Zones A, B and C) were obtained for the different analyses; each specimen contained the wound site with the sutures and some of the surrounding tissue (see Fig. 2.2.b).

From each LA zone, smaller samples with the suture located in the middle were extracted with a width:length ratio of next to 1:6 or 1:7 (see Fig. 2.2.c). This ratio was pursued to preserve the uniaxial hypothesis during the mechanical tests which requires to guarantee uniform stress at the central sample area. Table 2.2 shows the dimensions of the samples used in the tests.

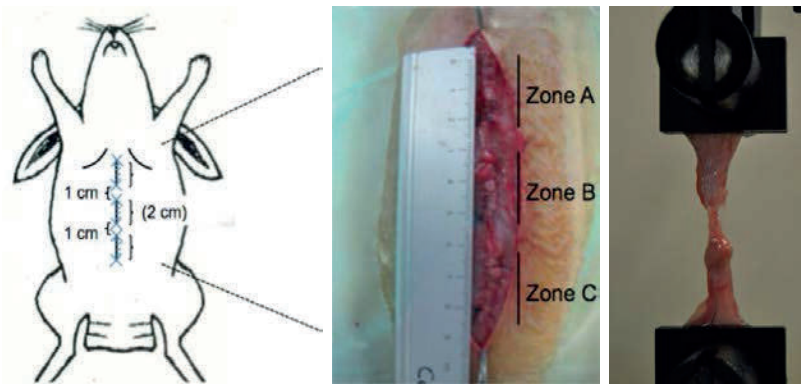

(a) Specimen locations (b) Samples from the animal model (c) Experimental setup

Figure 2.2: Experimental design and location of the sutures for the uniaxial tests.

2.2.4 Mechanical tests of linea alba specimens

Uniaxial tensile tests of the linea alba specimens were performed under displacement control on an Instron 3340 microtester with a 1-kN full-scale load cell. A displacement rate of $v = 5mm \cdot min^{-1}$, i.e. around 1.11% of stretch rate per minute, was estimated considering a quasi-static situation. Load and elongation were recorded until complete specimen rupture. Stretching data was obtained from $\lambda = \frac{L_0 + \triangle L}{L_0}$, where L_0 was the initial length between the clamps and $\triangle L$ was the clamp displacement. Cauchy stress was obtained from $\sigma = \frac{N}{CSA} \cdot \lambda$, where N was the applied loadand CSA the cross-section area, calculated as $CSA = Width \cdot Thickness$. Cauchy stress ($\sigma$) versus stretching ($\lambda$) for LA-closure samples were compared.

2.2.5 Morphological studies and collagen expression

For light microscopy, the specimens were fixed in F13 solution (60% ethanol, 20% methanol, 7% polyethylene glycol, 13% distilled water), embedded in paraffin, sliced into 5 mm thick sections, and stained with Masson's trichrome (Goldner-

		21 days		180 days	
		Sutured	Control	Sutured	Control
Zone A	Length	87.06 ± 4.17	85.30 ± 5.33	90.00 ± 2.93	87.32 ± 1.79
	Width	17.71 ± 2.90	14.87 ± 1.86	20.07 ± 2.14	19.24 ± 1.49
	Thickness	3.08 ± 0.49	2.48 ± 0.19	3.80 ± 0.44	2.92 ± 0.41
Zone B	Length	87.07 ± 6.88	84.98 ± 1.64	90.63 ± 3.37	92.14 ± 1.41
	Width	17.44 ± 3.11	14.05 ± 1.32	19.34 ± 1.61	17.65 ± 1.59
	Thickness	2.44 ± 0.28	1.81 ± 0.25	3.05 ± 0.45	2.27 ± 0.33
Zone C	Length	88.67 ± 3.98	86.72 ± 0.43	90.62 ± 4.19	91.56 ± 2.93
	Width	17.84 ± 1.90	13.41 ± 1.65	20.13 ± 2.34	19.33 ± 1.41
	Thickness	2.26 ± 0.34	1.55 ± 0.22	2.96 ± 0.52	2.17 ± 0.27

Table 2.2: Mean and standard deviations of length, width and thickness values for the tested samples (mm).

Gabe) stain. Images for analysis were captured using a digital camera (Axiocam HR, Zeiss) fitted to a light microscope (Zeiss Axiophot, Carl Zeiss, Oberkochen, Germany).

The collagen content was determined in the same sections by Sirius Red staining for collagen types I and III. This technique (Junqueira and Carneiro, 2007) is based on the orientation and interaction between the sulfone groups of the dye, the amine groups of lysine and hydrolysine and the guanidine groups of arginine in the collagen fibers, which give rise to different colors depending on the type of collagen. Type I collagen appears as a reddish-orange stain, while type III collagen takes on a yellowish-green shade when observed under a polarized light microscope (Zeiss Axiophot, Carl Zeiss, Oberkochen, Germany). For each type of collagen, relative staining was assessed in 10 digitized histological images per animal that were captured using a digital camera fitted to the microscope (Axiocam HR, Zeiss), and the images were analyzed using image analysis software (Axiovision AC 4.1). Each section was divided into 4 sectors, and one micro-

scope field (x100) was randomly selected from each sector to estimate the extent of staining. The following scale was used: $-$, no labeling ($< 10\%$); $+/-$, minimal labeling ($10 - 25\%$); $+$, moderate labeling ($25 - 50\%$); $++$, intense labeling ($50 - 75\%$); and $+++$, maximal labeling ($> 75\%$). The staining was assessed by 3 independent, blind observers.

2.2.6 Statistical analysis

All statistical tests were performed using the GraphPad Prism 5 computer package for Windows. The significance level was set at $p < 0.05$.

Mechanical behavior of individual sutures. Cauchy stresses at four levels of stretching were written down for each type of suture. Data were statistically analysed using an analysis of variance (ANOVA) and comparisons between the groups were performed using a Student's t-test to detect significant variations among the groups.

Mechanical behavior of linea alba closure. First, the three zones (A, B and C) in the control tissue and the four types of sutures were compared to determine any significant differences between zones. In addition, a statistical analysis was performed to determine possible significant differences between the four groups (PP, PUe, PDX, PDXb) and control tissue in the mechanical behavior at 21 and 180 days. Comparisons between groups were performed at four levels of stretching, selected regularly in the range $\lambda = [1.1 \div 1.4]$, using t-test if the data were normally distributed or the Wilcoxon test if not.

2.3 Results

2.3.1 Mechanical behavior of the sutures

Representative uniaxial stress-stretch curves for the different material sutures are presented in Fig. 2.3. At this figure, mean and ten error bars along the stress-stretch curves were displayed per each suture. PP, PDX and PDXb sutures showed a linear behavior, while PUe presented a non-linear behavior. Table 2.3 contains the failure stretch and stress and the Young's modulus for the three linear sutures. In the case of PUe, with non-linear behavior, the secant modulus was determined on the basis of the failure values. According to the results, PDX was the toughest suture, with failure occurring at a Cauchy stress of 657.94 ± 106.56 MPa. This suture also had the largest stretch failure of 1.39 ± 0.084. PP was the second-strongest suture, failing at Cauchy stress of $\sigma = 592.64 \pm 57.45$ MPa. PUe sutures were the second-weakest sutures tested and failed at a Cauchy stress of 565.76 ± 59.77 MPa, with the smallest stretch failure of 1.17 ± 0.060. PDXb sutures were the weakest sutures tested and ruptured at 477.720 ± 76.416 MPa. Both PDX sutures presented similar behavior, which indicates that the barbs do not affect the mechanical response of the suture.

Commercial name	**Failure stretch** $\lambda(-)$	**Failure stress** $\sigma(MPa)$	**Young's mod.** **E** (MPa)
$Surgipro^{TM}$ (PP)	1.294 ± 0.055	592.643 ± 57.452	$2.014 \cdot 10^3$
$Assuplus$® (PUe)	1.175 ± 0.060	565.756 ± 59.778	$3.239 \cdot 10^3$ *
$Assufil$® (PDX)	1.390 ± 0.084	657.940 ± 106.569	$1.685 \cdot 10^3$
$Filbloc$® (PDXb)	1.270 ± 0.027	477.720 ± 76.416	$1.767 \cdot 10^3$

Table 2.3: Means and standard deviations of failure values and Young's modulus of the sutures tested. *In the case of PUe, the secant modulus was determined due to its non-linearity.

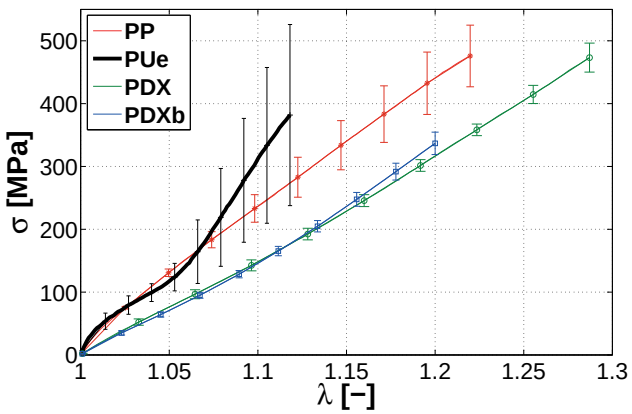

Figure 2.3: Experimental stress-stretch curves for the different suture materials. For each suture material, $n = 8$ specimens were tested and ten error bars were displayed, representing the standard deviation along the curve.

2.3.2 Animal model

None of the study animals died, and there were no signs of infection and/or rejection at the level of the different materials. Seroma was detected in two animals sutured with PDX and PP, in one animal sutured with PUe and in one of the controls. Macroscopically, at the test dates, there was no evidence of wound dehiscence or complications. As expected, due to their non-absorbable nature, PP and PUe remained present at 21 and 180 days after surgery. At the same test dates, there were still traces of both types of PDX sutures.

2.3.2.1 Linea alba closure mechanical behavior

Because the linea alba closure should mimic the mechanical response of a healthy abdominal wall, sutured and healthy tissues from the A, B and C zones were characterized and compared over time. When we compared the mechanical behavior of the three zones at 21 and 180 days, similar behavior was observed for the B and C zones ($p > 0.05$). According to these results, we assumed equal

behavior in the medial (Zone B) and inferior (Zone C) regions, so the samples from these two zones are grouped. Because the variable imposed during experimental tests was the stretching of the specimens, the variable measured and compared was the Cauchy stress needed to cause this stretching. The Cauchy stress-stretch curves for the different groups of studied samples were presented in Fig. 2.4. Ten error bars were displayed along each curve. All curves were cut off at $\lambda = 1.4$, due to the high dispersion found between the samples result at higher levels. As a result, some of the error bars were missed in Fig. 2.4.

When the behavior of the control and sutured tissues from the same time points were compared, distinct results were observed. At day 21, healthy and sutured tissue in zone A showed similar mechanical properties for small stretches ($\lambda < 1.3$)($p > 0.05$), since all of them deform in a similar stress-stretch curve. However, significant differences were found between three of the suture materials and the healthy tissue for $\lambda \geq 1.3$ ($p < 0.0459$), when healthy tissue showed a significant stiffer behavior than the PP, PDX and PDXb. Only PUe was able to mimic the control behavior for high stretches; see Fig. 2.4 (a). In Zone BC, different behavior was observed for low levels of stretch ($\lambda \leq 1.2$) between the PP, PDX and PDXb sutures and the healthy tissue ($p < 0.0079$), and only PUe showed a similar response to the control. For greater stretches ($\lambda \geq 1.3$), the four sutures presented similar behavior, and none of them reproduced the behavior of the control ($p < 0.0146$); see Fig. 2.4(b).

At 180 days, no significant differences were found between the sutured and the healthy tissues in Zone A ($p > 0.05$), see Fig. 2.4(c). In Zone BC, differences for low levels of stretching ($\lambda = 1.1$) were observed between PP, PDX and PDXb sutures and the healthy tissue ($p < 0.0079$). For $\lambda \geq 1.2$, none of the sutures showed behavior similar to that of the healthy tissue ($p < 0.0137$); see Fig. 2.4(d).

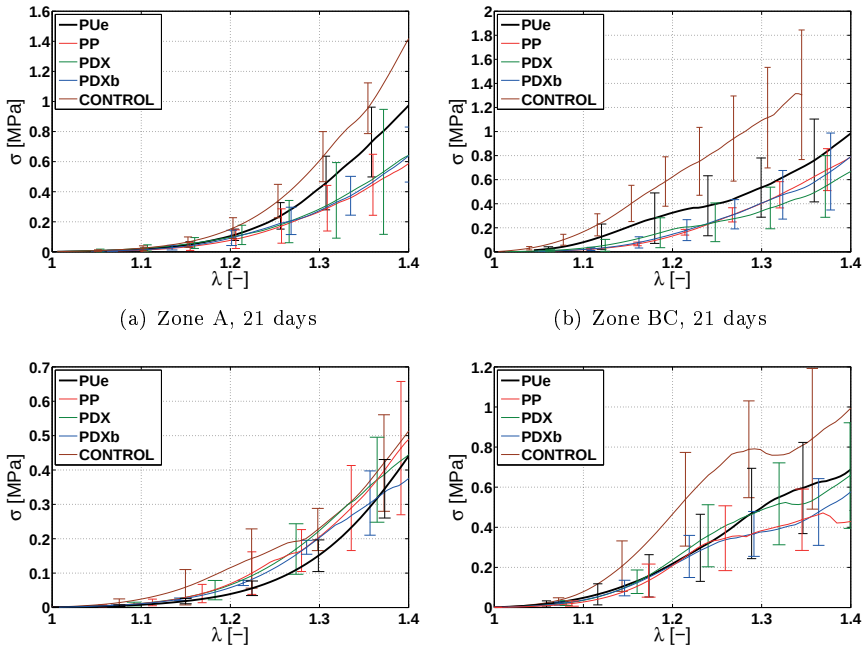

(a) Zone A, 21 days

(b) Zone BC, 21 days

(c) Zone A, 180 days

(d) Zone BC, 180 days

Figure 2.4: Experimental stress-stretch curves for the LA closures (all curves have been cut off at $\lambda = 1.4$). For each suture material, $n = 12$ in the case of Zone A and $n = 24$ specimens in the case of Zone BC were tested. Ten error bars were displayed per curve before cutting at $\lambda = 1.4$, representing the standard deviation along the curve.

2.3.3 Histology

2.3.3.1 Controls

Under light microscopy, Masson's trichrome staining revealed the linea alba, formed by connective tissue from the fusion of the prolongation of the premuscular and retromuscular aponeurosis/fascias in the midline. The linea alba, along with muscle fibers from the rectus abdominis, can be identified in a transverse section of the surgical specimens. Both the peritoneal and subcutaneous sides show

abundant adipose tissue (Fig. 2.5). This technique does not show remarkable morphological differences between the specimens at 21 and 180 days. Staining with Sirius Red showed the linea alba and the different fascias between muscle layers formed mostly by mature type I collagen at both 21 and 180 days (see Fig. 2.6).

2.3.3.2 Short-term behavior of the closure: 21 days

The area corresponding to the linea alba appeared to be thickened, with abundant disorganized connective tissue, which was much more cellular in the case of PUe and PDXb. There was a smaller amount of adipose tissue on both the subcutaneous and peritoneal sides compared with the control specimens (see Fig. 2.7). Sirius Red staining showed homogenous predominance of immature type III collagen in the area of the wound for the PP, PDX and PDXb sutures (Fig. 2.8). The three groups showed values above 75%in the semi-quantification of collagen type III (Table 2.4). The tissue from the wounds closed with PUe had a slight decrease in collagen III expression with respect to the other three groups. However, significantly more mature collagen I expression, similar to that in the control samples, was observed in this group when compared with the others (Fig. 2.8, Table 2.4).

2.3.3.3 Long-term behavior of the closure: 180 days

At 180 days, there was a noticeable increase in the amount of adipose tissue surrounding the connective tissue corresponding to the linea alba. In the closures performed with PP and PUe the connective tissue was very dense, and surrounded the suture filaments. Otherwise, Masson's trichrome staining did not show significant differences between the different suture materials (Fig. 2.7). Sirius Red staining showed that the total amount of collagen in the area of the wound had decreased due to the increase of adipose tissue (Fig. 2.8). Compared with the findings at 21 days, all suture materials showed a decreased amount of type III collagen except for PUe, where the amount of type III collagen remained stable.

No large differences were found in the percentage of type I collagen between 21 and 180 days (Fig. 2.8, Table 2.4).

	21 days		**180 days**	
	Col III	**Col I**	**Col III**	**Col I**
Control	+	+++	+	+++
Surgipro^{TM} (PP)	+++	+	++	+
Assuplus® (PUe)	++	+++	++	++
Assufil® (PDX)	+++	+	+	++
Filbloc® (PDXb)	+++	++	+	++

Table 2.4: Semi-quantification of the expression of type I and III (Sirius Red) collagen in control LA, and after closures performed with PP, PUe, PDX, PDXb at 21 and 180 days. The following scale was used for grading: no labeling ($<$ 10%);+/−, minimal labeling ($10-25\%$); +, moderate labeling ($25-50\%$); ++, intense labeling ($50-75\%$); and +++, maximal labeling ($>75\%$).

2.4 Discussion

In the present work, the behavior of four different suture materials were tested and subsequently compared to that of healthy tissue, which was the control. Two of these suture materials, polypropylene (PP) and polydioxanone (PDX), widely used in the medical field (Suzuki and Ikada, 2012; Nobile et al., 1997) represented the non-absorbable and absorbable monofilament sutures. The other two, polyurethane (PUe) and barbed polydioxanone (PDXb), represented new materials with possibly improved mechanical properties. To investigate whether these sutures were indeed an improvement, biomechanical and histological studies of the suture materials and their performance in an animal model were conducted.

Although all sutures were chosen to be the same size, 3/0, some differences were observed in the thread diameters when they were measured using scanning

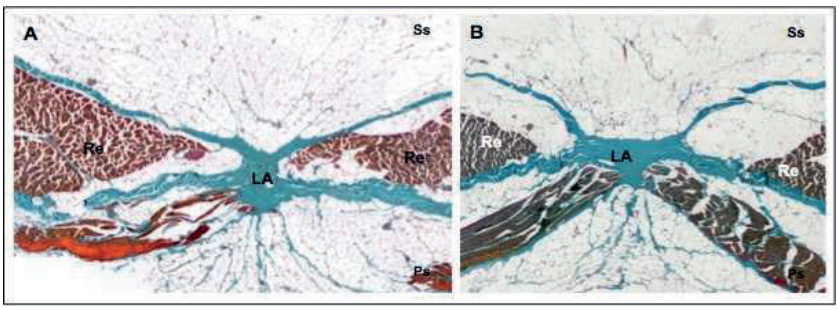

Figure 2.5: Panoramic view of the histological findings from Masson's trichrome (100x) staining of the linea alba (LA) of a control rabbit at 21 (A) and 180 days (B). Re: rectus abdominis muscle; Ss: subcutaneous side; Ps: peritoneal side.

electron microscopy. These size differences could affect the mechanical response of the sutures. To evaluate this mechanical behavior, uniaxial tensile tests were performed for all suture types. The test data showed that PUe was the stiffest material, followed by PP, and both types of PDX (barbed or non-barbed) were the most compliant and presented similar mechanical behavior. To understand the short- and long- term behavior of the sutures, samples were analyzed at two dates. During the first month, the wound starts to heal and the suture is responsible for absorbing the forces generated at the sizes of the incision (Franz, 2006, 2008; DuBay et al., 2006). Once this first period ends, the tissue starts recovering until it is strong enough to support typical loads (Franz et al., 2000). Owing to these mechanical differences during the healing process, the mechanical and histological properties were analyzed at 21 and 180 days.

At 21 days, PUe appeared to be the only suture able to mimic the control tissue behavior, regardless of the abdominal zone in the animal. Despite the high dispersion found between samples, significant differences were found between the rest of the sutures (PDX, PDXb and PP) and the control tissue. In all cases, healthy tissue presented a stiffer behavior than the obtained with sutured tissue, which explains why PUe was the suture that best reproduced the control behavior. When the histology and the collagen expression were analyzed at 21 days, it was observed that tissue from wounds closed with PUe had a slight decrease in collagen

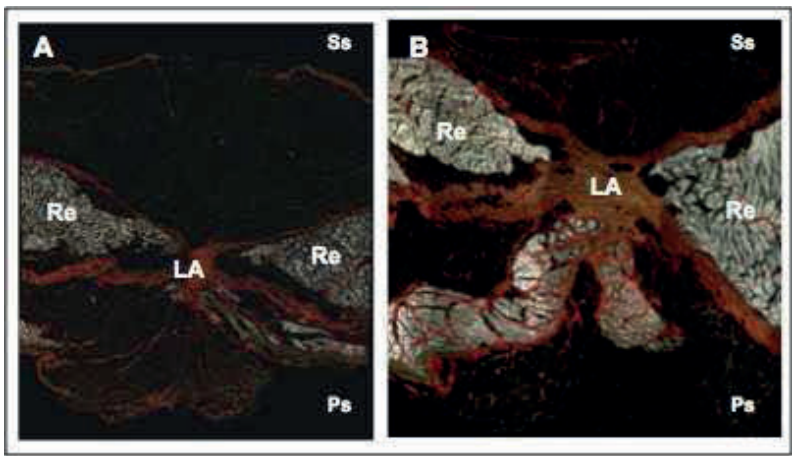

Figure 2.6: Panoramic view of the linea alba in control tissue at 21(A) and 180 days(B) (Sirius Red, 100x). LA: linea alba; Re: rectus abdominis muscle; S: suture; Ss: subcutaneous side; Ps: peritoneal side.

III with respect to the other groups, but an increased amount of mature collagen I.

As previously explained, collagen I or mature collagen, is the main fibrillar protein responsible for the mechanical properties of neoformed tissue. Type III collagen is also a fibrillar collagen and is found in extensible connective tissues, but more related to fast growing tissue, particularly at the early stages of wound repair. During healing, this collagen is replaced by the stronger and tougher type I collagen, giving the wound the strength needed to support loads. Accordingly, these differences in collagen content give the PUe increased resistance to elongation, which is in accord with the results obtained from the mechanical tests. Because the wounds were still starting to heal as much as 21 days after surgery, the higher resistance of the PUe during this period is a very interesting property.

At 180 days, no significant differences were found between the suture types. The high dispersion of the data may have contributed to this lack of differences between suture groups, considering that error bars overlap for high stretches.

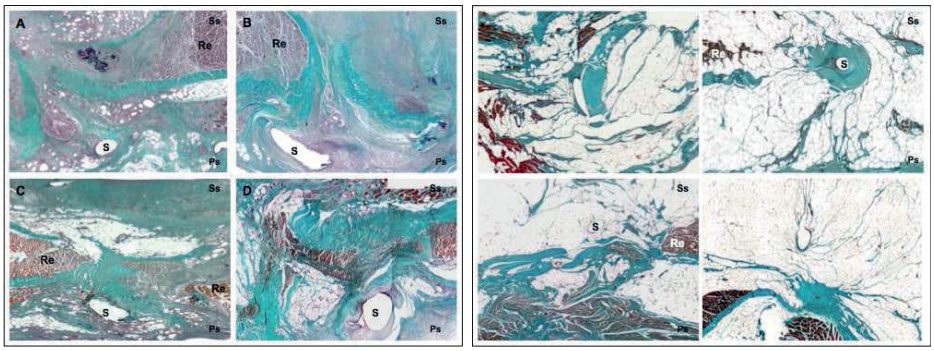

(a) 21 days (b) 180 days

Figure 2.7: Panoramic view of the linea alba after closure performed with PP (A), PUe (B), PDX (C) and PDXb (D) at 21 days (Masson's trichrome, 100x). Re: rectus abdominis muscle; S: suture; Ss: subcutaneous side; Ps: peritoneal side.

However, none of them was able to fully reproduce the control tissue behavior. With regard to the mechanical tests, maximum stresses were lower than at 21 days due to increased sample thickness. The collagen content of PUe-sutured specimens was similar to that of tissues sutured with the other suture materials, and no significant differences were found between the sutures. Although no suture material was able to reproduce the behavior of healthy tissue, this is not a vital drawback because at this time point, tissue should be able to bear the majority of wound tension.

Regarding the comparison between absorbable and non-absorbable sutures, no significant differences were found in this study. Polydioxanone is a slowly absorbable suture commonly used in surgery (Suzuki and Ikada, 2012), and its total absorption takes 180 days (Ceydeli et al., 2005). However, in this study, some traces still remained in the tissue after this time point. This finding could be related to the initial diameter of these two sutures, which was larger than those of the non-absorbable sutures, despite ostensibly being of the same size. According to histological results, at 180 days, PP and PUe present a noticeable increase in the amount of adipose tissue surrounding the connective tissue of the linea alba, as expected with non-absorbable sutures and unlike absorbable sutures

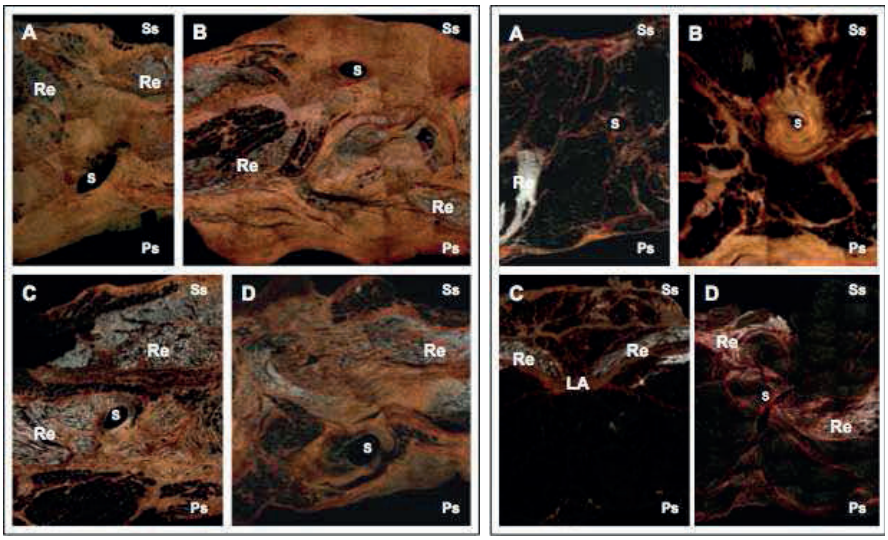

(a) 21 days (b) 180 days

Figure 2.8: Panoramic view of the linea alba after closure, performed with PP (A), PUe (B), PDX (C) and PDXb (D) at 21 days (Sirius Red, 100x). LA: linea alba; Re: rectus abdominis muscle; S: suture; Ss: subcutaneous side; Ps: peritoneal side.

(Weiland et al., 1998; Suzuki and Ikada, 2012; Docobo-Durantez et al., 2006).

Another interesting point examined in this work was the effect of barbed sutures. Previous studies have thoroughly evaluated the advantages of their use in tendons and in plastic surgery, but in most cases, they have been investigated as non-absorbable materials (Suzuki and Ikada, 2012; Villa et al., 2008; Oni et al., 2012; Ingle et al., 2010). In this work, a barbed polydioxanone suture was used. With regard to the mechanical analysis, no significant differences were found between barbed and non-barbed sutures, neither in individual threads nor in the sutured tissue. This result is in accord with those of Oni et al. (2012), who reported similar strength for barbed and non-barbed polydioxanone sutures. The main advantage of this type of suture seems to be the ability to avoid knots in wound closure, where a slip could turn into a complication during healing (Kim et al., 2007).

The last suture material studied herein was non-absorbable polyurethane (PUe). The existing literature about elastic sutures is scarce, and the only commercially available fully elastic suture is the *MonoMax*®, a long-term absorbable monofilament developed using poly-4-hydroxybutyrate (Odermatt et al., 2012). The non-absorbable elastic suture tested here is a novelty in the abdominal surgery field and is a starting point for a new way forward.

Some limitations of this study should be mentioned before concluding. First, only four suture materials were tested in this study, all of which were 3/0 monofilament. It would be interesting to test other sizes or arrangements (multifilament) to determine how these properties would affect the mechanical response. In addition, suturing technique could be varied (Weiland et al., 1998; Wissing et al., 1987; Richards et al., 1983). In this study, three midline laparotomies were performed on each animalÂt's abdomen with continuous sutures, that were 1 cm apart to preserve the boundary conditions of the suture. A complete and continuous 10-cm incision could be performed to investigate the influence of the wound size. Interrupted sutures would also be an interesting subject for study.

With regard to the mechanical analysis of the sutures, further information from other mechanical tests would be useful (e.g., biaxial tests) to reproduce in a more accurate way the tensional state of the abdomen. In addition, some simplifications have been assumed for the uniaxial tensile tests, such as the assumption of homogeneous tissue thickness, which is necessary for direct comparison of the experimental stress-stretch curves.

2.5 Conclusions

In this work, the mechanical behavior of four different suture materials (PP, PUe, PDX and PDXb) and the morphology and collagen expression have been investigated and subsequently compared to healthy tissue. Our results showed that PUe is the most appropriate material for abdominal wall closure, because it is the suture that best reproduces the mechanical behavior of healthy tissue.

At 21 days after the surgical procedure, tissue sutured with PUe presented a higher amount of collagen I, which permitted greater resistance to mechanical force during the first month of healing, just at the point when most loading of the wound devolved upon the sutures. At 180 days, all sutures showed similar behavior, and none of them could mimic healthy tissue. No significant differences were found between barbed and non-barbed sutures, nor there were mechanical differences between absorbable and non-absorbable materials.

3

In vivo mechanical testing on animal model

In vivo mechanical testing was divided into two stages, due to the complexity and novelty of the experimentation. The first one, included in this Chapter, presents the experimental process in depth and applies the method to a limited number of specimen. The second part is gathered in Chapter 5, where the application of the empirical method is widen and addressed to the mesh hernia repair.

Therefore, in this Chapter the experimental procedure followed during the *in vivo* testing on animal model is properly explained. Mechanical tests consisted on

recreating a pneumoperitoneum, which was carried out over two types of specimen: healthy specimen and herniated specimen, with a defect previously created and repaired through the implantation of a mesh a week before the testing. Specifications of both models are detailed. Based on the data acquired during the mechanical tests, the geometry at different timing were reconstructed and a 3D finite element model was created. A mechanical study developed from the measured displacements fields was performed, where pressure-displacement curves, radii of curvature and strain fields were also analysed.

During the experiments, muscle tissue mostly deformed during the first levels of pressure, showing the noticeable nonlinear passive behavior of abdominal muscles. This nonlinear behavior was also visible in the case of herniated specimen, but with a strong stiffening in the zone where the high density mesh was situated. Results from healthy and herniated specimen were compared. Cameras were able to discern differences, so this method can be used to measure the possible effect of other meshes.

3.1 Introduction

Although laparoscopic procedures have been applied to hernia repair for the latter half of past century, it was not until the 1990s that it accomplished a real step forward (Moreno Ruiz, 2011). As previously explained, a laparoscopy consists on performing a surgical procedure with out a big initial surgical cut, but only three or four small incisions where the surgical instruments are inserted. Through these incisions the laparoscope is introduced with a light and a viewer, allowing surgeons to see the interior of the abdominal cavity. In order to facilitate the laparoscope maneuvers, the first step of this procedure consists on blowing gas into the abdominal cavity so that the abdominal wall detaches from the internal abdominal organs (see Fig. 3.1). The gas inserted is carbon dioxide and it is controlled by an endoscopy device which monitors the pressure suffered by the end point of the laparoscope. The presence of air within the peritoneal cavity takes the name of pneumoperitoneum.

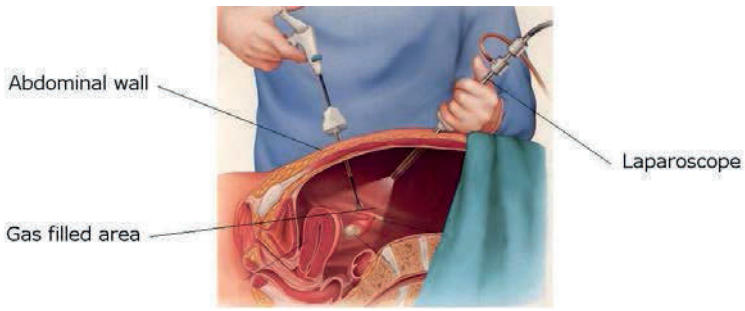

Figure 3.1: Scheme of the laparoscopic procedure.

This process of layer detachment, common in every abdominal laparoscopy, can be seen as a mechanical test where the pressure induced into the cavity is known. The rest of magnitudes involved, such as strain, stress or displacement field, remain unknown. The proposal of this Thesis is to measure the displacements undergone by the abdominal wall while the inner pressure is increased. In order to not to interfere with the mechanical behavior of the tissue, the displacements measurement has to be performed externally, in a non-invasive way. For this reason we propose photogrammetry, which allows estimating accurately 3D geometrical information of a scene only from photographs of the scene, without physical contact with the scene. The basics of this technique are explained in the following section.

3.2 Measurement using Photogrammetry

In its origins photogrammetry was an expensive technique mainly applied in cartography from aerial images (Slama et al., 1980). It was also used in high added value or critical measurements such as in the case of nuclear power stations or ships. In general, they were methods designed to make measurements of big scenes where the cameras were located far from the measured surfaces. More recently, due to the digitalization of the cameras and the availability of computers, these methods have significantly reduced their costs and are routinely applied not only in big scenes but also in small scenes close to the cameras (Mikhail et al., 2001;

Luhmann et al., 2014). There are also commodity softwares for applying these methods, such as PhotoModeler (2013).

Among the applications we can find its usage to measure displacements in biomedical applications (Goellner et al., 2010), and closer to our case (Buganza Tepole et al., 2015). We focus on the case of several synchronized cameras observing the same scene because this configuration can estimate 3D models of deforming scenes at a rate of several full scene reconstructions per second. In this Thesis we use the minimal configuration of two synchronised cameras gathering two synchronized videos at tens of frames per second. Regarding the scene, only a sparse set of points tattooed on the specimen surface are reconstructed in 3D.

A key element of photogrammetry is camera calibration. Each camera calibration is composed of two set of parameters: intrinsic and extrinsic. The intrinsic parameters are: focal length, pixel size, principal point and distortion. These attributes define the relation between the image in pixels and the ray to which the scene point P belongs (Fig. 3.2). Given the coordinates of a point in an image (u_L, v_L), the intrinsic define straight line, the ray, where the point belongs. The line is defined with respect to a frame local to the camera, in this case the left camera. On the other hand, the extrinsic parameters define the position of the camera (X_A, Y_A, Z_A in Fig. 3.2). Hence if both the intrinsic and the extrinsic parameters are defined, the absolute pose of the line can be defined. If a second camera is available a second line can be defined and the position of the point P in 3D can be accurately recovered by the intersection of the two rays. For this reason, to recover a point from image, it has to be observed at least by two images taken from different points of view. We call the distance between the cameras *baseline*.

The processing of a stereo pair consists first on determining the matches, i. e. what point of the left image (u_L, v_L) corresponds with a point of the right image (u_R, v_R). Then from the calibration, the corresponding projection rays are defined, and the position of the corresponding point is recovered. For a given camera resolution, the accuracy of the 3D measurement depends on the angle

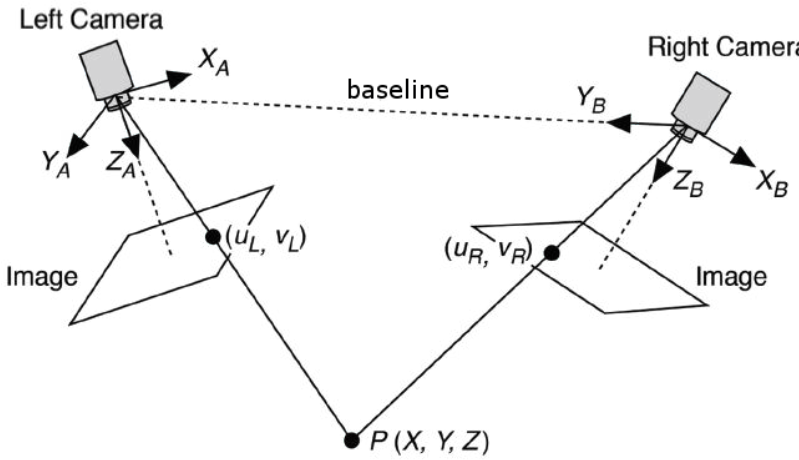

Figure 3.2: Stereoscopic vision approach.

between the two rays, which usually takes the name of *parallax*. The closer to 90 degrees the parallax is, the more accurate becomes the reconstruction. A second factor on the accuracy is the distances of the cameras to the scene, for a given parallax, the closer the camera to the scene, the more accurate the reconstruction is. The full scene to be measured has to be included in the image, in our case the specimen, what imposes the limit in the minimal distance of the cameras to the scene. As a result, the optimal configuration is cameras optical axes in a 90 degrees, and as close to the specimen as possible but observing the full specimen.

The intrinsic parameters of each camera are estimated previous to the experiments by the calibration, following the standard method of the planar pattern (Bouguet, 2011). The extrinsic parameters are estimated by the observation of coded fiducials in the scene, in our case the 20 coded markers fixed on the table in both sides of the specimen (Fig 3.3).

So far how to process an image pair has been described. Additionally, the observed points have to be tracked along the two synchronized sequences, in order to have available the evolution of the 3D point in time. The tracking of the

fiducials allows to accurately align the reconstructions produced by each stereo pair.

Therefore, in this Chapter an approach is proposed in which a discrete collection of points is tattooed on the external abdominal surface. These points can be safely matched across the stereo pair and tracked along the sequence. Resulting in a set of points of the surface tracked along the deformation what eases the comparison with the FE computations. There are other computer vision methods that can produce dense scene reconstruction (Scharstein and Szeliski, 2002), however in our case the skin surface has a poor texture what can reduce the reliability. More importantly, the texture severely changes when the abdomen deforms, what makes the tracking along the sequence less reliable.

The main drawback of this approach is that only points imaged on the two cameras can be reconstructed, what impedes detecting points close to the back of the specimen. It can alleviated with the addition of more synchronized cameras, virtually any number of cameras, however it comes at the expense of proportional increase in the cost of the experimental setup.

3.3 Material and methods

In vivo mechanical tests were performed in conjunction with imaging methods so that strain information could be obtained from the tissue in a non-invasive way. *In vivo* experiments consisted on the insufflation of carbon dioxide (pneumoperitoneum) into the abdominal cavity by laparoscopy, a technique largely used in hernia surgery, while observing the abdomen deformation with a stereo pair of digital cameras. The protocol here implemented was carried out on an animal model, specifically on New Zealand rabbits, species frequently used as an animal model in the study of surgical hernia repair (Bellón et al., 1996; LeBlanc et al., 2002; Hernández et al., 2011).

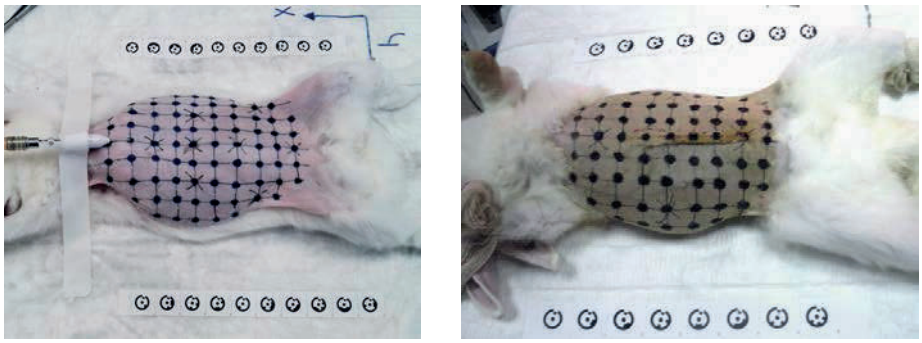

(a) Healthy animal. (b) Herniated animal.

Figure 3.3: Specimen preparation for the recorded pneumoperitoneum test. A tattooed grid was realized on the wall of the rabbit.

3.3.1 Specimen preparation

For the realization of this study, four New Zealand rabbits were subjected to several pneumoperitoneum tests. Animals were obtained from the Animal Experimentation Service of the Research Support Services of the University of Zaragoza, with an average weight ranged from 2 to 2.3 kg. They were housed singly, and were watered and fed a standard chow diet ad libitum (Finished feed n. 511; Food Corporation Guissona S.A., Lleida, Spain). Animals were healthy and free of clinically observable diseases.

Previously to the procedure, they were kept under stable conditions of light and temperature following the recommendations given by the Guide for the Care and Use of Laboratory Animals of the National and European Institutes of Health (Spanish Law 32/2007, Spanish Royal Decree 1201/2005, European Directive 2010/63/UE and European Convention of the Council of Europe ETS123). All procedures were carried out under Project Licence 01/11 approved by the in-house Ethics Committee for Animal Experiments of the University of Zaragoza.

Experiments were divided into two groups. The first group was compound by two healthy specimens while the second group was compound by two her-

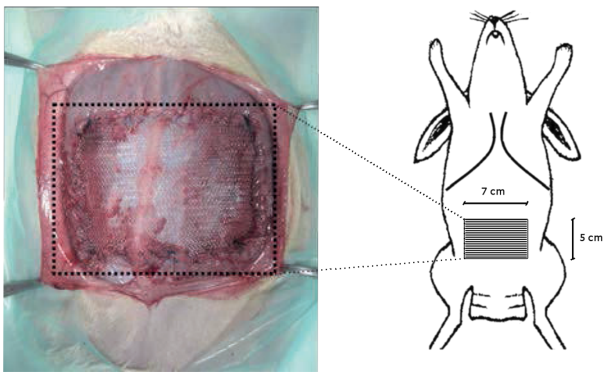

Figure 3.4: Defect on the abdominal wall repaired with a synthetic mesh and location on the specimen.

niated animals with a surgical mesh previously implanted (see Fig. 3.3). Animals were intramuscularly anaesthetized with a mixture of medetomidine (0,14 mg/kg, Medeson ®; Uranovet, Barcelona, Spain), ketamine (20 mg/kg, Imalgene 1000®; Merial Laboratorios S.A., Barcelona, Spain) and butorphanol (0.3 mg/kg, Torbugesic®; Fort Dodge Veterinaria S.A., Girona, Spain).

The hernia disease consisted on a total defect on the abdominal wall encompassing all abdominal layers (muscles, fascias and parietal peritoneum) and being replaced and repaired with a high density, non-absorbable surgical mesh made by polypropylene (*Surgipro*^{TM}, Covidien) with the size of 5x7 cm (see Fig. A.2). Tissue-mesh attachment was conducted by a continuous 4-0 polypropylene suture interrupted in the implant angles. This mesh was inserted one week before the pneumoperitoneum tests and its location on the animal is indicated in Fig. A.2. Skin was closed with a 2-0 polypropylene suture. Once the wound was closed, the visible scar was a 100-mm incision along the linea alba direction (see Fig. 3.3. b).

Before the test, specimens were cropped from front to rear legs in order to clear the visibility of the external abdominal cavity. Animals were placed over the surgical table in supine position, with the legs fixed to the table and the abdominal surface completely exposed. This surface was spotted with black points

which were used as fiducial markers to be tracked during the experiment. Fiducial markers had an average diameter of 8 mm and covered an almost diamond-shaped useful area of 100 cm^2. Coded targets were also added to the surgical table to define a reference for the 3D location estimates. Adding these coded markers ensures that 3D measurements correspond to the very same abdominal points along the whole range of pressures. Final setup is shown in Fig. 3.3.

3.3.2 Camera preparation

Procedure was recorded by a synchronized stereo rig, composed by two Prosilica GT1290 cameras with a Sony ICX445 EXview HAD CCD sensor. Image sequences were black and white having a 1280x960 resolution at a 5 fps frame rate stored in raw format to avoid compression losses.

The stereo rig was situated over the specimen so that both cameras were able to cover all the abdominal surface exposed. This was specially significant since 3D location estimates can be provided only for those points imaged in both cameras. Another determining factor was the parallax, which makes reference to the angle formed between cameras position in relation to the observed marker. In order to minimise the measurement error, this angle has to be as closer as possible to 90°, which is practically the value achieved in the experimental setup for all the markers (see Fig. 3.5). A prior camera calibration was needed to establish the intrinsic parameters of the camera and its internal geometry. A planar pattern method similar to Bouguet (2011) was applied.

To quantify the accuracy of further 3D reconstruction, additional tests were performed on a table with a micrometric XYZ translation stage (see Fig. 3.6, Modular Translation Stages, Newport® M-460P Series). In them, cameras were tested using the same resolution, pixel binning and technical parameters of the inflation tests. Spatial configuration between cameras and object were also kept in order to faithfully reproduce the conditions of animal experiments. These additional tests established an accuracy in the measurement method of 1 mm.

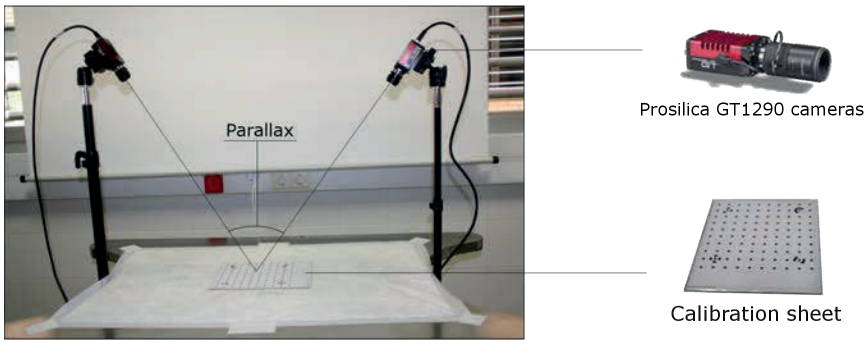

Figure 3.5: Cameras arrangement during the experiment.

3.3.3 Testing procedure

Once the animal and cameras were prepared, a Veress needle was inserted in the upper abdomen and fixed to a external reference. This needle was used for introducing carbon dioxide inside the cavity and was selected instead of the trocar for being considered less invasive during the experiment. In addition to this, a Standard Karl Storz endoscope was utilized for the gas supply. The whole setup is indicated in Fig. 3.7.

The experiment consisted on conducting a pneumoperitoneum in the abdominal cavity of the animal with carbon dioxide in a controlled manner, so that the deformed shape corresponding to determinate levels of pressure could be identified and extrapolated from the video. During the experiment, animals were kept alive but completely anesthetized. They were not intubated or ventilated, in order to not to modify the pressure level measured. The heart was beating with small rate, but blood pressure was considered irrelevant in terms of mechanical response of the wall.

Three tests were performed on the same specimen, returning to the zero pressure state after each test. To ensure that, pressure value inside the cavity was checked using a Fiber Optic Pressure sensor (Opsens®). The sensor was introduced in the opposite side of the cavity, at initial and final moment of the pro-

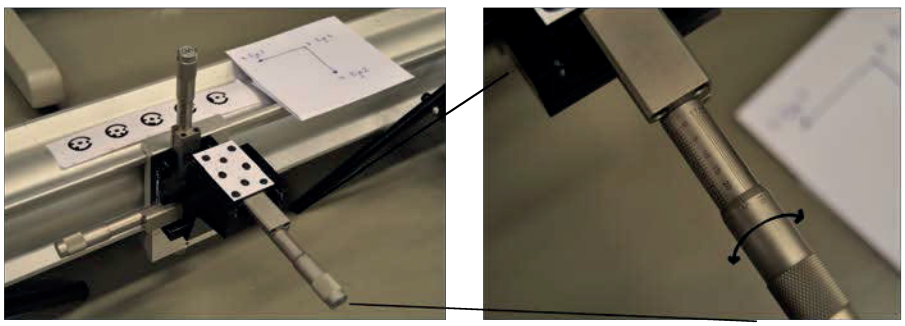

Figure 3.6: Micrometric table used to assess the accuracy of the experimental arrangement. On the right, detail of the micrometer.

cedure. First test of the same specimen was excluded from the study due to the preconditioning, so two tests per specimen were selected for the analysis of the results. A total of four pneumoperitoneum tests were analysed for each group, healthy and herniated rabbits.

During the experiment, the endoscope insufflated carbon dioxide increasing the inner pressure of the abdominal cavity from 0 to 12 mmHg, according to the human values commonly used in laparoscopy. In order to obtain data along the experiment the addition was carried out in 12 steps, one per mmHg, so the cameras could get images from determinate levels of pressure. In the cases conducted on herniated animals only 6 steps were able to be performed, obtaining pressure and frames data each 2 mmHg.

3.3.4 Data postprocessing

The digital photogrammetry PhotoModeler (2013) was used for processing the images. From the recorded video, a stereo pair of frames was selected for each level of pressure and these frames were post processed to estimate the 3D coordinates of the fiducial markers over the abdominal surface and over the surgical table.

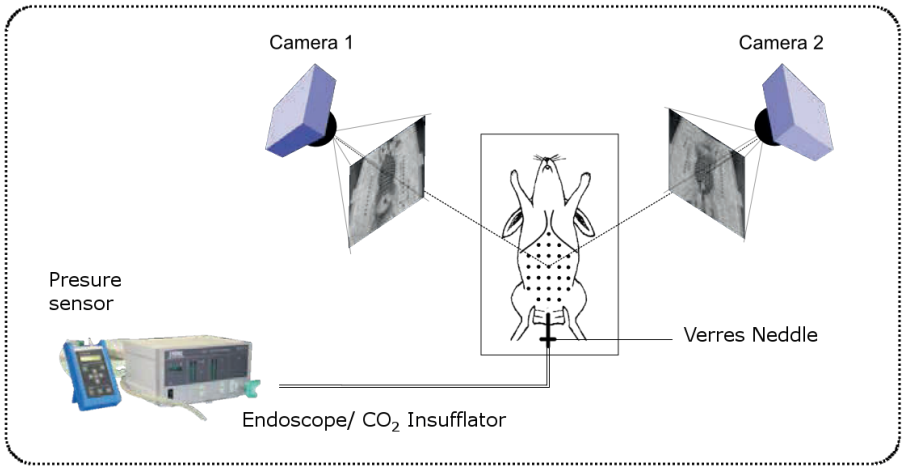

Figure 3.7: Experimental setup: the pneumoperitoneum was created in the abdominal cavity while two synchronized cameras recorded the volume change. Carbon dioxide was controlled by an endoscope with a pressure sensor in the end.

With these process, the aim was not only to obtain the 3D locations of the points for different levels of pressure, but also to calculate their variation (displacements) along the test.

A total of 43 points from the abdominal surface were tracked for the analysis of the results. The three-dimensional coordinates were therefore used to evaluate the displacements of those points, as well as to develop a 3D model of the cavity based on the reconstruction of the geometry for different pressures. From this model, principal radii of the surface were estimated using the 3D modelling software Rhinoceros (Rhinoceros, 2014).

3.4 Results

The abdominal wall response to the pneumoperitoneum test was analysed here, determining mechanical behavior from healthy specimen and those repaired with the $Surgipro^{TM}$ mesh. Longitudinal and transversal directions were also

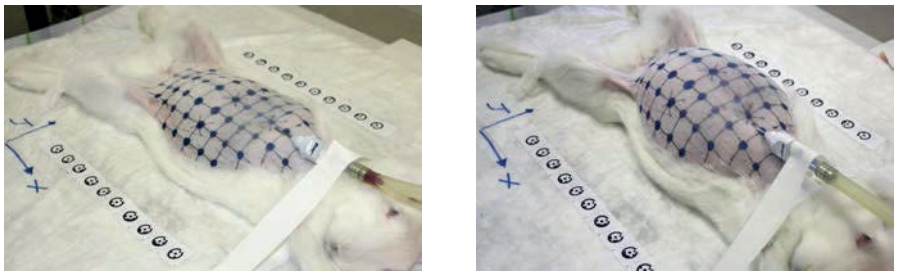

(a) $P = 0$ mmHg (b) $P = 12$ mmHg

Figure 3.8: Healthy animal in the initial (a) and final (b) instant of the inflation test.

distinguished during the post processing and sections in both directions were displayed to analyse the evolution with the pressure increase. Pressure-displacement curves of five main points of the surface were also constructed.

3.4.1 Response to the pneumoperitoneum tests

During the inflation test the abdomen shape changed from a flat cylinder to an ovoid contour, as can be seen in Fig. 3.8. In this figure, a healthy specimen is shown at the initial (a) and final (b) moment of the experiment. Tracking of points enabled to follow the evolution of abdominal displacement along the pressure increase. Inflation tests showed a maximum displacement of 42.3 mm in healthy animals and a significantly lower, 28.65 mm, in the case of animals repaired with the $Surgipro^{TM}$ high density mesh for $P = 12$ mmHg. Both values were measured at the black point corresponding to the center of the abdominal surface. The main component of the displacement was performed in the vertical direction, being the maximum value up to 2.5 mm in the X (longitudinal) direction for points on the lower abdomen, and 8 mm in the Y (transverse) direction for points on the side of the abdomen. A greater displacement was observed in points of the lower abdomen, towards the rear legs, rather than points of upper abdomen, closer to the head and front legs. This difference probably lies in the limiting effect of the rib cage that prevents the upper abdomen from a severe deformation.

All the experiments run in a comparable way showing the maximum gradient of deformation during the first half of the test. However, it was noted that the first test performed on the same specimen was fully different from the following. In this first test gas was inserted without causing an increase of pressure in the beginning, and the amount of gas needed to appreciate visible changes on the abdominal cavity was much greater than in the following tests. From the second experiment onwards, tests showed similar and reproducible behavior. Due to this, the first test on every specimen was considered preconditioning and was excluded from the study.

3.4.2 Pressure-Displacement curves

Aiming to parse the mechanical response of the abdominal wall, five main points were studied and compared in depth, corresponding to the central, sides, upper and lower zones of the abdominal surface (see Fig. 3.9(a)). Pressure-displacement curves for these points with mean and standard deviation of the four tests performed are shown in Fig. 3.9(b) and Fig. 3.10(b) for healthy and herniated animals respectively. In these figures, horizontal axis refers to the inner pressure reached in the abdominal cavity and vertical axis plots the displacement of each point, calculated from the coordinates transformation in the three principal axis.

Greater values of displacement for higher levels of pressure were observed in healthy animals rather than animals with the $Surgipro^{TM}$ mesh inserted. Specifically, a reduction of almost 30% was observed in points of maximum displacement between healthy and herniated cases (e.g. Point 2), while the value kept similar in points closer to the upper legs (e.g. Point 1). Considering these curves, it is also evident that the pressure-displacement relation for abdominal wall is not linear. At low pressures, muscle deformed much more than at high pressures, when the tissue got more rigid and the strain increment was much smaller.

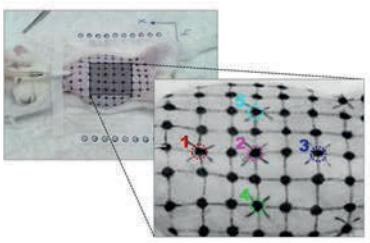

(a) Reference points of the surface.

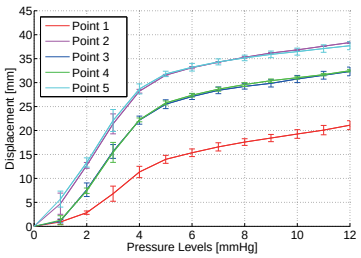

(b) Pressure-Displacement curves. Mean and standard deviation of healthy specimens.

Figure 3.9: Pressure-Displacement curves for main points of the healthy abdominal surface.

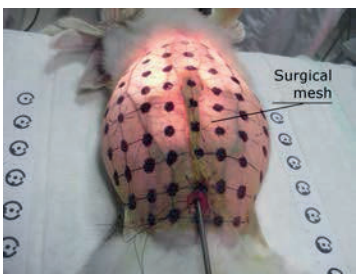

(a) *Surgipro*^{TM} mesh location inside the herniated animal.

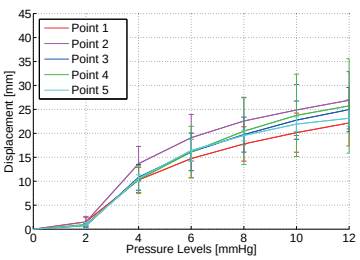

(b) Pressure-Displacement curves. Mean and standard deviation of herniated specimens.

Figure 3.10: Pressure-Displacement curves for main points of the herniated abdominal surface repaired with *Surgipro*^{TM} mesh.

In Fig. 3.10(a), the exact place where the surgical mesh was inserted is appreciated. According to the pressure-displacement curves the presence of the mesh provoked an increase of stiffness in the lower zone of the abdomen, where the mesh was inserted. This implies a smaller deformation of the muscle and therefore, a lower dispersion on the displacement values for different points of the surface. As a result, curves from Fig. 3.10(b) remain closer together than in the case of healthy animal, Fig. 3.9(b).

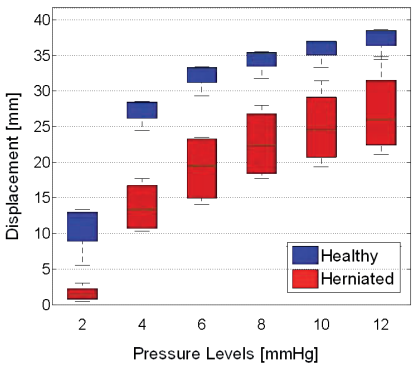

Figure 3.11: Displacements of the central point of the abdominal surface (point 2 in Fig. 3.9 (a)). Comparison between results of healthy and herniated specimens repaired with $Surgipro^{TM}$.

Fig. 3.11 compares the displacement obtained for the central point of the surface (Point 2) for both groups of animals, healthy and herniated repaired with $Surgipro^{TM}$ mesh. For that, means and standard deviations are displayed. The effect of rigidity due to the mesh presence is visible here, where the herniated line kept below the healthy one in all pressures.

3.4.3 3D Reconstructions

Based on the three-dimensional coordinates obtained from video frames along the experiment, a reconstruction of geometry was carried out for some levels of pressure, P = 0, 3, 6, 9 and 12 mmHg (see Fig 3.12(a)). For these reconstructions coordinates of the points were respected, and a smooth surface passing through the points was generated with the help of the modelling software Rhinoceros (Rhinoceros, 2014). The rest of the model was generated manually taking account geometrical considerations of the animal and the animal-table set in the experimental set-up.

Sections in both principal directions, longitudinal and transverse plane, were

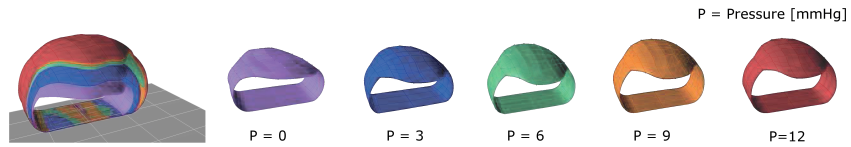

(a) 3D reconstructions according to the pressure level.

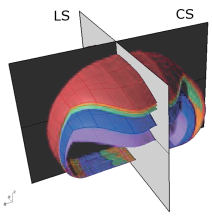

(b) Geometry sections.

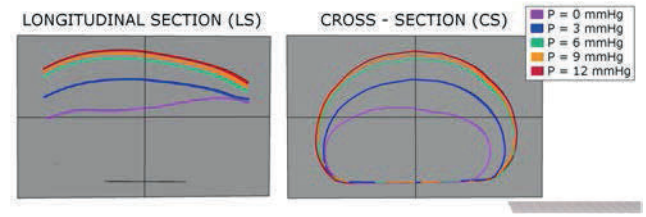

(c) Progress of the Longitudinal and Cross-Section with the pressure. LS=Longitudinal Section. CS=Cross-Section

Figure 3.12: 3D reconstruction of the wall for different inflation pressures.

also performed on the reconstructed model (see Fig. 3.12(b)). In Fig. 3.12(c) the progress of these sections with the pressure is shown. According to these outlines, the cavity deforms the most during the first levels of pressure, reaching the $80-90\%$ of the total strain at $P = 6$ mmHg.

Principal radii of curvature were also estimated based on the three-dimensional model reconstructed for several levels of pressure (see Fig. 3.13(a)). The evolution of the radii throughout the carbon dioxide insufflation, i.e. pressure increase, is observed in Fig. 3.13(b). According to this, the curvature change in longitudinal direction was bigger than in transverse. Again, it becomes clear that the main change of the principal radii and therefore in the volume of the cavity happened during the first half of the experiment.

3.4.4 Stretching data in abdominal wall

Stretching values in principal directions were also studied in case of maximum pressure. Fig. 3.14 shows the segments along the sections where the elongation

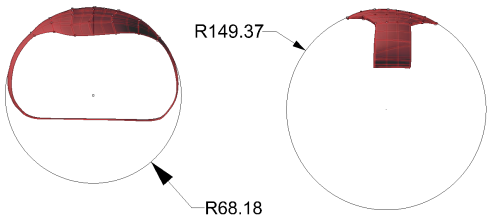

(a) Radio measurements (in mm) taken from the 3D model for P=12 mmHg.

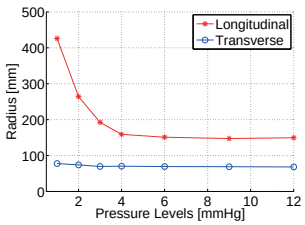

(b) Longitudinal and transverse radii vs. level of pressure.

Figure 3.13: Radii of curvature changes during carbon dioxide insufflation.

was analysed. This information was determined separately for healthy and herniated specimen repaired with $Surgipro^{TM}$, whose results are shown in Fig. 5.10 and Table 5.4 for the exact values.

For the transverse plane, results showed a greater elongation on segments of the side than in the center, which means that the tissue corresponding to the oblique muscles deformed much more than the rectus for the transverse direction. Same happened for herniated animals, although values obtained were lower than the healthy ones due to the high density mesh rigidity.

Similar results were found for the longitudinal plane, although quite cushioned. In this direction, segments situated closer to the legs (rear or front) stretched out slightly more than in the central zone, though the differences were small. This difference however was not found in the case of herniated animals, where the segments E and F deformed similar to the C and D, probably again due to the stiffening effect of the mesh.

Attending to the values obtained in Table 5.4, longitudinal direction (measured over the linea alba) seemed to be stiffer than the transverse direction (measured halfway on the abdominal surface). Differences between segments in each direction was explained taking account the rabbit anatomy. While longitudinal section was measured along the linea alba, where the junction between fascias and rectus abdominis lies moderately constant, cross-section goes through three different

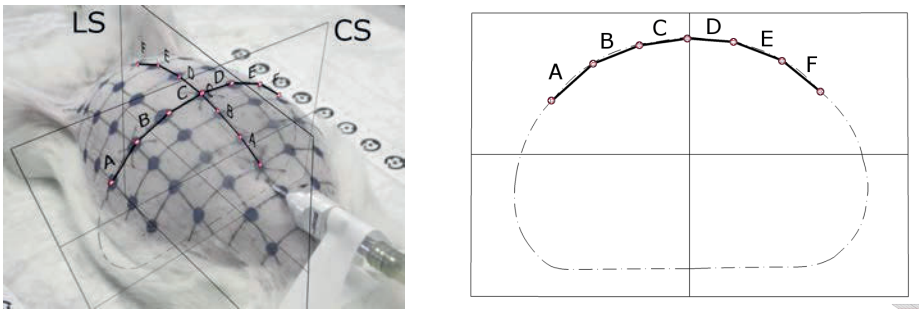

(a) Segments along the surface.

(b) Cross-Section detail.

Figure 3.14: Sections segments where the stretching was analysed.

Transverse	**A**	**B**	**C**	**D**	**E**	**F**
Healthy	22.41	20.33	3.23	3.01	15.42	19.85
Herniated	15.12	14.19	3.44	6.77	9.46	15.15
Longitudinal	**A**	**B**	**C**	**D**	**E**	**F**
Healthy	4.11	2.00	1.37	3.13	5.41	8.74
Herniated	4.03	6.25	2.89	1.54	2.97	2.39

Table 3.1: Mean stretching values for 12 mmHg in the transverse and longitudinal direction (%) according to the segments delimited in Fig. 3.14.

composite muscle layers: rectus abdominis (segments C & D), External-Internal composite (segments B & E) and External-Internal-Transversal composite (segments A & F) (Hernández-Gascón et al., 2011).

Lagrangian strain maps were also calculated from displacements of fiducial points. To do that, a rough mesh of quadrilateral elements was constructed over the abdominal surface where fiducial points worked as nodes of the mesh. This way, displacement of each point in the area was calculated from the nodal values, $\mathbf{u}^{nod}$, and the approximating functions of a bilinear quadrilateral, $\mathbf{N}(x, y)$, as $\mathbf{u}(x, y) = \mathbf{N}(x, y) \cdot \mathbf{u}^{nod}$. Lagrangian strain tensor $\mathbf{E}$ was calculated at Gaussian points in each quadrilateral element as

$$\mathbf{E}(x,y) = \frac{1}{2}[\mathbf{F}^T(x,y) \cdot \mathbf{F}(x,y) - \mathbf{I}] \tag{3.1}$$

where $\mathbf{F}$ is the deformation gradient tensor obtained when deriving the displacement field as $\mathbf{F} = \frac{\partial \mathbf{x}}{\partial \mathbf{X}} = \mathbf{I} + \frac{\partial \mathbf{N}}{\partial \mathbf{X}}\mathbf{u}^{nod}$.

General strain map is displayed in Fig.3.16(a) and strain in both principal directions, corresponding to the components $\mathbf{E_{11}}$ and $\mathbf{E_{22}}$ of the tensor $\mathbf{E}$, in Fig. 3.16 (b) and (c). Transversal components $\mathbf{E_{12}}$ and $\mathbf{E_{21}}$ of the tensor were close to zero which supports the hypothesis that the wall is working as a membrane, i.e., only in principal directions.

Stress values in principal directions were calculated using Laplace's Law and approximating the animal abdominal wall to an ellipsoidal shape, similar to a truncated rugby ball. Applying the same criteria in both principal directions, longitudinal and transversal stresses were estimated for each level of pressure and represented with regard to the stretching of the different segments along the sections (see Fig. 3.17).

3.5 Discussion

In the present work, *in vivo* mechanical behavior of abdominal wall was studied on an animal model. For that, several pneumoperitoneum tests were carried out on two groups of rabbits, composed of healthy specimens and herniated ones with a $Surgipro^{TM}$ high density mesh previously inserted. All experiments were recorded using a stereo system which enabled, by the postprocessing of the images, to extract three-dimensional coordinates of different points highlighted on the abdominal surface. Based on that information, the geometry of the cavity was successfully reconstructed for different levels of pressure. Pressure-displacement curves for reference points, principal radii of curvature and stretching in principal planes were also calculated.

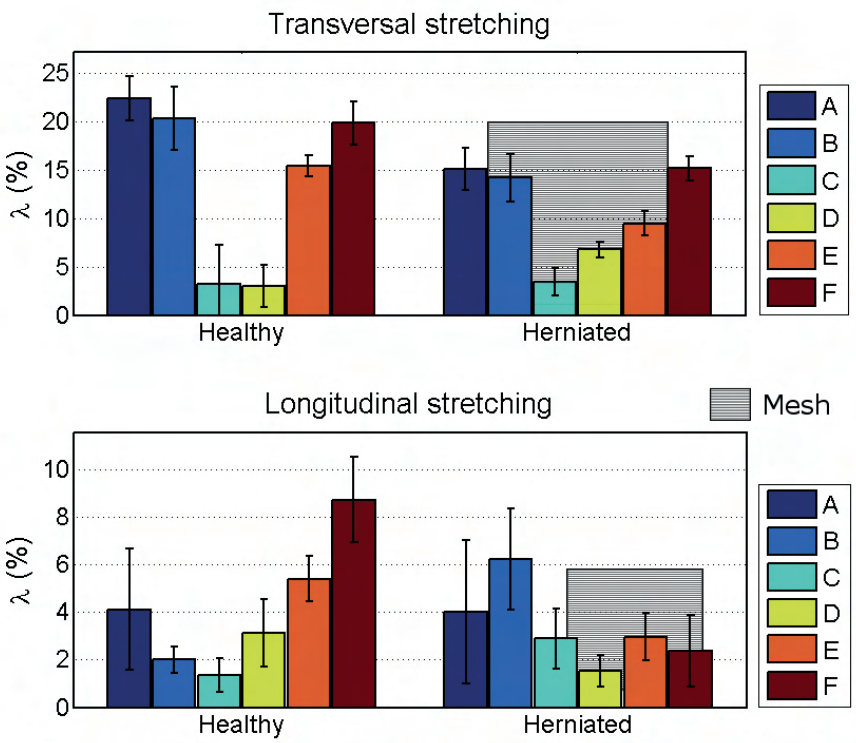

Figure 3.15: Mean and standard deviation of stretching values according to the segments delimited in Fig. 3.14. Exact values gathered in Table 5.4.

Experiments first showed differences between the initial inflation test performed on each specimen and the following. This may be related to a distribution of the gas inside the cavity, which contributed to squeeze internal organs before deforming the abdominal wall. These differences were also noted by Song et al. (2006), who associated this phenomenon to an unobserved internal reshaping in the form of diaphragm movement.

Pressure-displacement curves confirmed the strong nonlinear mechanical behavior when the whole abdominal wall is subjected to an inflation test. At low pressures, muscle deformed considerably for each level of pressure. At high pres-

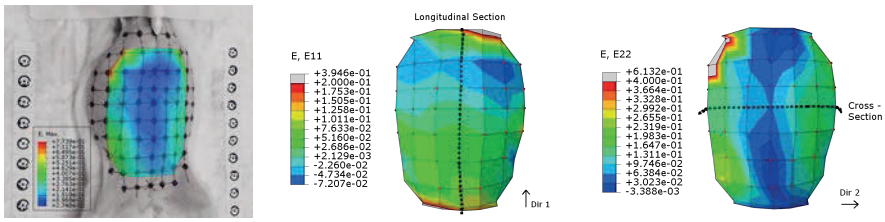

(a) Strain map along the abdominal surface. (b) Longitudinal direction. (c) Transversal direction.

Figure 3.16: Lagrangian strain maps on the abdominal surface of a healthy animal based on the fiducial points tracked.

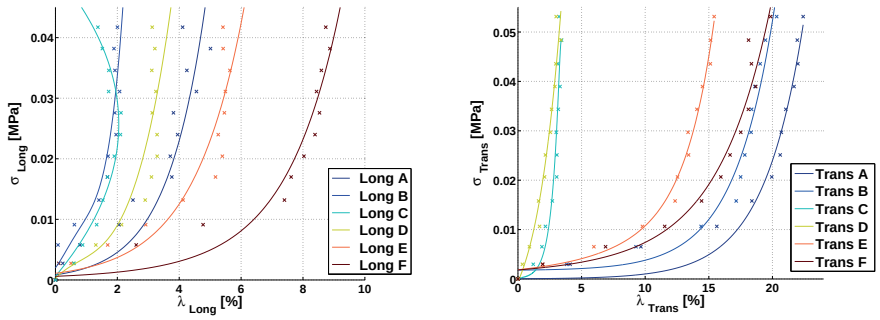

(a) Longitudinal direction. (b) Transversal direction.

Figure 3.17: Cauchy Stress-Strain relationship for both principal directions.

sures, the tissue got more rigid and the strain increment for each mmHg of pressure was much smaller (Fig. 3.9(b) and 3.10(b)). It was also shown in Fig. 3.13(b), when the main change of the principal radii happened during the first half of the experiment. This is associated with the fact that the abdominal muscles are considered an extracellular matrix with muscular and collagen fibers inserted, responsible for force generation and resistance of the tissue respectively. For low stresses collagen fibers present a wavy pattern which endows the tissue with a slight resistance, but it becomes more rigid when collagen fibers are oriented and stretched at higher pressures (Hernández-Gascón et al., 2011, 2012).

Differences between stretching of segments in each direction (see Table 5.4) were explained taking account the rabbit anatomy. The longitudinal section was measured along the linea alba, where the junction between fascias and rectus abdominis lies moderately constant and the small differences between stretching of the segments can be explained due to the changes in the stretch response of the linea alba along its length (Cooney et al., 2015). However, cross-section goes through three different composite muscle layers besides the linea alba: rectus abdominis (segments C & D), External-Internal composite (segments B & E) and External-Internal-Transversal composite (segments A & F) (Hernández-Gascón et al., 2011). The distinct mechanical response of these three composites could explain the differences of stretching founded between segments.

Attending to the effect of the surgical mesh on the mechanical behavior of the abdominal wall, in the case of the $Surgipro^{TM}$ mesh, the study showed a strong stiffening on the part of the surgical mesh which caused a decrease of deformation of the wall during the experiment. This stiffening was visible in Fig 3.11, where the herniated line kept below the healthy one in all pressure levels, and also in the stretching values gathered in Table 5.4. For herniated animals, values obtained in the transverse direction were lower than the healthy ones due to the high density mesh rigidity. Similar results were found for the longitudinal plane, but only in segments D, E and F, where the mesh was situated. It is also noticed that some regions showed a lower tissue stretching in healthy animals rather than the herniated ones. It could be that the presence of the mesh, which stiffens some segments (e.g. longitudinal segments D, E & F), leads in a pull to the adjacent segment (e.g. segment C) provoking an increase of stretching in this area.

Some authors have previously studied the mechanical response of abdominal tissue when it has been repaired with a surgical mesh. Podwojewski et al. (2013) reported that there were not significant differences in stiffness between intact specimens and repaired with a surgical mesh, but that was a polyester $Parietex^{TM}$ Composite, a synthetic mesh different from the $Surgipro^{TM}$ used here. Henández et al. (Hernández-Gascón et al., 2011, 2012) studied the mechanical behavior of the $Surgipro^{TM}$ mesh together with other synthetic surgical meshes and both

studies ended with the assumption that the $Surgipro^{TM}$ mesh leads to suppose an increase in stiffness. The methodology developed in this work was able to measure this stiffening in a complete non invasive way, and could be used with other meshes after surgery to determine if they are affecting the rigidity of the abdomen. This factor is important since it is directly related to the patient comfort.

According to the strain field measured over the abdominal surface, the longitudinal direction (measured over the linea alba) seemed to be stiffer than the transversal one (measured halfway on the abdominal surface). This fact may appear to be opposed to previous studies in abdominal muscle, but actually there is a great dispersion about this issue in literature and some differences should be explained. Hwang et al. (2005) agreed with this assumption in his work about canine abdominal muscles, which has a special relevance considering that is a quadruped animal case. Also Kirilova et al. (2011) and Martins et al. (2012) had the same results studying mechanical behavior of fascias and rectus sheaths respectively, but working on human samples and when each element was working alone.

On the other side, some authors (Förstemann et al., 2011; Tran et al., 2014; Podwojewski et al., 2014) found a higher compliance in the longitudinal than in the transverse directions when performing *in vitro* and *ex vivo* tests of the whole abdominal muscle samples of human. Similar results were found in Song et al. (2006) with the only *in vivo* experiment, according to author's knowledge, performed on abdominal human tissue. This disagreement could be explained considering that different types of species are being compared here, biped and quadruped animals, so that muscle elongations between them could differ due to the posture. Also Hernández-Gascón et al. (2011), who performed *in vitro* tests on different composite layers of abdominal rabbit muscle, proved a stiffer behavior in the transverse direction for all composites. Nevertheless, those tests were carried out until failure, which means a higher level of stress than the obtained in this study as physiological range ($\sigma \simeq 0.06MPa$). If strain values for physiological stresses are analysed in that study longitudinal reveals to be stiffer than the transversal direction, which is consistent with the findings observed in this work.

This experimental study is not exempt from some limitations. First of all, the number of specimens used for inflation tests should be increased in order to obtain a certain pattern to compare healthy and herniated animals. Different types of synthetic meshes could be tested, so the convenience of distinct materials, pore sizes or thread arrangement would be analysed. These both limitations (number of specimen and meshes) were solved in the Chapter 5 of this Thesis.

Regarding the measurement process, the number of cameras could be increased. This way the measured area along the abdominal wall would grow and the strain of the back muscles of the wall could also be studied. Besides, the post processing of the images needs to be automatized to speed up the obtainment of the 3D model. Finally, this measurement method should be tried on human tissue, since the main objective of this methodology is to be applied in hernia diseases on human beings.

4

Numerical FE simulation on the abdominal wall

In this Chapter, a numerical approach to the abdominal wall is preformed. Considering the 3D patient-specific geometry, obtained by photogrammetry (see Chapter 3), a finite element model was reconstructed in order to numerically simulate the experimental response of the tissue. By comparing the experimental and numerical results, mechanical properties of the abdominal wall may be estimated. Thus, considering the main features in the abdominal muscles three material models were selected to attempt to reproduce the mechanical behavior of the wall. As a first approach the response surface methodology (RSM) was

performed, which studies the relationship between variables in a problem and determines which explanatory variables affect the response variable(s) of interest. By using this method, a preliminary characterization of the wall was achieved assuming same mechanical response of the whole abdominal tissue.

In a next step, a second numerical approximation was applied. Considering one of the material models presented in the RSM, the Demiray's model dependent on two parameters, the experimental tests were reproduced allowing these parameters to vary along the abdominal surface. By assuming different values of the material parameters, an heterogeneous response of the abdominal tissue is expected. The optimal values of the model were obtained by an inverse analysis procedure, where experimental data was used as the input of the problem while material model remained as the solution.

4.1 Constitutive modelling

The passive and active finite strain response of the abdominal muscle is usually simulated within the framework of continuum mechanics. In this section, the main concepts about the constitutive modelling of the passive mechanical behaviour of skeletal muscles are presented.

4.1.1 Theoretical frame

According to the classic nonlinear continuum solid mechanics, given a three-dimensional solid determined by its coordinates in the reference system ($\mathbf{X}$), motion can be defined as the change of these coordinates in the initial state to a second and deformed state (Ogden, 2001). Considering $\mathbf{X}$ the coordinates of Ω_0 defined in the initial or reference configuration labeled φ_0, and $\mathbf{x}$ the coordinates of Ω_t defined in the actual or deformed configuration φ_t, the deformation gradient tensor $\mathbf{F}$ can be obtained as the quotient $\mathbf{F} = \partial\mathbf{x}/\partial\mathbf{X}$.

Based on this tensor, the Jacobian of the transformation J is calculated as $J = det(\mathbf{F})$ and provides a measure of the volume change suffered by the solid during the transformation. Additional measure of deformation is given by the right Cauchy-Green deformation tensor, defined as $\mathbf{C} = \mathbf{F}^T \cdot \mathbf{F}$. In order to avoid numerical problems due to the characteristic incompressibility present in soft tissues, the decomposition of the deformation gradient introduced by Flory (1961) and generalized by Simo and Taylor (1991) has been considered. This decomposition allows to rewrite the tensors $\mathbf{F}$ and $\mathbf{C}$ as follow

$$\mathbf{F} = [J^{1/3}\mathbf{I}] \cdot \overline{\mathbf{F}} \tag{4.1}$$

$$\mathbf{C} = [J^{2/3}\mathbf{I}] \cdot \overline{\mathbf{C}} \tag{4.2}$$

where J terms represent the volumetric part, that is the deformation caused by the volume changes, while the $\overline{\mathbf{F}}$ and $\overline{\mathbf{C}}$ correspond to the distortional (or isochoric) part of the decomposition which do not imply any change in volume.

Since abdominal muscles are composed by different types of fibers, it is necessary to distinguish between collagen fibres, which are mainly responsible for the passive mechanical response, and muscular fibres, which are associated with the contractile muscle behaviour. Moreover, muscular and collagen fibres are frequently not aligned in the same direction (Hernández-Gascón et al., 2011; Linden, 1998). The direction of collagen fibres is assumed to determine the direction of material anisotropy in order to study the passive behaviour of the tissue (Arruda et al., 2006), whereas muscle fibres have to be considered in the modelling of the active behaviour. Thus, the anisotropy of a point $\mathbf{X} \in \Omega_0$ is associated with the active and passive responses, is described by unit vectors $\mathbf{m}_0 \cdot \mathbf{X}$ ($|\mathbf{m}_0| = 1$) and $\mathbf{n}_0 \cdot \mathbf{X}$ ($|\mathbf{n}_0| = 1$), respectively. In this work only passive response was considered, so families defined in the general description of the constitutive model only refer to possible collagen fiber families.

According to the existing literature (Spencer, 1954), in order to characterize an isotherm process in reversible materials is common to postulate the existence of an unique strain energy function Ψ. Attending to the case of the *passive hyperelastic tensorial response*, this function is dependent on the deformation tensor $\mathbf{C}$ and the structural tensors that define the direction of the fiber families contained in the tissue (Weiss et al., 1996; Holzapfel, 2000). Similarly to the deformation tensors $\mathbf{F}$ y $\mathbf{C}$, the strain energy function may be written in the decoupled form

$$\Psi(\mathbf{C}, \mathbf{M}, \mathbf{N}) = \Psi_{\text{vol}}(J) + \overline{\Psi}(\overline{\mathbf{C}}, \mathbf{M}, \mathbf{N}) \tag{4.3}$$

where $\mathbf{M}$ y $\mathbf{N}$ are structural tensors associated to the anisotropy, that in this case correspond to the collagen fiber families (Linden, 1998; Jenkyn et al., 2002; Odegard et al., 2008). The strain energy function Ψ may be also written in terms of nine strain invariants dependent of the tensors $\overline{\mathbf{C}}$, $\mathbf{M}$ and $\mathbf{N}$ (Valanis and Landel, 1967; Holzapfel, 2000), resulting

$$\Psi(\mathbf{C}, \mathbf{M}, \mathbf{N}) = \Psi_{\text{vol}}(J) + \overline{\Psi}(\overline{I}_1, \overline{I}_2, \overline{I}_4, \overline{I}_5, \overline{I}_6, \overline{I}_7, \overline{I}_8, \overline{I}_9) \tag{4.4}$$

with Ψ_{vol} and $\overline{\Psi}$ correspond to the volumetric and isochoric contributions of the strain energy function respectively. The terms $\overline{I}_1$ and $\overline{I}_2$ are the first and second strain invariants of the symmetric modified Cauchy-Green tensor $\mathbf{C}$. The rest of invariants, $\overline{I}_4$ to $\overline{I}_9$, are related to the anisotropy associated to the fibers. $\overline{I}_4$ and $\overline{I}_6$ have a clear physical that define the square of the fibers length. On the other hand, $\overline{I}_5$, $\overline{I}_7$, $\overline{I}_8$, $\overline{I}_9$ refer to transversal strain of fibers ($\overline{I}_5$, $\overline{I}_7$) and interaction between them ($\overline{I}_8$, $\overline{I}_9$). Regarding the fiber families above described the invariants mas be defined as

$$\begin{aligned}
&\overline{I}_1 = tr\overline{\mathbf{C}}, \quad \overline{I}_2 = \frac{1}{2}((tr\overline{\mathbf{C}})^2 - tr(\overline{\mathbf{C}})^2) \\
&\overline{I}_4 = \mathbf{m}_0 \cdot \overline{\mathbf{C}} \cdot \mathbf{m}_0, \quad \overline{I}_5 = \mathbf{m}_0 \cdot \overline{\mathbf{C}}^2 \cdot \mathbf{m}_0, \quad \overline{I}_6 = \mathbf{n}_0 \cdot \overline{\mathbf{C}} \cdot \mathbf{n}_0 \\
&\overline{I}_7 = \mathbf{n}_0 \cdot \overline{\mathbf{C}}^2 \cdot \mathbf{n}_0, \quad \overline{I}_8 = \mathbf{m}_0 \cdot \overline{\mathbf{C}}\mathbf{n}_0, \quad \overline{I}_9 = (\mathbf{m}_0 \cdot \mathbf{n}_0)^2
\end{aligned} \tag{4.5}$$

However, due to the strong correlation of $\overline{I}_5$ and $\overline{I}_7$ to $\overline{I}_4$, $\overline{I}_6$ respectively, and considering that interaction between families is not usually included, $\overline{\Psi}$ is commonly simplify as a function of $\overline{I}_1$, $\overline{I}_2$, $\overline{I}_4$ and $\overline{I}_6$.

The tensional response is obtained by applying the Clausius-Plank inequality to the strain energy function Ψ, so that the second Piola-Kirchhoff stress tensor $\mathbf{S}$ remains defined as

$$\mathbf{S} = \frac{2 \cdot \partial\Psi(\mathbf{C}, \mathbf{M}, \mathbf{N})}{\partial \mathbf{C}} = Jp\mathbf{C}^{-1} + 2\frac{\partial\overline{\Psi}(\overline{\mathbf{C}}, \mathbf{M}, \mathbf{N})}{\partial \mathbf{C}} = \mathbf{S}_{\text{vol}} + \overline{\mathbf{S}} \tag{4.6}$$

In this equation the first addend corresponds to the volumetric part $\mathbf{S}_{\text{vol}}$, where hydrostatic pressure p may be defined as $p = \frac{d\Psi_{\text{vol}}(\mathrm{J})}{d\mathrm{J}}$ for quasi-incompressible material, and the second addend is the modified Piola-Kirchoff tensor $\overline{\mathbf{S}}$. Based on this tensor, the Cauchy stress tensor $\boldsymbol{\sigma}$ can be obtained by applying $1/\mathrm{J}$ times the *push forward* operation of $\mathbf{S}$, i.e. $\boldsymbol{\sigma} = J^{-1}\boldsymbol{\chi}_*(\mathbf{S}) = J^{-1}\mathbf{F}\mathbf{S}\mathbf{F}^T$.

The linearization of the constitutive equations is required for the numerical solution of the nonlinear problem by means of the Newton method. Differentiating Eq. 4.6 with respect to $\mathbf{C}$ leads to the material elasticity tensor $\mathbb{C}$.

$$\mathbb{C} = 2\frac{\partial\mathbf{S}(\mathbf{C})}{\partial\mathbf{C}} = 2\frac{\partial\mathbf{S}_{\text{vol}}}{\partial\mathbf{C}} + 2\frac{\partial\overline{\mathbf{S}}}{\partial\mathbf{C}} \tag{4.7}$$

To obtain the elasticity tensor in the spatial representation, denoted as $\mathbf{c}$, it is necessary to apply the *push forward* to the tensor $\mathbb{C}$ multiplied by a factor of J^{-1}, i.e. $\mathbf{c} = J^{-1}\boldsymbol{\chi}_*(\mathbb{C})$ (Holzapfel, 2000).

4.1.2 Selection of hyperelastic material models

Since stress tensors of an hyperelastic material model are derived from the strain energy function Ψ, the selection of a determined mathematical form for Ψ will directly condition the mechanical response of the material. In literature, there is a wide range of constitutive models frequently employed to describe the mechanical behavior of soft tissues, such as tibialis anterior muscle (Davis et al., 2003), ligaments (Calvo et al., 2008), arterial wall (Holzapfel et al., 2000) or cornea (Nguyen and Boyce, 2011) among others. The selection of a specific type of model is conditioned by the features of the soft tissue under examination, in this case abdominal muscles.

As described in Chapter 1, abdominal muscles are known for the wavy pattern typical of the collagen fibers that confers a strong non linear behavior to the tissue. Other determinant factors are that abdominal wall suffers large deformations and that due to the high water content present in the muscle (around 60%-70% on weight), it can be considered almost incompressible. Finally, although each muscle layer shows an anisotropic response when is studied isolated (Hernández et al., 2011), further studies has shown that the behavior approaches to isotropic when the whole tissue, compound by all muscle layers, skin and other components, are analyzed together (Hernández-Gascón et al., 2013).

Taking these tissue characteristics into account, several types of quasi-incompressible isotropic hyperelastic material models were considered in this Thesis for the numerical analysis.

- **Demiray model**

  Proposed by Demiray in the seventies and refined in the eighties (Demiray,

1972, 1981; Demiray et al., 1988), this exponential material law assumed that biological materials to be elastic, homogenous, isotropic and quasi-incompressible. The constitutive law is only function of the first invariant I_1.

The strain energy function (SEF) is dependent on two material parameters, D_1 and D_2, and it can be written as

$$\Psi = \Psi_{\text{vol}} + D_1[\ \exp\ (D_2(\overline{I}_1 - 3)) - 1] \tag{4.8}$$

- **Holzapfel-Gasser-Ogden model**

  This exponential model (HGO), fully explained in Holzapfel (2000); Gasser et al. (2006), was originally applied to the arterial walls and subsequently extended to other materials reinforced with two fiber families. A general description of the strain energy function may be the following

$$\begin{aligned}\Psi = \Psi_{\text{vol}} + C_{10}(\overline{I}_1 - 3) + \\ \frac{k_1}{2k_2}\sum_{\alpha=1}^{N}\left[\exp[k_2(\kappa(\overline{I}_1 - 3) + (1 - 3\kappa)(\overline{I}_{4(\alpha\alpha)} - 1))^2] - 1\right]\end{aligned} \tag{4.9}$$

  where $\overline{I}_1$ and $\overline{I}_4$ are strain invariants associated to the isotropic and anisotropic response of the tissue respectively. In this equation, N is the number of fiber families present in the material and κ is related to the level of dispersion in the fiber directions. When this factor takes the value of $\kappa = 1/3$ the contribution of $\overline{I}_4$ becomes invalidated. In this case, the fibers are considered to be randomly distributed and the material becomes isotropic, remaining the SEF as

$$\Psi = \Psi_{\text{vol}} + C_{10}(\overline{I}_1 - 3) + \frac{k_1}{2k_2}[\ \exp\ (k_2(\overline{I}_1 - 3)^2) - 1] \tag{4.10}$$

  In this Thesis, the isotropic adaptation of the HGO model dependent on three parameters (C_{10}, k_1 and k_2) has been applied.

- **Yeoh model**

  The Yeoh model (Yeoh, 1993) is a particular case of a polynomial form of the strain energy function that together with other polynomial models (Mooney-Rivlin, Neo-Hookean, etc) have been frequently used to describe isotropic materials as rubber-like materials. The Yeoh model has also been called the reduced polynomial model, since it is used to describe nearly incompressible materials and therefore it only depends on the first invariant. The particular form on the SEF used in this work is the following

$$\Psi = \Psi_{\text{vol}} + C_{10}(\overline{I}_1 - 3) + C_{20}(\overline{I}_1 - 3)^2 + C_{30}(\overline{I}_1 - 3)^3 \tag{4.11}$$

  dependent on three material parameters C_{10}, C_{20} and C_{30}.

- **Veronda-Westman modified model**

  The last constitutive law considered for the numerical analysis is the Veronda-Westman model (Veronda and Westmann, 1970). This exponential model is almost equivalent to the Demiray's model, denoting only minor differences in the material parameters influences, and it has been widely applied to soft tissues (Kauer et al., 2002; Oberai et al., 2009; Goenezen et al., 2011). The strain energy function is given by

$$\Psi = \Psi_{\text{vol}} + \frac{\mu}{2\gamma}[\exp\gamma(\overline{I}_1 - 3) - 1] \tag{4.12}$$

  The Veronda-Westman model is dependent on two parameters, the shear modulus at zero strain μ and the non linear parameter γ, both with distinct physical interpretations: μ governs the small strain behavior independent of the value of γ, while γ controls the exponential stiffening. To observe the respective roles of these two parameters a sensitivity analysis with biaxial tension was performed. Fig. 4.1 the Cauchy stress-stretch curves shows the influence of each parameter: variation of μ (Fig. 4.1 (a)) and variation of γ (Fig. 4.1 (b)). The response becomes more rigid with the increasing values of γ and μ.

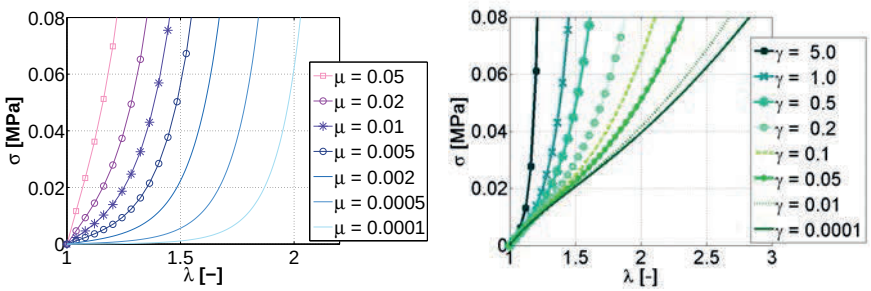

(a) Cauchy stress vs stretch for $\gamma = 1$ (b) Cauchy stress vs stretch for $\mu = 0.01MPa$

Figure 4.1: Effect of the material parameters in the Veronda-Westman model.

4.2 Response surfaces methodology

The response surfaces methodology (RSM) was introduced in 1951 by Box and Wilson (1951) and originally focused on the statistics area. However, since then this methodology has been widespread and applied to other a priori different fields, such as food distribution chain, titanium dioxide films or analytical chemistry (Giovanni, 1983; Tien and Lin, 2006; Bezerra et al., 2008).

RSM basically explores the relationships between variables in a problem (or equation), trying to determine how the variables affect the response of the problem. This methodology uses quantitative data from appropriate experimental designs, and solve multivariate equations that can be graphically represented as response surfaces. These surfaces describe in a visual way how the test variables affect the response, which facilitates the initial understanding and dissemination of the problem. Moreover, it may provide information on the interrelationships among the test variables or describe the combined effect of all test variables on the response.

As seen in the prior section, the mechanical response of each material model is subject to the mathematical form of the strain energy function and the value of the material parameters. Unfortunately, the variables that provoke a mechanical

response close to the obtained during the experimental part of the abdominal tissue, remain unknown. The RSM was used in this work to determinate their optimal value, it means the combination of parameters for each material model that better reproduces the experimental deformation.

To quantify how good the numerical approach was, an objective function was defined. In this aspect, the estimator chosen as objective function consisted on the mean square error (MSE) defined as

$$MSE = \sqrt{\frac{1}{n_p}\frac{1}{n_k}\sum_{i=1}^{n_p} w_i \sum_{k=1}^{n_k}(e_k^i)^2} \tag{4.13}$$

where n_k is the number of study points taking into account in the abdomen to calculate the MSE, n_p the number of pressure levels where the error was evaluated and w_i the weight given to each pressure level to normalized the error value. The individual error committed for each study point was denoted by e_k and it can be defined as

$$e_k = \sqrt{(u_{num}^k - u_{exp}^k)_x^2 + (u_{num}^k - u_{exp}^k)_y^2 + (u_{num}^k - u_{exp}^k)_z^2} \tag{4.14}$$

For the three material models (Eq. 4.8, Eq. 4.9 and Eq. 4.11), a total of 500 simulations were performed. For each case, a random combination of the material parameters was assumed, resulting in a different deformed shape for each simulation. The MSE (defined as Eq. 4.13) was therefore calculated for each combination. A general scheme of the process is explained in Fig. 4.2. The parameter combination that led in a minimum MSE was considered to be the optimal value to reproduce the experimental behavior.

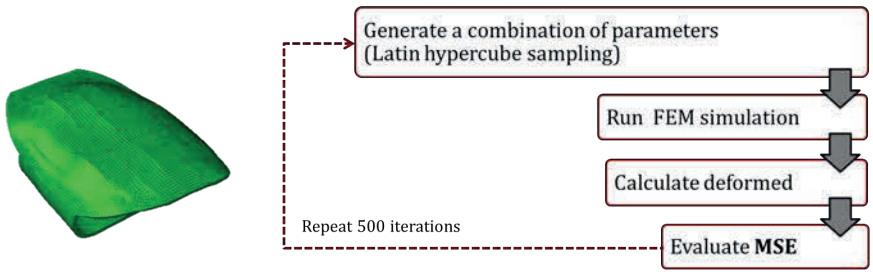

Figure 4.2: Response surfaces methodology followed in this Chapter.

SEF	**Fixed**	**Variable**	
Demiray	-	$D_1 = [0 - 0.01]MPa$	$D_2 = [0.7 - 10][-]$
HGO	$C_{10} = 5 \cdot 10^{-3} MPa$	$k_1 = [0 - 0.01]MPa$	$k_2 = [20 - 2000][-]$
Yeoh	$C_{20} = 1 \cdot 10^{-4} MPa$	$C_{10} = [0 - 0.01]MPa$	$C_{30} = [0 - 0.1]MPa$

Table 4.1: Variation range of the material parameters for the three constitutive models analyzed.

The graphical representation of the solution when it is dependent on two parameters, can be given by a three dimensional surface plotted on cartesian axis, as shown in Fig. 4.3. When there are more than two parameters involved the graphic representation becomes more problematic. In the reference system of Fig. 4.3, the X and the Y axis represented the value of the material parameters while the third axis measured the MSE. For each simulation one point was plotted on the reference system up to a total of 500 points. Then a surface was interpolated through the points by using the MATLAB software and its toolbox DACE (Design and Analysis of Computer Experiments) (Lophaven et al., 2002). This toolbox uses the kriging approximations (Olea, 1974; Rossi et al., 1994) to obtain computer models based on data from a computer experiment, it means, a collection of pairs of inputs and responses that come from runs of a computer model. The particular option of Latin Hypercube Sampling was chosen to interpolate the surface because its generation of random sample points ensures that all portions of the vector space is represented (McKay et al., 1979).

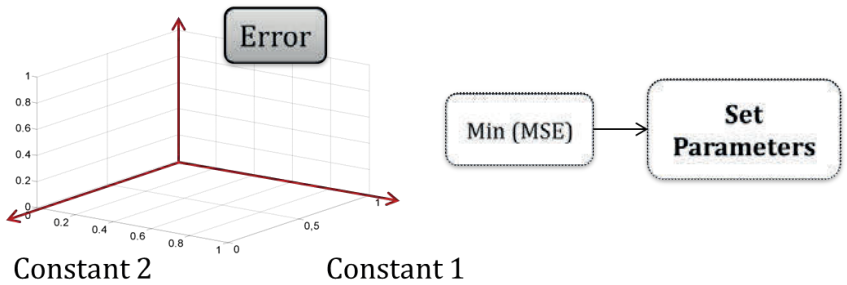

Figure 4.3: Graphical representation of the MSE versus the material parameters.

The graphic response of the MSE was given according to two material parameters, represented by axis X and Y respectively. However, the HGO and the Yeoh models were three-parameter dependent so the graphic representation was not viable. To solve it, in these cases the parameter considered to be the least determinant in the mechanical response, was previously fixed. This way, the benefits of the simple visualization of the results remained. The material parameter fixed in each model as well as the variation range of the other two parameters are gathered in Table 4.1. The 500 cases per material model were obtain by a random combination of the material parameters, which were allowed to vary inside the interval indicated in the Table 4.1.

4.2.1 Finite element model

To run the numerical simulations a finite element model was reconstructed based on the measurements obtained during the experimentation. Once the coordinates of the fiducial markers were determined in the reference state (Fig. 4.4 (a)), they were used to reproduce the initial geometry of the whole external abdominal cavity. To do so, the 3D modelling software Rhinoceros (2014) was used to interpolate a surface through the fiducial points (Fig. 4.4 (b)). The rest of the geometry was closed considering the geometrical references of control points in the surgical table.

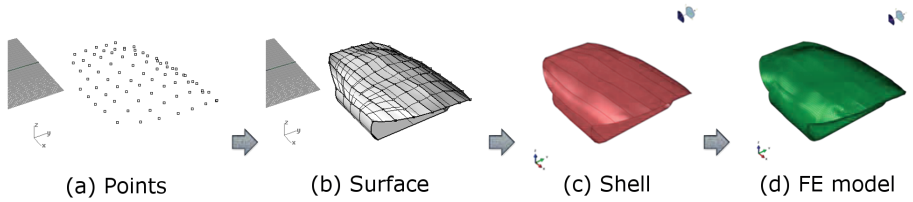

Figure 4.4: Process to reconstruct the abdominal cavity in the reference state.

Once the geometry of the abdominal wall was completely defined, a finite element mesh was generated using $ABAQUS^{®}$ (Simulia., 2011) (Fig. 4.4 (c) and (d)). The mesh was constructed with 19,796 nodes and 87,191 3D hexahedral hybrid elements (C3D8H). A constant thickness of 3 mm normal to the surface was considered based on previous abdominal wall studies (Hernández et al., 2011). The thickness of the abdominal wall was covered by three finite elements (see Fig. 4.5 (b)).

Boundary conditions reproducing the pneumoperitoneum tests were applied by clamping sides and back of the model. Displacement of the side nodes were constricted according to the limited displacement of the side black dots observed during the experiments. Nodes of the back were restricted considering the contact of this zone with the surgical table. Both boundary conditions can be seen in Fig. 4.5 painted in orange: sides, Fig. 4.5 (a); back, Fig. 4.5 (b). A internal load of $12mmHg$ applied normal to the inner surface was considered to simulate de pneumoperitoneum pressure.

4.2.2 Results

A response surface was obtained for each material model based on the 500 simulations performed varying the value of the material parameters. The graphical results are shown in Fig. 4.6 to Fig. 4.8. In those figures, the left one corresponds to the response surface in a three dimensional view, where the spatial form of the surface can be appreciated, while the right one relates the zenithal view of the

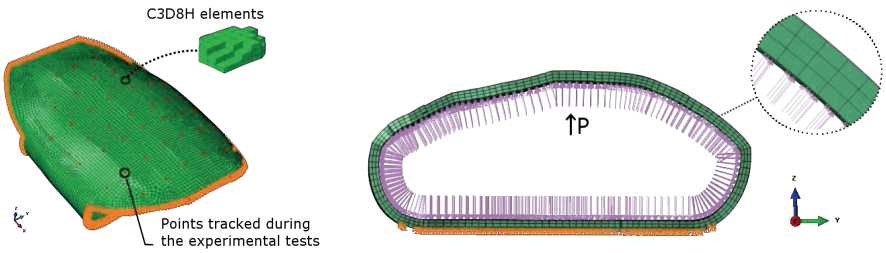

(a) (b)

Figure 4.5: Features of the abdominal wall mesh. (a) Fiducial markers are denoted by red points; nodes fixed are denoted by orange points. (b) Section view: fixed nodes are indicated by orange dots and the pressure field through purple arrows.

surface. This view has the advantage of presenting the distribution of the error by colours, which facilitates the search of the area with minimum error.

The three MSE presented a similar pattern where there were a peak range (red), a minimum zone (dark blue) and a wider area comparable to a tableland (turquoise). The peak range was related to those combinations that yield in extremely compliant geometries, sometimes even reaching to unsteady material. The tableland, on the contrary, implicated those combinations that provoke a response much more rigid. The area between is the crossing part from excessive compliance to too much stiffening, and therefore the range with less MSE.

SEF	**Fixed**	**Variable**	
Demiray	-	$D_1 = 2.6 \cdot 10^{-3} MPa$	$D_2 = 1.4[-]$
HGO	$C_{10} = 5 \cdot 10^{-3} MPa$	$k_1 = 5.3 \cdot 10^{-7} MPa$	$k_2 = 377.32[-]$
Yeoh	$C_{20} = 1 \cdot 10^{-4} MPa$	$C_{10} = 4.5 \cdot 10^{-3} MPa$	$C_{30} = 3.6 \cdot 10^{-3} MPa$

Table 4.2: Material parameters that yield in a minimum MSE.

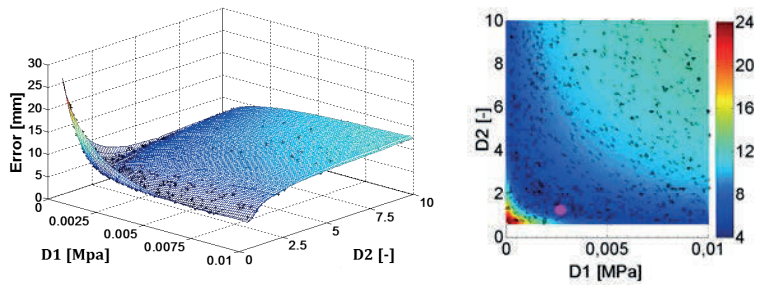

(a) 3D view (b) Zenithal view

Figure 4.6: Response surface for the Demiray model.

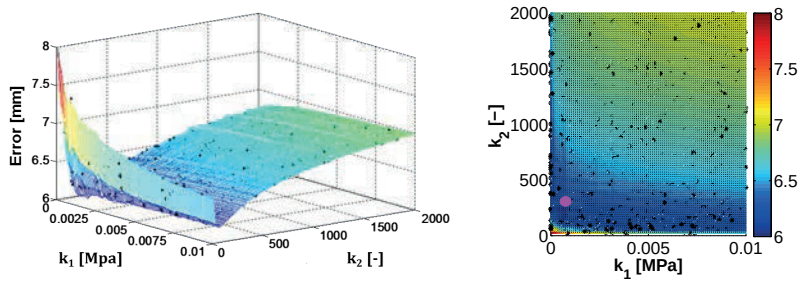

(a) 3D view (b) Zenithal view

Figure 4.7: Response surface for the HGO model.

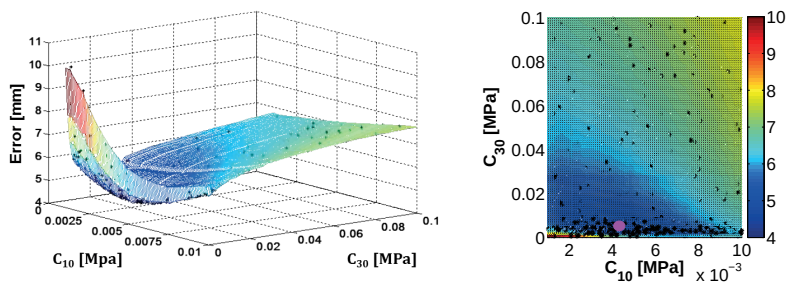

(a) 3D view (b) Zenithal view

Figure 4.8: Response surface for the Yeoh model.

Any of those combinations in the dark blue would satisfy the model in a similar way, although only the one that provide the minimum MSE was considered for the next analysis. These *optimal* combinations were marked in the zenithal view with a pink circle and their exact values were gathered in Table 4.2.

Once the *optimal* combination was obtained and with the aim of assessing the benefits of each model, the finite element analysis performed with each combination were compared. Displacement results are shown in Fig. 4.6 (a), Fig. 4.7 (a) and Fig. 4.8 (a) for the Demiray, HGO and Yeoh models respectively. These images show the numerical displacement field obtained in the anterolateral abdominal wall for the last level of pressure, $P = 12mmHg$. In order to correlate these numerical geometries and the experimental one, a external surface was reconstructed based on the experimental data measured at $P = 12mmHg$. Then, this experimental surface was directly compared to each numerical one, plotting their difference in an contour map shown in Fig. 4.6 (b), Fig. 4.7 (b) and Fig. 4.8 (b).

In this figures the axis X and Y refer to the 2D coordinates (in mm) considered in the model, thus the vertical axis (named as **X**) refers to the craneocaudal direction of the animal and the horizontal one denotes the transverse direction. These maps show the substraction of the numerical data from the experimental one. Consequently, a positive difference denotes that the experimental surface is above the numerical one (this area displaced more) while a negative error means the opposite. Consequently, the closer to zero was the difference, the better the numerical solution could be considered.

Finally, not only the last instant but also the behavior along the test was analysed. To that end, pressure-displacement curves of a central point of the abdomen were obtained for the three *optimal* combinations. Data from the same point was extracted from the experimental tests. Results are shown in Fig. 4.12.

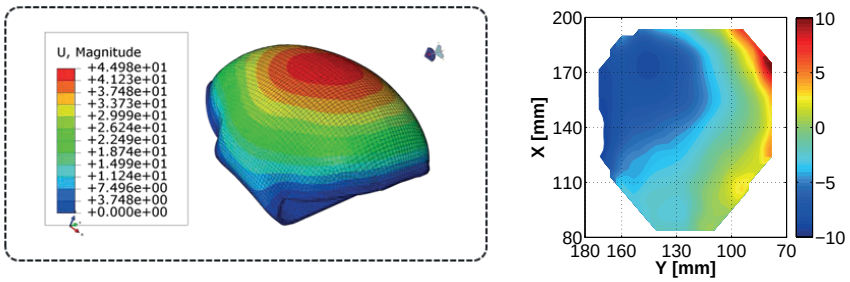

(a) Deformed geometry (b) Error contour map

Figure 4.9: Displacement results (mm) for the *optimal* case of Demiray model.

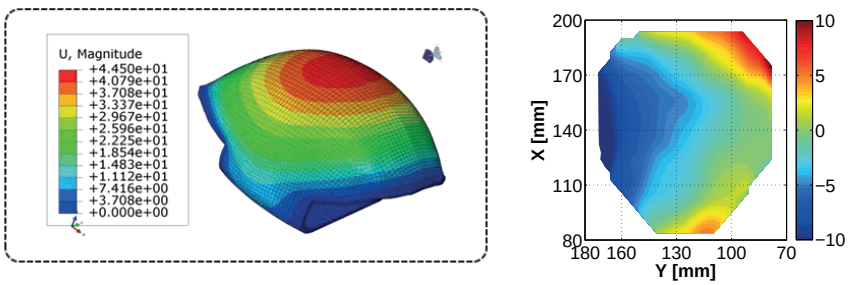

(a) Deformed geometry (b) Error contour map

Figure 4.10: Displacement results (mm) for the *optimal* case of HGO model.

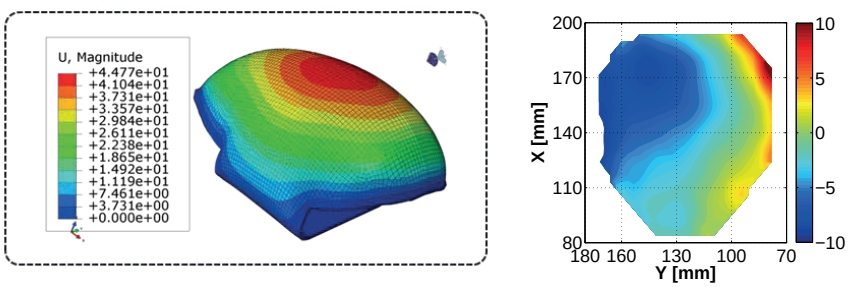

(a) Deformed geometry (b) Error contour map

Figure 4.11: Displacement results (mm) for the *optimal* case of Yeoh model.

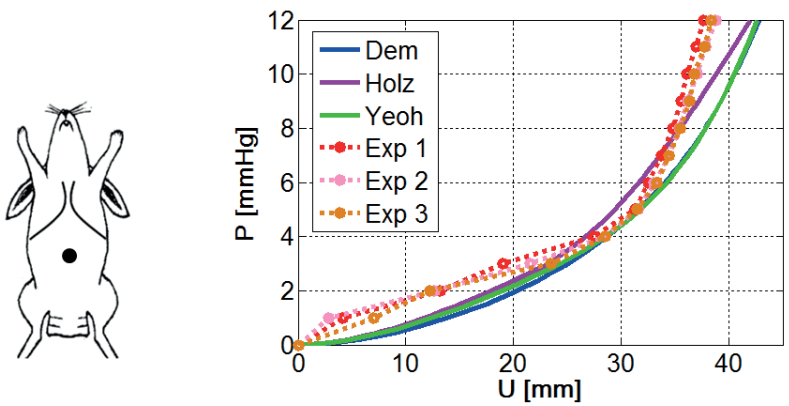

Figure 4.12: Pressure-displacement curve of a central point of the abdomen: numerical versus experimental data.

4.2.3 Discussion

The response surface methodology is a very useful analytic tool to obtain the optimal parameters that minimize a determine function. However, the initial assumption of considering the same response from the whole abdominal tissue was indeed a generalization far from the reality. The proposal was not therefore to fully characterize the abdominal tissue, but to obtain a set of parameters that applied to a simplified model was able to roughly reproduce the mechanical response of the abdominal wall. Considering three isotropic incompressible hyperelastic material models this objective was partly achieved.

The three models were able to create a response surface with a minimum in the range selected for the parameters. This minimum, although not very close to zero, was stable and continuous in the area surrounding, which guaranteed that a small perturbation in the measurement would not lead to a big alteration in the results.

The minimum value of MSE was obtained for the Yeoh model (MSE= $4.910mm$), but very close to the Demiray model (MSE= $4.961mm$). HGO model on the con-

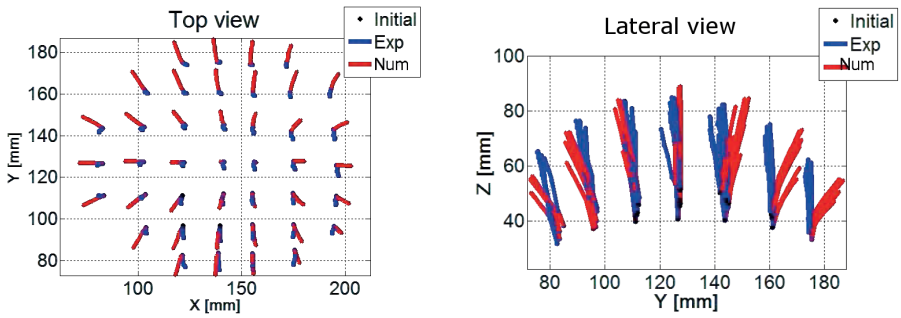

Figure 4.13: Evolution of fiducial points with the pressure increment.

trary showed a slightly higher value (MSE=6.123mm). However this value still remained higher than expected considering that maximum displacements observed in the numerical and experimental reconstruction were similar.

To understand this discrepancy, the tracking of the fiducial points was studied and compared to the numerical case of the model with minimum MSE (Yeoh model). This tracking can be seen in Fig. 4.13, where a top and a lateral views of the fiducial points evolution through the test are shown. It is very noticeable how the numerical data (red lines) seems to pursue the experimental measurements (blue lines) for the central points of the abdomen, but loses them for the points on the borders. These can be explained in two ways, either the boundary conditions were badly designed for the FE model or different mechanical response should be considered for the center and the sides of the abdominal wall.

Regarding to the error contour maps, it was noticeable how these maps showed the same asymmetry for the three material models. On the left side the numerical geometry seemed to displace much more than the experimental one, while results on the right side were the opposite. This could indicate that a possible deviation of the anterolateral wall during the pneumoperitoneum, as a result of the asymmetry of the inner organs location or even the needle position during the test.

When the pressure-displacement curves were analyze for the central point of

the abdomen (Fig. 4.12), it was noted that none of the models were fully able to reproduce the fast rigidization of the experimental curves. This may be achieved through the introduction of a constitutive model reinforced with fibers, where the fiber orientation was considered as a new variable. This way, the first half of the curve would respond to the fiber unrolling while the second one would correspond to the fiber stretching.

The implementation of the RSM to the abdominal wall problem was not exempt from some limitations. As said before, this approach should not be considered as a characterization but an analytic tool able to obtain an acceptable mechanical model. Anatomical zones that form the abdominal wall should be considered in a future, distinguishing those zones with distinct mechanical response. The inclusion of constitutive models with fibers could be very interesting, since it would help to reproduce the fast rigidization beyond $P = 6mmHg$. However, both approaches would mean the introduction of a lot of variables that would complicate the numerical analysis and eliminate the benefits of the RSM. Some of these limitations were attempt to be solved in be following section.

4.3 Inverse analysis

As previously introduced in Chapter 1, an inverse problem is known as the process of calculating from a set of observations the causal factors that produced them. Through the use of the response surface methodology, it has been able to solve this problem by assuming same material parameters for the whole abdominal wall. However, the error contour maps shown in the prior section underlined the lack of symmetry and uniformity in the abdomen tissue. Because of this, this new approach allowed the material parameter to vary along the abdominal location in order to get a more rigid or more compliant response with respect to the obtained in the experimental data.

To solve the inverse problem here proposed, an optimization algorithm developed in conjunction by the Rensselaer Polytechnic Institute and Boston University

(both in United States) was used. This algorithm covers the solution of the inverse problem for several classic materials. In this case, the solution of the finite element inverse problem for incompressible materials was searched, whose complete description was discussed in detail in Goenezen et al. (2011). In this section, a brief review of basic concepts is provided, necessary for understanding the results obtained.

The material model considered for solving the inverse analysis was the Veronda-Westman model (Section 4.1.2) dependent on two material parameters: the shear modulus μ and non linear parameter γ. Since this model is equivalent to the Demiray model, the results obtained from the RSM for this model were used as the initial seed in this section.

The approach followed by the optimization algorithm faced the inverse problem in two steps. First, based on the reconstructed finite element model used in the prior section, a simulation of the pneumoperitoneum test was performed assuming nominal values for the material properties of the abdominal wall. These nominal values were determined considering the results of the RSM. This step takes the name of *forward problem* since it solves a common finite element problem where the initial inputs are known.

Then, in a second step an inverse problem was solved interactively by minimizing an objective function under the constraint that the predicted displacement fields satisfy the *forward problem*. This objective function measured the difference between the predicted and the measured displacement fields. This difference was driven to a minimum by iteratively updating the spatial distribution of the material properties through a quasi-Newton algorithm. The gradient was efficiently computed through the use of an adjoint equation (Gokhale et al., 2008; Goenezen et al., 2011).

The objective function considered in section was defined as follows

$$\Pi = \frac{1}{2}\sum_{i=1}^{n_{meas}} w_i \|\mathbf{u}_i - \mathbf{u}^i_{meas}\|_0^2 + \frac{1}{2}\sum_{j=1}^{N_\beta} \alpha_j R(\beta_j) \tag{4.15}$$

where $\mathbf{u}^i_{meas}$ are the measured displacements fields obtained during the experimental part, $\mathbf{u}^i$ are the predicted displacements fields obtained in each numerical iteration and n_{meas} is the number of independent measured displacement fields. The vector $\beta = [\beta_1, \beta_2, ...\beta_{N_\beta}]$ is the vector of material coefficients required to describe the abdominal muscle material. For this model $\beta_1 = \mu$ and $\beta_2 = \gamma$. The spatial distribution of these parameters is determined by solving the optimization problem, where the optimization variables are the nodal values of these material parameters. Further, $\|.\|_0$ denotes the L_2 norm and w_i are weighting factors selected to ensure that the contributions to the objective function from all measurements are of the same order.

The second term in Eq. (4.15) is the regularization term which ensures a certain smoothness to the material parameters. In this term, α_j is the regularization parameter. The regularization term also embeds prior information about the material parameter distribution into the inverse problem.

For the purpose of this Thesis, two different types of regularization were considered. The first one is the Total Variation Diminishing (TVD), whose regularization term is given by

$$R(\beta_j) = \int_{\Omega_0} \sqrt{|\nabla \beta_j|^2 + c^2}\, d\Omega_0 \tag{4.16}$$

where c is a small non-zero number that ensure that (4.16) is differentiable when $\nabla \beta_j = 0$. TVD suppresses oscillations in the reconstructions and smooths the solution for noisy data without penalizing large gradients in the reconstruction. It is able to detect sharp spatial changes in material parameters, and is robust to noise in a small convergence region.

Regularization type	α_μ	α_γ	**c**
H^1 (Eq. 4.17)	0.2	1	-
TVD (Eq. 4.16)	0.01	0.1	0.125

Table 4.3: Regularization parameters for μ and γ, for material property reconstructions.

The second regularization type implemented in the algorithm was the Tikhonov (H^1) term, defined as

$$R(\beta_j) = \int_{\Omega_0} |\nabla \beta_j|^2 d\Omega_0 \tag{4.17}$$

In contrast to TVD, H^1 tends to smooth out sharp spatial changes in material parameters. However it is quite accurate is determining the spatial location of large changes in material parameters (Ito et al., 2011; Liu et al., 2013).

In both methods the optimal value of the regularization parameter α_j (present in eq. 4.15) was evaluated by finding an equilibrium between the smoothness of the distribution reconstruction and the variation in the objective function value. The regularization parameters for both μ and γ are listed in Table 4.3.

This method was applied to the abdominal geometry to evaluate the distribution taken by the material parameters along the anterolateral wall.

4.3.1 Finite element model

In order to assess differences intra specimen (different tests performed on the same specimen) and inter specimen (tests performed on different specimen) two healthy specimen were reconstructed following the same procedure than in Section

4.2.1. The only disparity consisted on the hexahedral hybrid elements (C3D8H), that were substituted by tetrahedral hybrid elements (C3D4H) in order to satisfy the algorithm requirements. Consequently, two specimen (denoted by Spec1 and Spec2) and two tests per specimen were considered for the inverse analysis.

Regarding to the material model, values of the *optimal* combination obtained from the RSM for the Demiray model were used as a seed for the inverse analysis, due to the equivalence between Demiray and Veronda-Westman SEF. This equivalence included a needed parameter transformation, consisting on $\gamma = D_2$ and $\mu = 2D_1D_2$.

The algorithm thus began with a homogeneous initial value of $\mu = 7{\cdot}10^{-3}MPa$ and $\gamma = 1.4[-]$. During the solution of the inverse problem these parameters were allowed to vary in a range of $[0.0001 - 0.05]MPa$ for μ and $[0.0001 - 5]$ for γ.

Since μ governs the small strain behavior γ controls the exponential stiffening, each parameter was assessed using data from different levels of pressure. To determinate the shear modulus μ, experimental displacement field corresponding to the sixth level of pressure ($P = 6mmHg$) was used. Once this parameter distribution was established, the nonlinear parameter distribution was obtained with the displacement data at the highest level of pressure ($P = 12mmHg$).

4.3.2 Results

Results of the inverse analysis were visualised with ParaView (Ahrens et al., 2005). The solution of the inverse analysis consisted on a distribution of material parameters along the abdominal surface that yield in a displacement field close enough to the experimental data to satisfy the algorithm. The input of the problem was thus the displacement of the fiducial markers in the pnemoperitoneum tests. To assess if the accuracy of the distribution, the final displacement field was evaluated and compared to the experimental one.

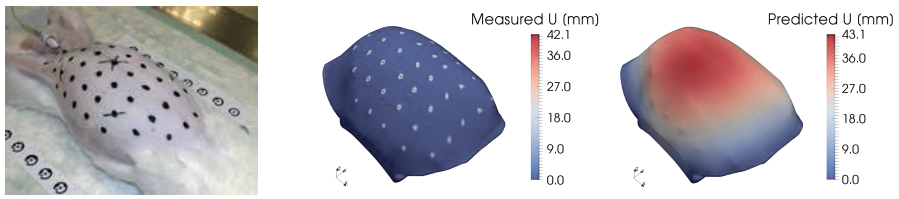

(a) (b) (c)

Figure 4.14: (a) Deformed shape of the abdominal wall at $P = 12mmHg$. (b) Measured vertical displacement of the fiducial markers, plotted on the predicted deformed shape. (c) Predicted vertical displacement field obtained after solving the inverse problem with the TVD regularization, plotted on the predicted deformed shape.

In Fig. 4.14 the deformed shape of the abdominal wall based on the predicted displacement field obtained from the reconstruction with TVD regularization is shown. In Fig. 4.14 (b) the colour scale presents the displacement value of fiducial markers, which constitute the primary input to the inverse problem. Furthermore, in Fig. 4.14 (c) the predicted displacement field obtained after solving the inverse problem with the TVD regularization is plotted.

The accuracy of the final solution was then examined by determining the error committed between the measured and predicted displacement field at the highest applied pressure ($12mmHg$). Additionally, the correlation of regions with higher material parameter values with the anatomical composition of the animal model wall was evaluated.

4.3.2.1 Material parameter reconstructions

The spatial distribution of the material parameters with the TVD regularization for the two tests conducted on each specimen are shown in Fig. 4.15: (a) Specimen 1, (b) Specimen 2. Left images represent the distribution for μ (calculated from displacements at $P = 6mmHg$) and right ones represent the distribution for γ (calculated from displacements at $P = 12mmHg$). Red zones represent a stiffer behaviour while blue zones have a more compliant response.

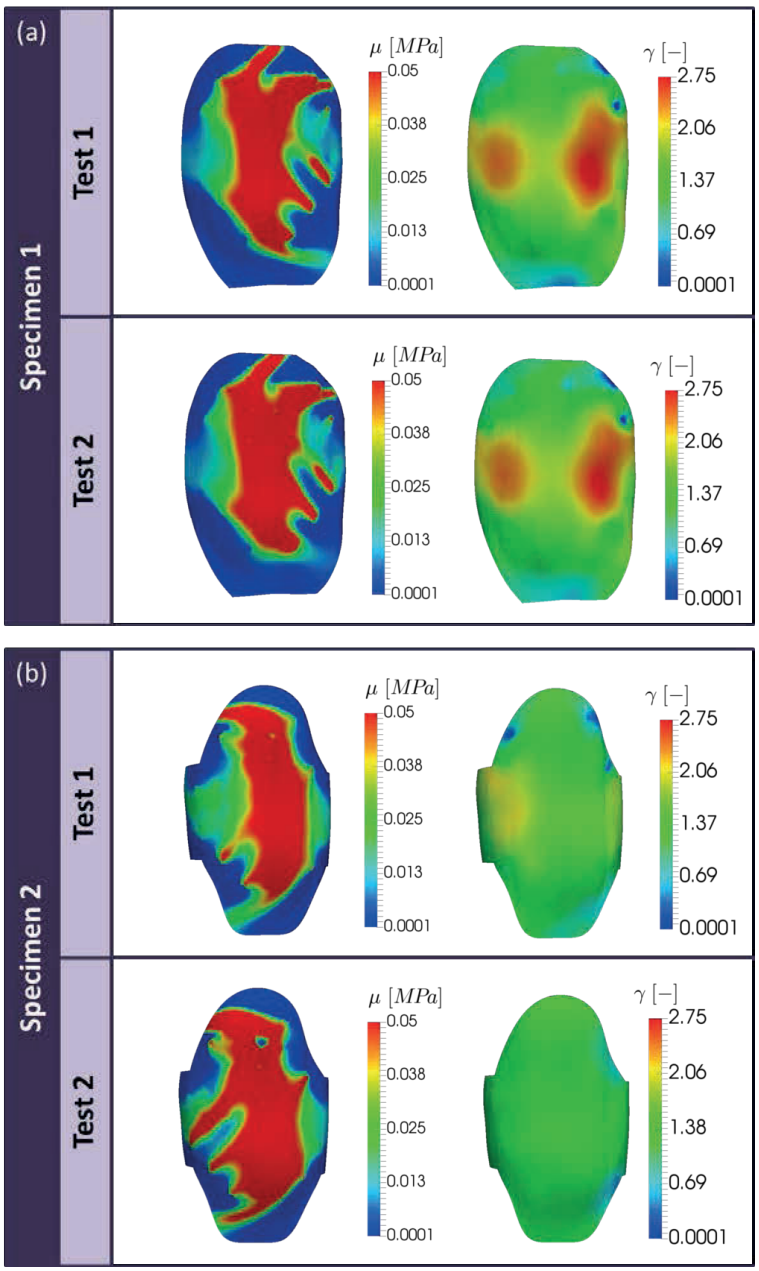

Figure 4.15: Reconstruction of the material parameters after solving the inverse problem with TVD regularization.

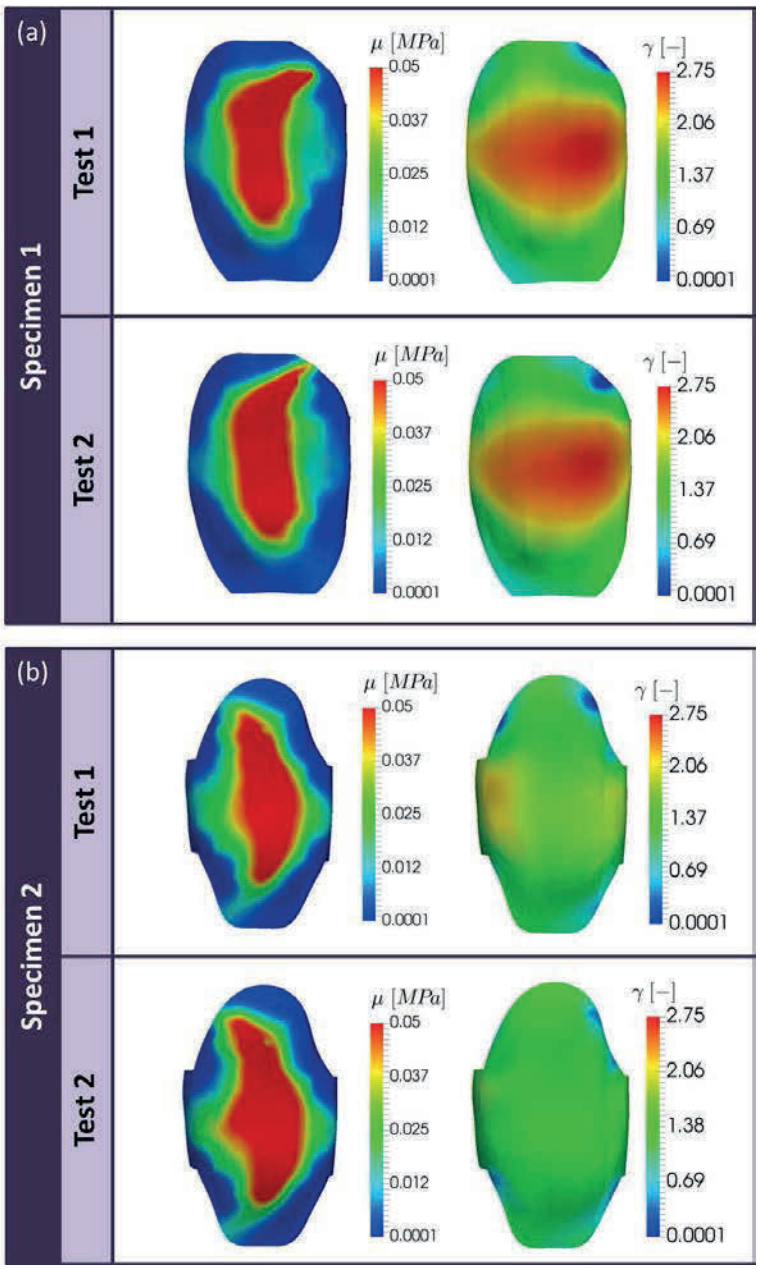

Figure 4.16: Reconstruction of the material parameters of after solving the inverse problem with H^1 regularization.

Only the frontal abdominal surface was plotted here since it is the area where experimental data was measured. The material parameters of the surface in contact with the table were fixed at their initial values. In each reconstruction, a wide red strip in the middle of the abdomen was observed for the shear modulus. The nonlinear parameter showed a more uniform distribution along the surface, with values slightly higher in case of Specimen 1. There were some spots with larger value of shear modulus that are absent in the images for the nonlinear parameter.

Similar results were found for Specimen 1 when using H^1 regularization (shown in Fig. 4.16). With this regularization a smoother distribution for the shear modulus was found in all tests. The red strip of high μ in the middle of the abdomen appears to be slightly thinner and more regular than for the TVD case. In contrast to this, in Specimen 1 the zone with the larger value of γ appears to be bigger with this regularization type.

4.3.2.2 Accuracy of the solution

In order to quantify the accuracy of the reconstructed material property distributions, the surface obtained from the experimental measurement and the predicted surface resulting from the parameter distributions determined by inverse analysis, were directly compared. Thus, similarly to the prior section an error contour map was calculated for each test and regularization type, so that the error committed between the experimental and numerical data in the frontal abdominal surface was graphically determined. These maps were calculated for several levels of pressure but results from last level ($P = 12mmHg$) were chosen as reference to draw a comparison between models.

As comparison, this difference was first computed for the displacement field obtained by solving the forward elasticity problem using the initial guess, it means assuming homogeneous distribution of material parameters along the wall. Maps are shown in Fig. 4.17 for both specimen. It is noticeable that there are significant regions where this difference exceed 6 mm.

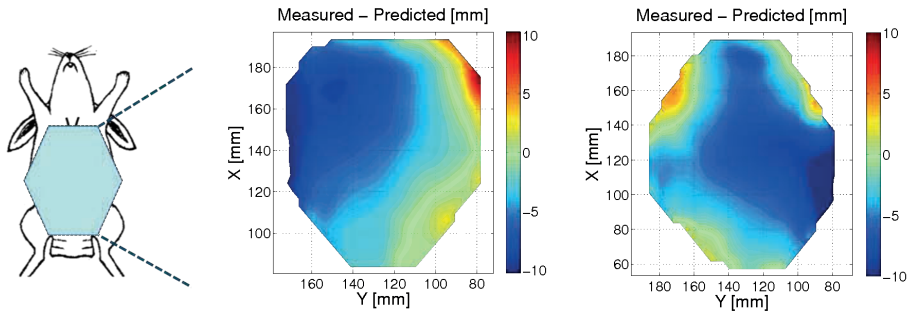

(a) Specimen 1 (b) Specimen 2

Figure 4.17: Error contour maps for the forward problem. Difference in mm between the measured and predicted surface at $12 mmHg$.

In Fig. 4.18 the error contour maps with the predicted displacements resulting from the inverse analysis are shown. TVD results are displayed in figures on the left and H^1 in figures on the right. It is observable that in most cases these errors were significantly smaller ($\leq$ 3mm) that those found with the homogeneous distribution for both regularization types.

It is also visible that regions with larger errors are close to the edges where boundary conditions were applied, indicating that better matches could be achieved by re-evaluating the boundary conditions of the FE model.

4.3.2.3 Stress stretch behavior

In order to graphically observe the different mechanical response between abdominal zones with distinct material parameters, two points on the upper abdominal surface were chosen (one of the center and one of the side, see Fig. 4.19 for their location) and their stretch stress curves were plotted.

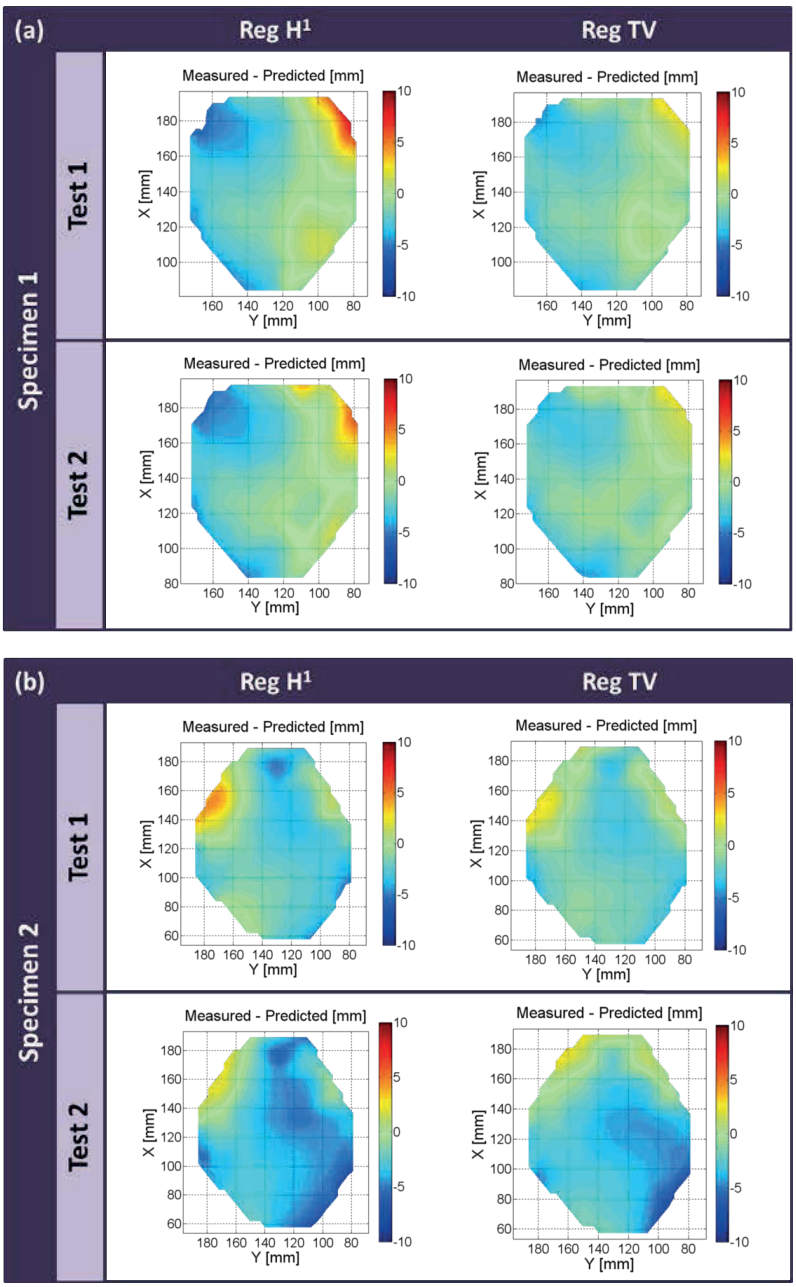

Figure 4.18: Error contour maps after solving inverse problem. Difference in mm between the measured and predicted surface at $12 mmHg$.

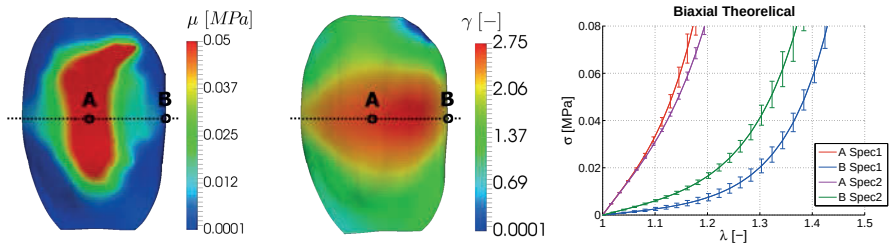

(a) Shear Modulus μ. (b) Nonlinear parameter γ. (c) Cauchy stress vs stretch

Figure 4.19: Mechanical differences between two areas of the reconstructed material properties along the transversal direction.

	Specimen 1	
Point	**A**	**B**
μ [MPa]	$5.0 \cdot 10^{-2} \pm 0$	$3.90 \cdot 10^{-3} \pm 1.08 \cdot 10^{-3}$
γ [-]	2.25 ± 0.35	1.83 ± 0.19
	Specimen 2	
Point	**A**	**B**
μ [MPa]	$4.99 \cdot 10^{-2} \pm 6.74 \cdot 10^{-5}$	$9.65 \cdot 10^{-3} \pm 7.72 \cdot 10^{-4}$
γ [-]	1.55 ± 0.11	1.57 ± 0.14

Table 4.4: Material parameters of points A and B for both specimen (see Fig. 4.19).

The situation of the points in regard to the material parameter distributions is shown in Fig. 4.19 (a) and (b). Using these parameters, biaxial tension simulations were performed in order to obtain the theoretical stress-stretch curves (see Fig. 4.19 (c)). To do so, for each point and specimen, the four results (2 tests x 2 regularization) were considered, and media and standard deviation were calculated (values in Table 4.4).

4.3.3 Discussion

In this Section, a methodology to characterize *in vivo* the passive mechanical behaviour of the abdominal wall using an animal model was evaluated. Assuming an incompressible hyperelastic isotropic model with a SEF depending on two parameters, the experimental tests were reproduced numerically to obtain the distribution of these material parameters that better reproduce the experimental data. These values were calculated by inverse analysis and two different types of regularization were used for the analysis.

Material parameter reconstructions for both regularizations are given in Fig. 4.15 and Fig. 4.16 respectively. Distributions of tests of the same specimen were found really similar, proving that the test is repeatable giving the same results. Regarding to different specimen similar order in the parameter values were found, although showing minor differences mainly in the γ reconstruction. This fact highlights the necessity of testing each individual specimen.

The TVD regularization was found to introduce artifacts into the reconstructions, in the form of small islands of stiffness surrounding the measurement points. This artifacts could be observed in the μ distributions and they were considered a bad aspect of this regularization since there was no anatomical reason for those points to be there. On the contrary, H^1 regularization did not introduce such artifacts. Rather, it smoothed the distribution around the locations of the fiducial markers. Overall values of the parameters were similar to the ones obtained with the TVD regularization, which proved that both approximations worked for characterizing the material.

Both the spatial distribution and absolute values of the material property distributions were determined. The accuracy of both of these depend on experimental and analysis parameters. For example, the spatial resolution at which we can reconstruct the material properties is roughly equal to the distance between fiducial markers. We cannot detect a change that occurs on a scale smaller than this length. Further, the reconstructed modulus values are influenced by our

assumed thickness of 3mm for the abdominal wall.

The red strip found for μ reconstructions indicates that this zone had a more rigid behaviour than the sides for low pressures. This is logical considering that this is the place where rectus abdominis lies, together with the fascias and the linea alba, which greatly increase the stiffening of the tissue (Grässel et al., 2005).

The stress stretch curves shown in Fig. 4.19 (c) provide useful mechanical information about strategic zones of the abdomen. This information could be used in a future in a surgical room, when the mechanical response of the specific area (for example where the hernia takes place) is needed. The low deviation found between tests on same specimen proves the repeatability of the tests. Likewise, both specimen resulted in parameter distribution of the same order. However, the slight differences found between specimens underline the necessity of *in vivo* tests, which provide information of the specific tissue of the specimen under study.

To fully understand the implications of the material parameter distributions it is useful to attend to the anatomical distribution of the abdominal wall in a New Zealand rabbit. In Fig. 4.20, main abdominal muscles situated in different layers are represented: Rectus abdominis, external oblique (EO), internal oblique (IO) and transversus abdominis (TA). The points analyzed and shown in Fig. 4.19 correspond to a different muscle or muscle composite: Point A is on the rectus abdominis while Point B is situated on the EO-IO-TA composite. The mechanical differences found between these points, determined by the change of value in the material parameter distribution, seem to be associated to the mechanical differences between muscle layers and could be use as a characterization of those layers (or composite layers) when working in *in vivo* conditions.

To evaluate the accuracy of the solution, predicted and measured surfaces were compared at last level of pressure. When the forward problem was analysed (homogeneous response, see Fig. 4.17), high differences were found between the experimental and the numerical surfaces. After the inverse analysis was performed the material parameters were allow to vary to better reproduce the experimental

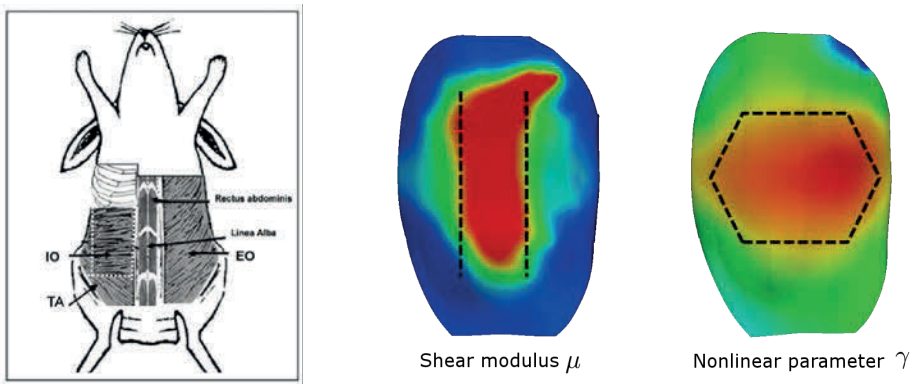

Figure 4.20: Model of the muscle composition in the abdominal wall of the New Zealand white rabbit (EO: external oblique; IO: internal oblique; TA: transversus abdominis). Image obtained from literature (Hernández et al., 2011).

data, which yields to a allocation of the parameters along the surface. This entails an heterogeneous response of the wall, which is closer to the characteristic anisotropy of the abdomen. This improvement wass seen in Fig. 4.18, where the error committed between numerical and experimental surfaces significantly decreased. The fact that no meaningful differences were found between regularization types, indicated that both approaches were resulting in a similar numerical surface close to the experimental one. Extreme levels of error found on the borders of the contour maps probably appeared as a result of imposing restrictive boundary conditions in the FE model.

It is worth mentioning that this algorithm has been previously tested adding different levels of noise to the measured displacement field in order to assess the noise effect in the final inverse approach. In Gokhale et al. (2008) and Goenezen et al. (2011), authors guarantied the performance of the approach on synthetically generated displacement data until 3% of noise. In this study the measurement technique here used can assure an accuracy of $1mm$, which considering the $40mm$ of maximum displacement suppose an noise of 2.5%.

Some limitations of this study should be mentioned here. The 3D FE model

was reconstructed from several points measured during the pneumoperitoneum at different pressures. Increasing this amount of points would better adjust this initial model and subsequently would improve the accuracy of the results. Likewise, widening the surface tracked during the tests would help to avoid the effect of boundary conditions imposed on the FE model. A constant thickness was considered along the model of the wall but it may be better obtain by ultrasound in a future.

Concerning to the formulation model, an isotropic incompressible hyperelastic material model was proposed here to reproduce the abdominal wall. However, this initial simplification should become more complex in future works: to distinguish separate layers or assuming an anisotropic model with preferential directions associated to collagen fibers arrangement would definitely help to improve the abdominal muscle characterization. These would require significantly more experimental observations than what is currently available.

5

Application to the mesh hernia repair

In this Chapter, the characterization obtained with the inverse analysis was applied to different cases of hernia repair. In order to assess the goodness and adequacy of each prothesis, four non-absorbable, biocompatible and polypropylene monofile meshes with different density and mechanical response were subjected to biaxial tests. Then, the four meshes were characterized by a numerical approach, consisted on an iterative process to minimize the error between experimental and analytical curves.

Concurrently, two of these meshes were also implanted in an animal model and then subjected to the pneumoperitoneum tests detailed in Chapter 3. Based on the herniated specimen, a finite element model was reconstructed to numerically assess the response of the whole abdomen when repaired with each of the four meshes. The model was validated by comparing the experimental data to the simulation. The herniated model was use to predict the response for the different protheses. Disturbances from the healthy tissue were also determined.

5.1 Introduction

Since the introduction of Lichtenstein's tension-free mesh procedure (Lichtenstein and Shulman, 1986; Amid et al., 1995; Sakorafas et al., 2001), the classic suture techniques have gradually given way to the use of a biomaterial for the surgical repair of an abdominal wall hernia, which is today practically standard practice (Rutkow, 2003; Kulacoglu, 2011). However, despite the widespread use of the surgical meshes, there is not a guide or extended acceptance about which protheses is the ideal for each hernia case or patient typology. Surgeons are often forced to choose a mesh mostly based on their experience and knowledge.

In order to facilitate the mechanical aspects of this selection some technical data may be provided. Specifically, there are two information sources that would definitely contribute to improve this choice: the *in vivo* mechanical response of the specific patient and the behavior of the surgical mesh in conjunction with the tissue. In the prior Chapter a methodology to determinate the *in vivo* mechanical behavior of the abdominal wall was presented, only through the use of the first steps of the laparoscopy. This non invasive way of measure assures a truly passive response of a specific abdomen. The mechanical behavior of the whole mesh-tissue is impossible to measure before the operation. Thus, a prediction of this interaction becomes a very interesting tool to determinate which mesh better reproduces the response of the healthy wall.

To perform this prediction, numerical simulations arise as the perfect solu-

tion, but they must be provided with some mechanical information of each mesh. Nowadays, it is common that manufacturers supply the medical equipment with a technical data sheet. It would be very easy as well as useful, if these data sheets included the response of a mesh to a biaxial loading test, since this type of mechanical test is close to reproduce the loading state suffered in the abdomen. Based of their biaxial response, meshes could be classified and characterized from a mechanical point of view.

Besides that, if the biaxial characterization was included in the patient specific model developed in the prior Chapter, a reliable prediction of the repair abdomen may be obtained. This prediction might be used to determinate which mesh leads in a deformation close to the expected in a healthy abdomen.

In order to verify the viability of this idea, this approach was applied to four commercial meshes: two meshes were used to validate the methodology proposed and the other two were used as an example of the mechanical response prediction in the repaired wall.

5.2 Materials and methods

5.2.1 Surgical meshes

Four surgical meshes were used for this study, all of them non-absorbable, biocompatible and polypropylene monofile meshes (see Table 5.1): *Neomesh Soft*® (NM, DIMA S.L.), an isotropic light-weight mesh (40 g/m^2); *Neopore*® (NP, DIMA S.L.), a slightly anisotropic ultra light-weight mesh (32.4 g/m^2); *Neomesh SuperSoft*® (SS, DIMA S.L.), a highly anisotropic ultra light-weight mesh (18.10 g/m^2); and *Surgipro*^{TM} (SUR, Covidien), a slightly anisotropic heavy-weight mesh (84 $g/m2$). All meshes are designed for abdominal and inguinal hernia repair as well as tissue reinforcement. Two directions, Direction 1 and 2 (see Fig. 5.1), were identified in the meshes in order to assess possible anisotropy.

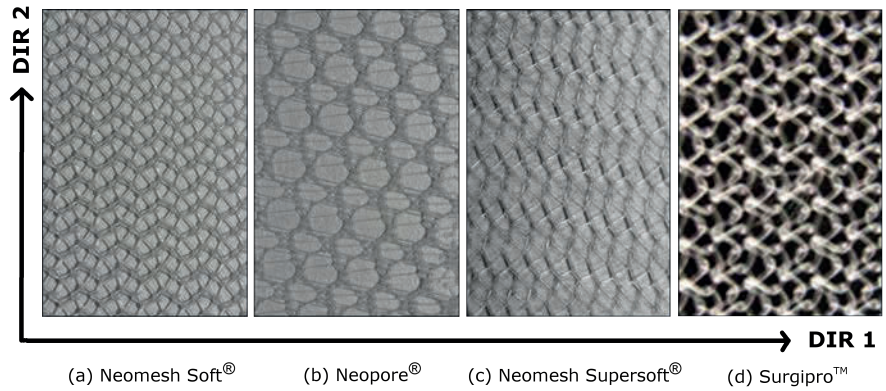

Figure 5.1: Details of the four synthetic meshes.

Commercial Name	Isotropic/Anisotropic	Density
Neomesh Soft® (NM)	Isotropic	40 g/m^2 (LW)
Neopore® (NP)	Slightly Anisotropic	32 g/m^2 (ULW)
Neomesh SuperSoft® (SS)	Highly Anisotropic	18.10 g/m^2 (ULW)
Surgipro^{TM} (SUR)	Slightly Anisotropic	84 g/m^2 (HW)

Table 5.1: Description of the four surgical meshes tested in this study.

5.2.2 Experimental characterization of surgical meshes

Mechanical tests were carried out on three surgical meshes: *Neomesh Soft*®, *Neopore*® and *Neomesh Supersoft*® (DIMA meshes). Mechanical data from *Surgipro*^{TM} was obtained from previous works (Cordero et al., 2015).

With regard to the mechanical tests, six 35×35 [mm] strips of DIMA meshes were cut and subjected to biaxial tests. They were conducted using a Instron BioPulsTM low-force planar-biaxial Testing System, with four independently 50 N full scale load cell and minimal resolution of 5 N, and a sensibility of 0.125 N (0.25%). For all samples, Direction 1 defined on the meshes was aligned with the

Test TA:TB	Longitudinal displacement [mm]	Transversal displacement [mm]	Longitudinal velocity [mm/s]	Transversal velocity [mm/s]
1:1	4.0	4.0	0.4	0.4
1:0.5	4.0	2.0	0.4	0.2
1:0.75	4.0	3.0	0.4	0.3
0.5:1	2.0	4.0	0.2	0.4
0.75:1	3.0	4.0	0.3	0.4

Table 5.2: Loading protocols biaxial tests.

A axis of the machine. Custom-made clamps (grips) equipped with sandpaper at the clamping faces were used to grip the samples to the biaxial machine (see Fig. 5.2), keeping a distance between clamps of about 30 mm. Each specimen was then preloaded 0.1 N along both axes in order to obtain a perfectly planar shape and define the zero load level. All samples were subjected to ten loading and unloading cycles were acquired for each protocol, where the first nine cycles ensured that the specimen was preconditioned and the tenth was used for subsequent analysis. For each sample, five different ratios TA : TB in A and B directions were tested (see Table 5.2), following protocols similar to those previously described by (Sacks, 2000) for biaxial mechanical evaluation. All tests were carried out in displacement control modality. In the case of SUR, since data was taken from literature, only three ratios were shown.

To compare the mechanical response of the four meshes, force per unit width (Equivalent Piola Stress, EPS) was obtained using the expression $EPS = \frac{Force[N]}{Width[mm]}$, where Force [N] is the load acquired during the test.

5.2.3 Calculation

To fit the experimental results obtained, a strain energy function (SEF) which reproduces isotropic and anisotropic responses was considered:

$$\overline{\Psi} = \frac{k_1}{2k_2}\left[e^{k_2(1-\rho)(\overline{I}_1-3)^2+k_2\rho(\overline{I}_4-1)^2}-1\right] \tag{5.1}$$

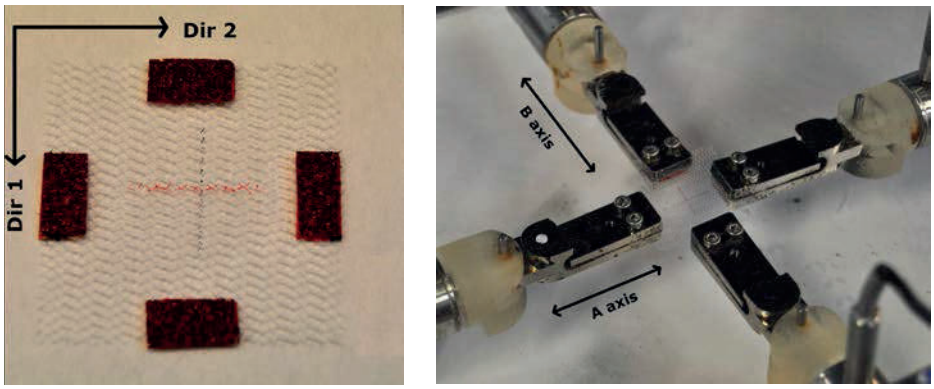

(a) Directions on the mesh (b) Mesh setup.

Figure 5.2: Biaxial setup.

This equation corresponds to a exponential strain energy function similar to that introduced by Holzapfel (2000) and Gasser et al. (2006), and previously used in the Chapter 4. This SEF is dependent on two main material parameters k_1 and k_2, and a third one ρ that controls the contribution of each term in the equation. The term that includes I_1 is associated to the isotropic response of the material, while I_4 concerns the anisotropic response. This anisotropy is determined by the insertion on a family of fibers, that in the specific case of the surgical meshes considered in this Chapter, they run aligned Direction 2.

The isotropic or anisotropic character of the mesh is conditioned by the parameter ρ, which is related to the fiber dispersion. When $\rho = 0$ fibers are randomly distributed, so the material can be considered isotropic. On the contrary, when $\rho = 1$ fibers are totally aligned in the Direction 2, and therefore the response of the material becomes fully anisotropic. When ρ takes a value between those limits, both contributions (isotropic and anisotropic) have influence and the parameter $\rho = 0$ works as a regulator of each one.

Material parameters and the coefficient ρ were fitted by an iterative process minimizing the error committed between experimental and analytical curves. In the approach followed in this work, experimental curves were first averaged and

then fit once using the Levenberg-Marquardt minimization algorithm (Marquardt, 1963). This algorithm is based upon minimization of an objective function, which for the case of biaxial tests takes the form of

$$\chi^2 = \sum_{i=1}^{n} \left[(EPS^{exp} - EPS^{num})_{i1}^2 + (EPS^{exp} - EPS^{num})_{i2}^2 \right] \tag{5.2}$$

where EPS^{exp} and EPS^{num} represent the experimental (measured) and numerical values of EPS respectively. This equation is evaluated in each data point (i) up to the total number of data points (n). The subscripts 1 and 2 make reference to the axis A and B indicated in the tests.

The quality of data fitting was assessed by calculating the coefficient of determination R^2 (Steel and Torrie, 1960), defined as

$$\begin{aligned} R^2 &= 1 - \frac{SS_{res}}{SS_{tot}} = \\ &= 1 - \frac{\sum_{i=1}^{n} \left[(EPS^{num} - EPS^{exp})_{i1}^2 + (EPS^{num} - EPS^{exp})_{i2}^2 \right]}{\sum_{i=1}^{n} \left[(EPS^{exp} - \mu)_{i1}^2 + (EPS^{exp} - \mu)_{i2}^2 \right]} \end{aligned} \tag{5.3}$$

In this equation, SS_{res} is the residual sum of squares and SS_{tot} the total sum of squares, both defined as indicated in the second part of the equation. Lately, μ is the mean stress define as $\mu = \frac{1}{n} \sum_{i=1}^{n} [EPS]_i$. The coefficient R^2 is an indicative of the goodness of the fitting, being 1 the solution that fits the data exactly.

5.2.4 Animal model: experimental design

Nine adult male New Zealand white rabbits obtained from the Animal Experimentation Service of the Research Support Services of the University of Zaragoza

were used. Their weight ranged from 3.7 to 4.2 kg. The animals were housed singly, and were watered and fed a standard chow diet ad libitum (Finished feed n. 511®; Food Corporation Guissona S.A., Lleida, Spain). All animals were healthy and free of clinically observable systemic diseases. All procedures were carried out under Project Licence PI 01/11 approved by the in-house Ethics Committee for Animal Experiments of the University of Zaragoza. The care and use of animals were performed accordingly with the Spanish Policy for Animal Protection RD53/2013, which meets the European Union Directive 2010/63 on the protection of animals used for experimental and other scientific purposes.

Surgical procedure

Experiments were divided into two groups: the group A (control) was compounded by five healthy specimens and the group B by four herniated animals with a surgical mesh previously implanted. The abdominal defect was repaired with two meshes referred in Section 5.2.1, *Neopore Mesh*® (NP) and *Neomesh Soft*® (NM). Each mesh was inserted in two rabbits.

Mesh anisotropy was considered to establish the orientation of the mesh in relation to the anatomy of the animal. According to (Hernández-Gascón et al., 2013), an anisotropic mesh situated with the most compliant direction perpendicular to the craneo caudal axis produces more alteration in the abdomen than the orthogonal position. In order to study the effect of the meshes in the worst case, the stiffest direction (Direction 2 in Fig. 5.1) was longitudinally aligned in the rabbit whereas the most compliant direction (Direction 1) lied transversally.

Animals were intramuscularly anaesthetized with a mixture of medetomidine (0.5 mg/kg, Medeson; Uranovet, Barcelona, Spain), ketamine (25 mg/kg, Imalgene 1000® ; Merial Laboratorios S.A., Barcelona, Spain) and buprenorphine (0.05 mg/kg, Buprex® ; Fort Dodge Veterinaria S.A., Girona, Spain). Using a sterile surgical technique, an abdominal wall defect was created through a 7-cm midline incision beginning 2 cm below the xiphoid process. A 5x7-cm portion was excised of the anterior abdominal wall comprising the aponeurotic, muscular

and peritoneal planes (see Fig. 5.3 (a)). The corresponding mesh was attached to the tissue defect by a continuous suture with 4/0 non-absorbable monofilament polypropylene (Premilene®, B-Braun Vet-Care S.A., Barcelona, Spain) interrupted in the implant angles. The underside of the implants was placed in direct contact with the visceral peritoneum, whereas the upper side was in contact with the subcutaneous tissue. The subcutaneous tissue was then closed over the implants by a continuous suture and the skin by an intradermal suture, both with 4/0 absorbable monofilament glyconate (Monosyn®, B-Braun Vet-Care S.A., Barcelona, Spain). Once the wound was closed, the visible scar was a 100-mm incision along the linea alba direction (see Fig. 5.3).

Immediately after the surgical procedure, to minimize pain and avoid infections, intramuscular buprenorphine (0,05 mg/kg twice a day, Buprex®; Fort Dodge Veterinaria S.A., Girona, Spain) and enrofloxacine (10 mg/kg twice a day, Alsir 5® ; Esteve Veterinaria S.A., Barcelona, Spain), and subcutaneous meloxicam (0,2 mg/kg once a day, Loxicom® ; Laboratorios Karizoo S.A., Barcelona, Spain) were administered in all animals for a week. Throughout the study, the animals were visually inspected for signs of seroma formation, wound infection and/or areas of mesh incompatibility.

After 15 days of the surgical procedure and immediately after the pneumoperitoneum tests, each animal was humanely euthanized with an overdose of intravenous sodium pentobarbital (150 mg/kg, Dolethal®; Vétoquinol E.V.S.A., Madrid, Spain).

Experimental testing

Using the protocol previously described in Chapter 3 of this Thesis, several pneumoperitoneum tests were performed on each animal, increasing the inner pressure from 0 to 12 mmHg. By proceeding similarly to the Chapter 3, specimens were cropped from front to rear legs and their abdominal surface was spotted with black dots. Then, the intraabdominal pressure was increased from 0 mmHg to 12 mmHg while tests were recorded by a stereo rig necessary to the track-

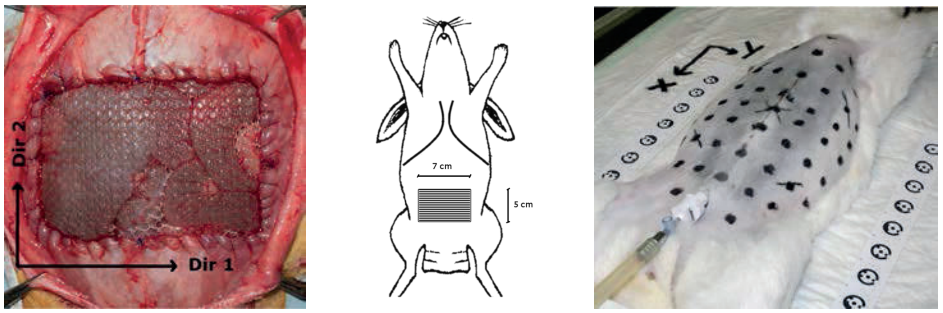

(a) (b) (c)

Figure 5.3: Details of the implanted mesh in in the rabbit: (a) *Neopore*® mesh at the moment of mesh implantation. (b) Mesh location in the abdomen. (c) External aspect of the abdomen after wound closure.

ing of the points. Tests were repeated for four times, reaching zero state after each pneumoperitoneum, and first one was excluded from the study due to the preconditioning.

During the experiment, animals were kept alive but completely anesthetized.

Finite element model

Following the same procedure performed in Chapter 3, frames for each level of pressure were extracted from the video recorded and post processed with the software ?). Based on the 3D measurements obtained after the postprocessing, three finite element models were reconstructed: one for the *Neomesh Soft*® protheses, one for the *Neopore*® one and the last one for the healthy case. A constant thickness of 3 mm (and 3 elements) was considered again for the abdominal surface. On the contrary, the mesh was simulated by a surface of 1 mm (and 1 element) of thickness in the place where it was supposed to be situated according to the surgical procedure.

To simulate the continuous suture that joins the implant and the subcutaneous tissue, nodes of the mesh perimeter where merged to the surrounding tissue, so

Mesh	D_1 [MPa]	D_2 [-]	k_1 [MPa]	k_2 [-]	ρ [-]	R^2
NM	-	-	14.92	40.1	0	0.973
NP	-	-	11.28	51.4	0.02	0.919
SS	-	-	0.153	40.5	0.25	0.917
SUR	1.73	11.7	$3.51 \cdot 10^{-2}$	88.8	1	-

Table 5.3: Material parameters for the NM, NP, SS and SUR meshes generated by the fitting procedure.

that no slipping was allowed between mesh and tissue.

In order to determine the effect of each mesh on the abdomen response, the four prothesis were simulated on the same FE model. To do so, the NM was chosen as a model where healthy and repaired results were compared. Once the FE model was reconstructed, material properties were assigned with respect to the particular tissue. Material properties of the abdomen were based on the material parameter distribution obtained after the inverse analysis in the previous Chapter. Thus, a central band in the abdomen was assumed to take higher value of μ and an oval area was delimited to assign higher value of γ, following the material distributions obtained after the inverse analysis with the Tikhonov regularization.

For the properties of the mesh, material parameters resulted from the biaxial fitting procedure were considered (see Table 5.3). Consequently, five finite element model were analysed: one considering the space of the mesh as abdominal tissue, and therefore simulating the behavior of the healthy specimen, and four models simulating the response on the abdomen after repaired with four synthetic meshes.

5.3 Results

5.3.1 Biaxial test response

Figs. 5.4 and 5.5 shows the mean EPS vs. stretch curves obtained in the biaxial mechanical tests to provide a meaningful comparisons between the four meshes studied. All curves started with an initial low stiffness region, which then changed into a high stiffness region. The Fig. 5.4 plot the five load ratios tested during the biaxial tests. The NM mesh showed an isotropic behavior (see Fig. 5.4(a)), with similar response in both axis. On the contrary, the other three meshes presented anisotropic behavior, with tensile mechanical behavior along B direction stiffer than the A direction. In this group, NP and SUR showed a slight level of anisotropy (Fig. 5.4(b) and (d) respectively) when compared to the high level of anisotropy presented by SS (Fig. 5.4(c)). Besides, SUR mesh revealed as the stiffest behavior of the four meshes and SS as the most compliant. The comparison of the four meshes for the equibiaxial test (T:T) is shown in Fig. 5.5.

The SEF used to model the mechanical behavior of the meshes was defined in Eq. 5.1. The results of parameter estimation for all meshes obtained by fitting the experimental curves are shown in Table 5.3. The fitting corresponding to the SUR mesh was obtained from prior works developed by Cordero et al. (2015), who employed a Demiray's SEF to model the isotropic contribution and Holzapfel for the anisotropic. The value of the fitting parameters is also included in the Table 5.3. In all cases, coefficient of determination R^2 (see Eq. 5.3) took values above 0.9, which confirms the goodness of the fit.

Fig. 5.6 provides the results of the fitting process for the equibiaxial case. In the figure, curves constructed using the experimental biaxial test data (dash-dot line) and the results of the simulation (solid line) are compared. The plots of EPS vs. stretch indicate the good fit of the parameters.

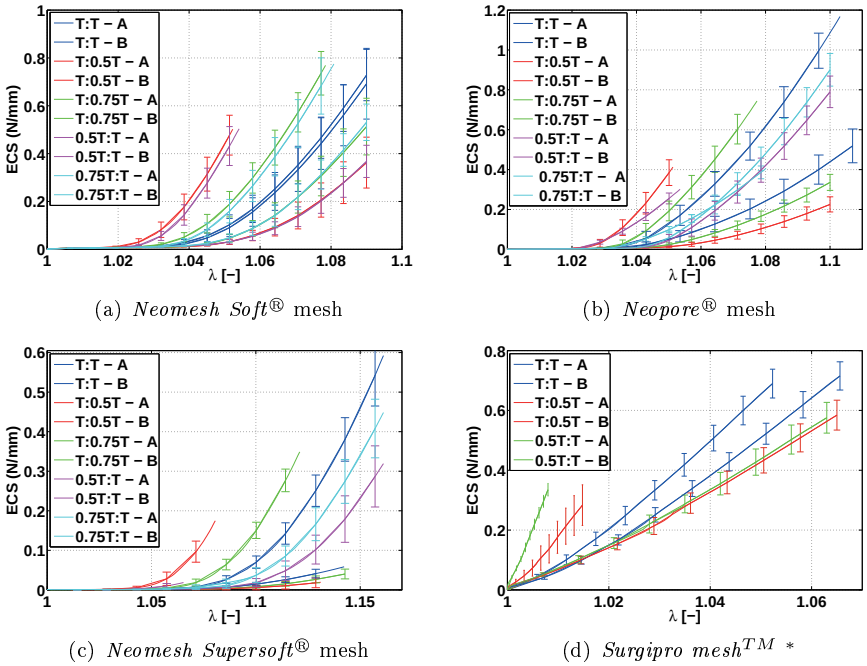

(a) *Neomesh Soft*® mesh

(b) *Neopore*® mesh

(c) *Neomesh Supersoft*® mesh

(d) *Surgipro mesh*^{TM} *

Figure 5.4: Experimental data obtained in the biaxial tests for the four meshes. * Figure obtained from Cordero et al. (2015).

5.3.2 In vivo mechanical response

Similarly to the results found in Chapter 3, abdominal surface changed from a cylinder to a dome shape during the tests, as can be seen in Fig. 5.7. In this figure, a specimen with the *Neopore*® mesh is shown at the initial ($P = 0$ mmHg) and final instant of the pneumoperitoneum test ($P = 12$ mmHg).

During the pneumoperitoneum, none of the sutured animals exhibited any sign of opening or breakage in the wound despite the pressure increase. Furthermore, no visible differences were found between healthy and operated specimen during the development of the test.

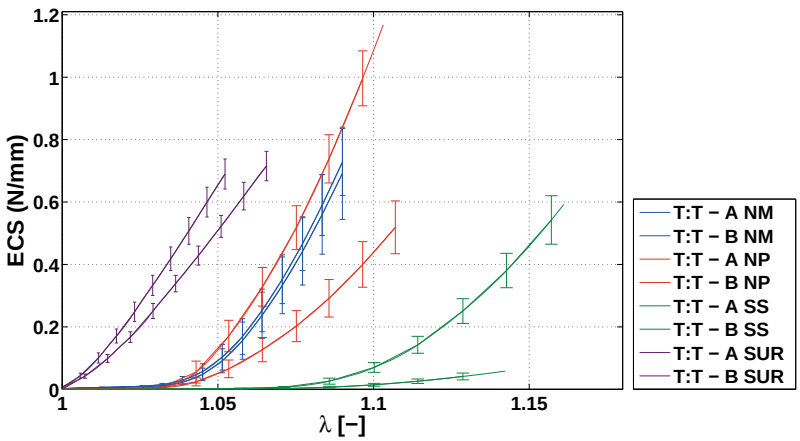

Figure 5.5: Comparison of the equibiaxial test (T:T) for the four meshes.

Inflation tests showed a maximum displacement of 44.011 mm in healthy animals, and 44.911 mm and 42.697 mm in specimen repaired with *Neomesh Soft*® and *Neopore*® meshes respectively. Maximum displacements were found in the central zone of the abdomen for all cases while minimum displacement values corresponded to the area between the front legs, probably given by the rigid effect of the rig cage and the breastbone. During the pneumoperitoneum test, abdomen deformed symmetrically about the longitudinal axis (craneo caudal direction) but unsymmetrically in the perpendicular axis. With respect to the transversal axis, a greater displacement was observed in points of the lower abdomen, towards the rear legs, rather than points of upper abdomen.

No clear alteration resulting from the mesh presence was noticed to the human eye at the end of the pneumoperitoneum, except for one specimen which presented a case of emphysema. In this case, corresponding to a specimen operated with the *Neomesh Soft*®, the inner gas went through the abdominal cavity to the subcutaneous tissue. This provoked an excessive elongation of the skin surrounding (visible in Fig. 5.8) which led in an extra displacement of the dots situated on this area. This displacement was *false* though, since it came from the skin elongation instead of the muscle strain. Due to this, the four points altered

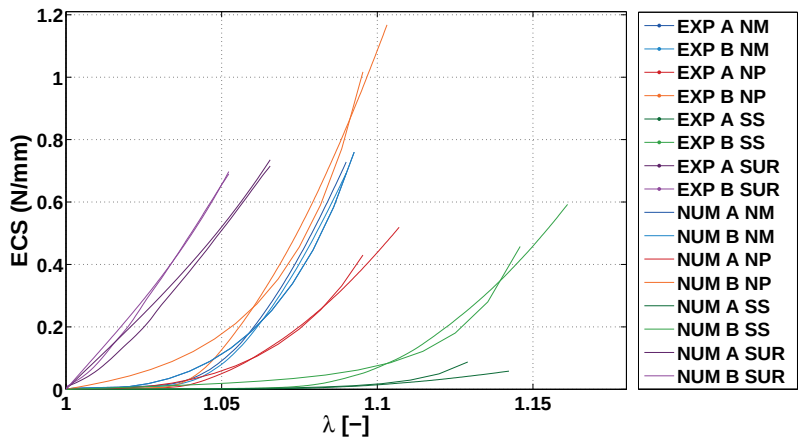

Figure 5.6: Numerical fitting of the biaxial tests for the four meshes.

by the emphysema were removed from the analysis.

Five main points were studied and compared in depth, corresponding to the central, sides, upper and lower zones of the abdominal surface (see Fig. 5.9(a)). Pressure-displacement curves for these points with mean and standard deviation of the four tests performed are shown in Fig. 5.9(b) for healthy specimen and Fig. 5.9(c) and (d) for the NM and NP mesh respectively. In these figures, horizontal axis refers to the inner pressure reached in the abdominal cavity and vertical axis plots the displacement of each point, calculated from the coordinates transformation in the three principal axis.

According to these curves, dispersion was higher between the second and the sixth level of pressure, when maximum gradient of deformation was found. No great differences were found in the pressure-displacement curves between healthy and repaired specimen although slight discrepancies should be mentioned. It was noticed that NM started the big gradient of deformation right before the healthy group and the repaired with NP. Furthermore, the central point (point 2) of the NP showed a greater difference in displacement with respect the following point (point 3), difference which was not found in the healthy or NM group.

(a) $P = 0$ mmHg (b) $P = 12$ mmHg

Figure 5.7: Specimen with the mesh inserted in the initial (a) and final (b) instant of the inflation test.

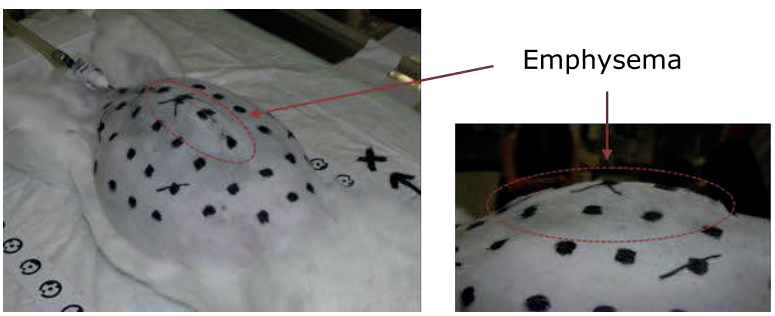

Figure 5.8: Emphysema resulting from the test in one of the specimen.

Stretching values were analysed in both principal directions, longitudinal (parallel to the craneo caudal) and and transversal (perpendicular to the craneo caudal). As previously performed in the Chapter 3, six segments were analysed in each direction, named A, B, C, D, E and F. In longitudinal direction, segments were named in order from the head to the tail; in transversal direction, from the right to the left side. According to this nomenclature, stretching values for the last level of pressure were calculated for the three groups (see Fig. 5.10). Exact values at 12 mmHg are gathered in Table 5.4.

According to this bar diagram, the insertion of the NP mesh contributed to increase the elongation in the central area of the abdomen for the transversal direction, precisely where the most compliant direction of the mesh was aligned.

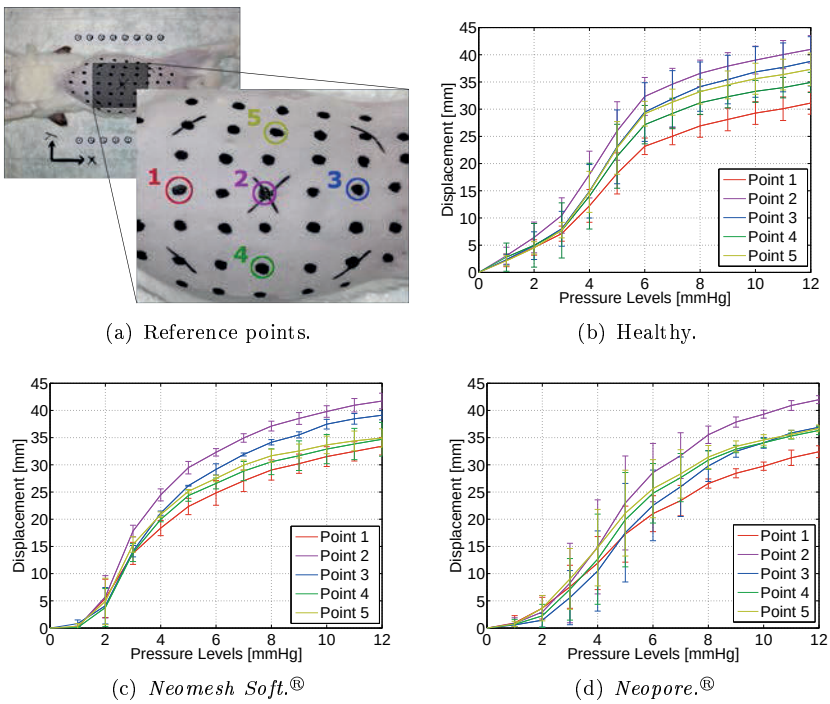

(a) Reference points. (b) Healthy.

(c) *Neomesh Soft.*® (d) *Neopore.*®

Figure 5.9: Pressure-displacement curves for main five points of the abdominal surface for the healthy and repaired specimen. Mean and standard deviation are shown.

On the contrary, no alteration was noticed in the longitudinal direction. With regard to the NM mesh, it was noteworthy that NM mesh provoked a shortening of the segments B and C in the longitudinal direction, probably due to the increase of stretching in transversal direction.

5.3.3 Numerical results

On the reconstructed FE model, results for the healthy and repaired cases were compared. In order to determine alterations provoked by the mesh insertion, maximal displacements (MD), maximal principal stresses (MPS) and lagrangian

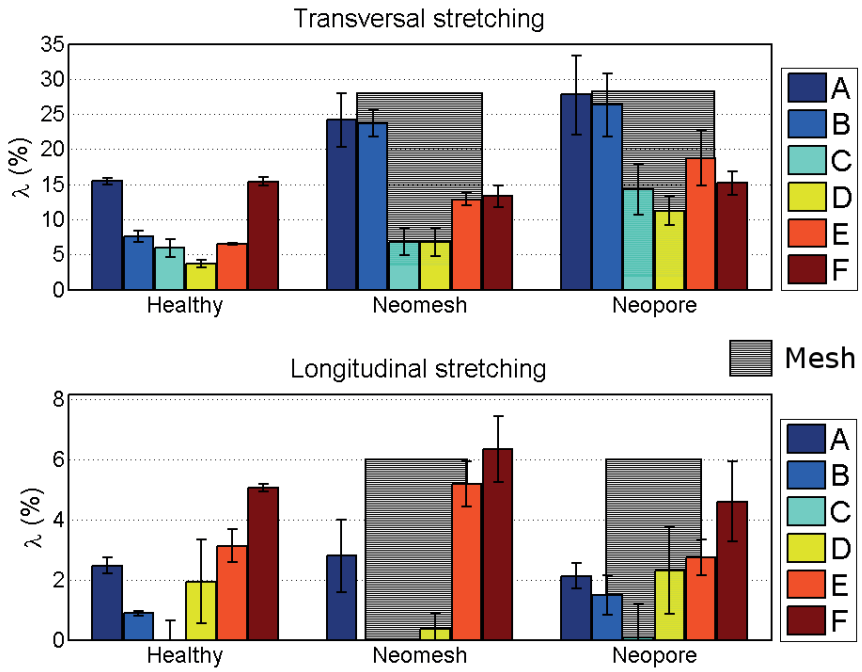

Figure 5.10: Mean and standard deviation of stretching values according to the segments delimited in Fig. 3.14. Exact values are gathered in Table 5.4.

strain (LS) were analysed. Results were also graphically presented along the two preferential directions of the abdomen: longitudinal and transversal.

Maximal displacements (MD) along the abdominal surfaces are shown in Fig. 5.11. As expected, maximum values were found in the central zone of the abdomen for all cases, corresponding to the mesh implantation area. MD for the healthy abdominal wall was about 37.21 mm at the frontal zone of the abdomen. NM and NP were the closest to the healthy response, reaching the maximum displacement on the mesh area with 36.07 and 36.13 mm respectively.

Transverse	**A**	**B**	**C**	**D**	**E**	**F**
Healthy	15.445	7.560	5.904	3.676	6.487	15.362
Neomesh Soft	24.139	2.715	6.783	6.795	12.849	13.301
Neopore	27.793	26.301	14.235	11.248	18.709	15.165
Longitudinal	**A**	**B**	**C**	**D**	**E**	**F**
Healthy	2.463	0.888	0.386	1.938	3.123	5.056
Neomesh Soft	2.788	-1.157	-1.876	0.353	5.172	6.327
Neopore	2.1223	1.485	0.073	2.310	2.736	4.598

Table 5.4: Mean stretching values for 12 mmHg in the transverse and longitudinal direction (%).

No great differences were noticed between the anisotropic NP and the isotropic NM behavior concerning the MD map. With regards to the other two meshes, SS presented a MD up to 42.84 mm, greater than any other case, while SUR showed a the stiffest response with a MD of 34.41 mm.

Maximal principal stresses (MPS) computed on the abdominal wall model are presented in Fig. 5.12. MPS on the healthy model were uniform distributed, presenting only small variations due to the change of material parameters assumed along the surface or in zone close to the boundary conditions. In the frontal abdomen, MPS for the healthy case reached a maximum value of $4.015 \cdot 10^{-2}$ MPa.

When the hernial defect was computed MPS were also modified at the frontal zone of the abdomen. Simulations of the repaired model returned higher values of MPS than those found the healthy wall. When an element in the center of the hernial defect was examined in the implant simulations, MPS took values of 0.127, 0.125, 0.101 and 0.133 MPa for the NM, NP, SS and SUR mesh respectively. Close to the suture zones, where there is a stress concentration due to the discontinuity provoked by the surgical mesh, MPS on the prothesis were 0.159, 0.158, 0.107 and 0.241 MPa for the NM, NP, SS and SUR mesh respectively.

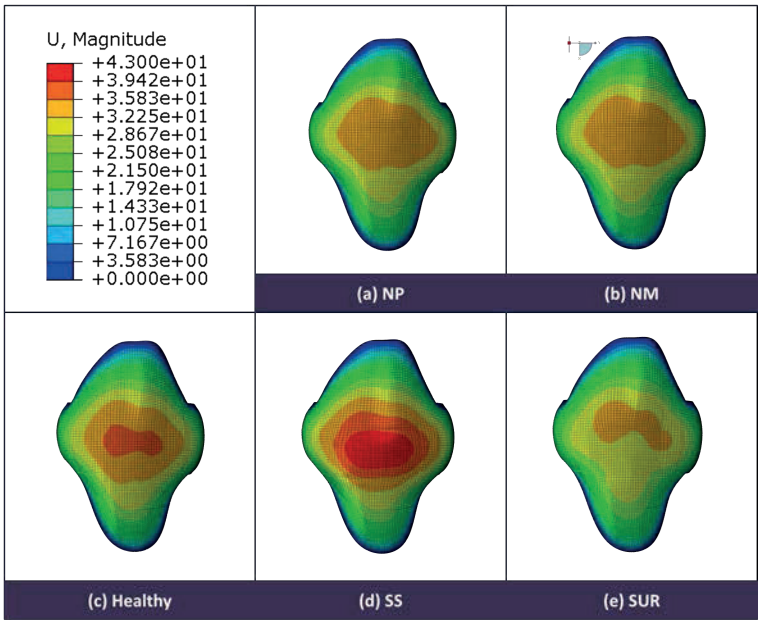

Figure 5.11: Displacement [mm] computed on the same model for the healthy and four meshes considered in the study.

This peak of stresses caused by the surgical implant, provoked another increase of stress on the abdominal tissue surrounded. The MPS created on the soft tissue resulting from the prothesis pull were 0.087, 0.0823, 0.152 and 0.153 MPa for NM, NP, SS and SUR mesh respectively. This peak values did not appeared on the same element but it varied depending on the stiffness shown by the mesh in each direction. For the SUR mesh, the MPS appeared on the tissue joined to the mesh sides closer to the laterals of the abdomen, while in the SS it was in the mesh sides closer to the head and tail. NM and NP shown a uniform distribution of the MPS in the tissue around the mesh.

Finally, results obtained for the healthy case and those repaired by a synthetic mesh were compared along longitudinal and transversal direction. Similarly to the prior section, longitudinal direction was defined parallel to the craneo-caudal direction and was denoted by the path A-B (see top of the Fig. 5.13), whereas the

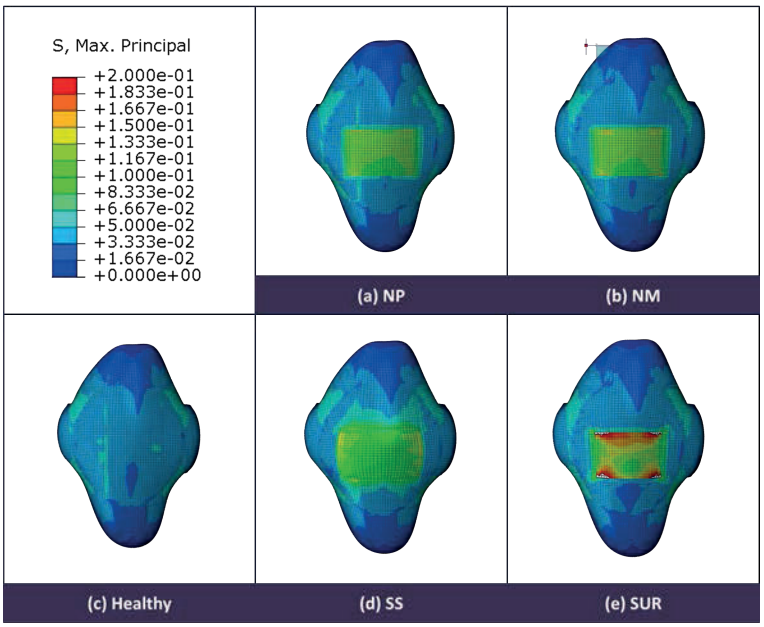

Figure 5.12: Maximal principal stresses [MPa] computed on the same model for the healthy and four meshes considered in the study.

transversal direction lied perpendicular, denoted by the path C-D. In all cases, the abscissa shows the normalized distance of the paths A-B and C-D, where $x = 0$ and $x = 1$ correspond to points A/C and B/D respectively. Maximal displacements are shown in Fig. 5.13(a) and (b), maximal principal stresses in (c) and (d) and logarithmic strain in (e) and (f).

According to the MD, SUR mesh restricted movement throughout of the repaired defect due to the greater stiffness. In contrast, the MD recorded throughout the SS mesh notably exceeded the displacement corresponding to the natural distensibility of a healthy abdomen. NM and NP presented the most similar response in displacements to the obtained by the healthy case. Both of them slightly decreased the natural distensibility of the abdomen although quite cushioned.

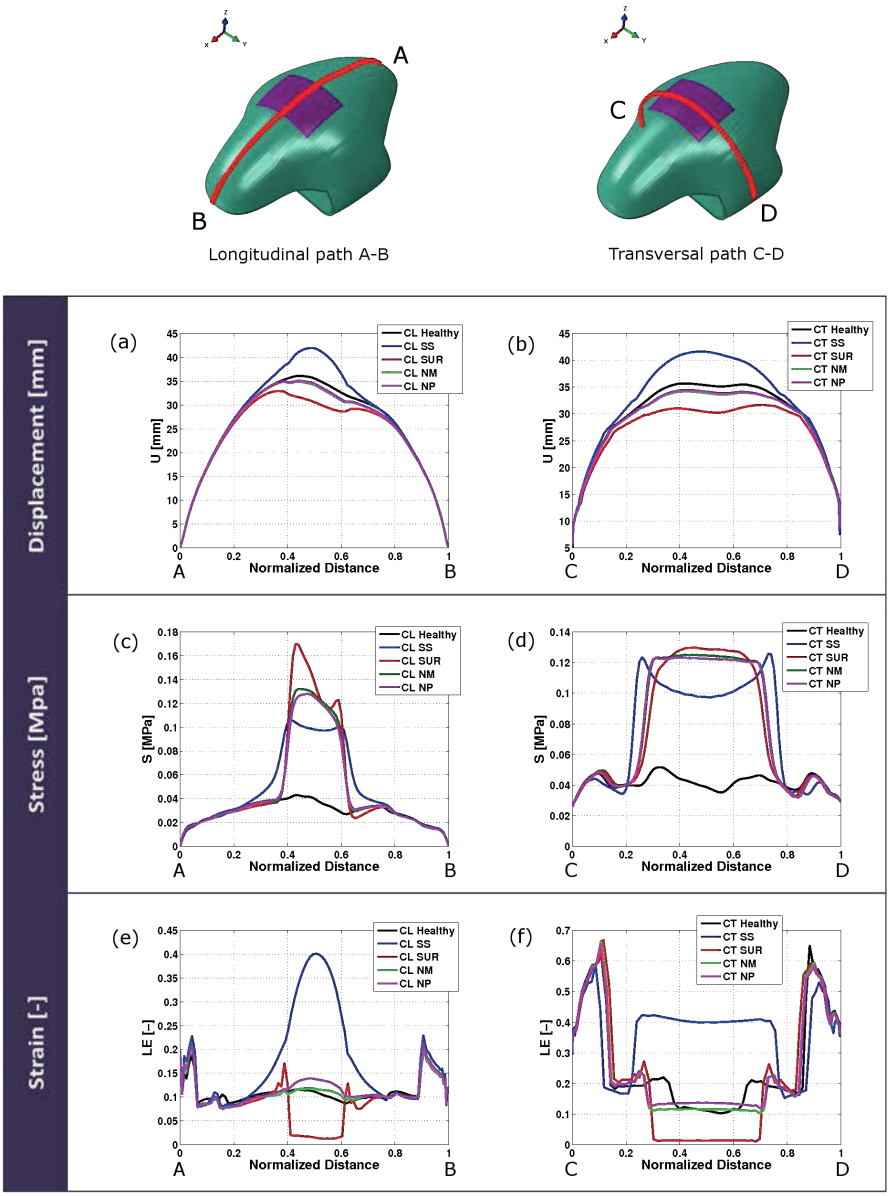

Figure 5.13: Displacements (a,b), maximal stresses (c,d) and logarithmic strain (e,f) computed along the longitudinal (A-B) and the transversal (C-D) paths the healthy specimen and those repaired with four surgical meshes.

Regarding the MPS, the greater stiffness of the prostheses compared to that of the tissue led to a marked increase in MPS in the area of the defect. The difference of the thickness considered for the abdominal wall and the synthetic meshes also contributed to mark this effect. This increase of MPS was specially noticeable for the NM, NP and SUR meshes, and lightly lower in the case of SS due to its great compliance.

Logarithmic strain shown in the Figs. 5.13(e) and (f), came influenced by the change in the material parameters, which explains the side LE peaks of both longitudinal and transversal graphics. Attending to the defect area, SUR presented a strong stiffening with respect to the healthy response, while SS mesh shown a compliance much higher than the healthy case. Again, NM and NP shown a LE quite similar to that assessed to the central area, corresponding to the rectus abdominis.

5.4 Discussion

In order to improve the mechanical aspects of the surgical hernia treatment, mechanical properties of the surgical mesh need to approximate the mechanical properties of the abdominal wall (Conze and Klinge, 1999). Moreover, the mechanical response of the mesh once inserted into the abdominal tissue should mimetize the response of a healthy abdomen. That is why reliable numerical simulations become so relevant for the future of hernia surgery.

In this Chapter, the mechanical response of four synthetic meshes have been determined and subsequently compared to the mechanical behavior of a healthy abdominal wall. In a first stage, isolated meshes were subjected to biaxial loading tests and then they were characterize based on the biaxial results. Concurrently, two of these meshes were implanted in an animal model to repair a total defect and the whole repaired abdomen was subjected to pneumoperitoneum tests. *In vivo* passive response was compared to the healthy response. Finally, a FE model of a repaired specimen was reconstructed and the mechanical tests was simulated

for the four surgical meshes analysed in the biaxial tests.

The mechanical biaxial tests performed on the surgical meshes confirmed the anisotropy supposed on each mesh, showing a higher level of anisotropy in the case of SS, followed by the NP, SUR and finally the NM, which behaved as an isotropic material. Biaxial tests revealed SUR mesh as the stiffest one, which agreed with prior works that remarked the stiff behavior of this implant (Hernández-Gascón et al., 2011; Röhrnbauer and Mazza, 2013), and SS as the most compliant mesh used here. NP and NM remained between the other two, stiffer than SS and more compliant than SUR. Unfortunately, to the author's knowledge there is not any existing work in literature where the material properties of DIMA meshes were analysed, so results here obtained cannot be compared.

SUR material parameters, obtained from work developed by Cordero et al. (2015), agreed with the findings of Röhrnbauer and Mazza (2013) and can be correlated with Hernández-Gascón et al. (2011), although mechanical tests performed in this work were uniaxial. *In vivo* response of the SUR mesh was studied in Chapter 3, when this mesh was inserted in a healthy abdomen and analysed following the same procedure than in this Chapter. Results obtained in that section shown how the stiff behavior of the SUR provoked a decrease on the natural mobility of the healthy tissue in about 30% . The *in vivo* results were properly reproduced with the numerical simulation performed in this Chapter on the FE model of a repaired specimen although lightly cushioned, since FE analysis computed a decrease in MD about 15-20% . This difference could be explained by the fact that distinct specimen were considered.

When *in vivo* response of the DIMA meshes was analysed, both meshes NP and NM exhibited a mechanical response in the abdomen very close to the healthy specimen, which indicates the goodness of these implants from the mechanical approach. The anisotropy of the NP can be noticed in the increase of transversal stretching in the area where the mesh was inserted. However, this anisotropy was not visible in the longitudinal direction where NM was stiffer than the NP, contrary to the expected from biaxial tests. This difference can be explained

by the fact that according to the biaxial tests, the longitudinal direction of the NP mesh behaves more similar to the NM than the transversal direction, which presents a more compliant behavior (see Fig. 5.5).

With regard to the numerical simulations performed on the FE model, results agreed to those obtained during the *in vivo* tests. NP and NM were the closest to the healthy response (see Fig. 5.11) and MD computed in numerical simulations were similar to the MD obtained after the pneumoperitoneum. The anisotropy of the NP is not visible in the displacement maps, but it can be seen in Fig. 5.13 (e) and (f) where the strain computed for the NP was lightly greater than the NM, concurring with the stretching analysis performed on the *in vivo* specimen (see Fig. 5.10). Based on the stretching measured along the longitudinal and transversal direction, NP seems to better reproduce the healthy results. This assumption is endorsed by the pressure displacement curves shown in Fig. 5.9, where NP also exhibited a mechanical behavior along the test closer to the healthy group.

Regarding the computed response of the macroporus ultralight-weight SS mesh, this implant permitted greater displacements to those needed to mimic the natural distensibility of the abdomen. Despite the benefits associated to a LW or ULW mesh in terms of foreign body reaction, infection risk or postoperative pain (Klosterhalfen et al., 2002; Brown and Finch, 2010; Li et al., 2012), this type of meshes are also frequently related to a higher risk of breakage (Lintin and Kingsnorth, 2014; Blázquez Hernando et al., 2015). Although additional mechanical tests should be performed to address breaking stretch and stress and properly determine the risk of breakage, based on the excessive elongation observed in this mesh, the use of SS is not recommended for hernia repair.

This study is not exempt from some limitations. First, experimental data for the mechanical characterization of meshes was obtained by a fitting procedure of biaxial tests. Further information from other mechanical tests, such as inflation or bulge test, would be useful to complete the characterization. Concerning to the *in vivo* study, it is subjected to the same limitations that those previously

mentioned in Chapter 3. Besides, widen the *in vivo* experimentation to the use of the other two meshes involved in the study, SS and SUR, would help to complete the results. During the pneumoperitoneum tests, only the passive response at low pressure is studied. However, it would be necessary to analyse the response of the abdomen when inner pressure is increased, as a result of physiological actions such as sneeze or standing cough. This may imply to spread the analysis to the active response of the muscle. Attending to the FE model and numerical simulation, 3D model was based on the measurements taken by cameras during the experimental tests. This method should be improved in order to increase the accuracy of the reconstruction, specially in the zones were the boundary conditions were assessed. Additionally, material parameters assumed for the healthy abdominal tissue were extrapolated from the distribution obtained after the inverse analysis. However, those distributions were obtained for a specific specimen and they may vary when a different specimen is considered. Lastly, this study makes reference to the short term response of the mesh after insertion. Long term study, complemented to a biological analysis of the interaction mesh-tissue would definitely improve significance of this findings.

Despite this limitations, relevant and useful information was provided here. Based on biaxial data of four surgical meshes, their effect after being used to correct a total defect performed on a healthy abdominal was analysed. Results were given in terms of maximal displacements, stresses and strains provoked on the abdomen. This information may contributed to help surgeons to choose which mesh better reproduce the mechanical response of the healthy tissue, and thereby reducing the risk of mesh breakage, pain or discomfort in the patient.

6

Conclusions and future work

This Chapter includes a brief summary of the work developed in this Thesis along with the main conclusions extracted from the fulfillment of this work. In addition, some future lines in the research field of the *in vivo* characterization of abdominal muscle are suggested.

6.1 Conclusions

Through this Thesis, several aspects of the mechanical characterization of the abdominal wall has been considered. Previous works developed on this area used

to tackled this problem by determining mechanical properties of each component and muscle layer of the abdominal wall and computing the whole when working together. Although this approach presents the benefits of working with higher number of samples and a more accurate fitting of each element, it does not go beyond an *in vitro* approximation so real features of abdominal wall when subjected to physiological loading state are inevitably missed. Thus, an *in vivo* approach and its implementation to the hernia repair is presented here.

First, an initial biomechanical study of a wound closure in abdominal wall was performed. In this study, four different types of suture were tested on three locations of the linea alba and their progress was analysed at short and long term from biological and mechanical point of view. Then, the *in vivo* passive response of the whole abdominal wall was determined in an animal model by photogrammetry and subsequent mechanical research was carried out. Experimental data was post processed by an inverse analysis algorithm, which provided the material parameter distribution that better reproduced the experimental response, determining the mechanical characterization for the anterolateral abdominal wall. This characterization was used to recreate a FE model where different surgical meshes, used in the hernia repair field, were tested and evaluated.

Main conclusions extracted from this work are listed below:

- The *Assuplus*® suture (non-absorbable, polyurethane) revealed as the most appropriate material for a wound closure linea alba. At short term, when the tissue has not started to heal and most loading of the wound is devolved upon the sutures, the tissue closed with this material presented greater resistance to mechanical force due to a higher amount of collagen I presented on the tissue. At long term, all sutures closure showed similar behavior and none of them could mimic healthy tissue. No significant differences were found between absorbable and non-absorbable materials and the new model of barbed suture did not entailed any additional benefit beyond the possibility of avoiding knots during the wound closure.

- The pneumoperitoneum test needed during the first steps of any laparoscopy can be used to obtain mechanical information of the passive response of abdominal tissue. To that end, non invasive measurement techniques must be used so that the *in vivo* response was not altered. This method can provide pressure displacement relations on different zones of the abdomen.

- Pressure-Displacement curves obtain from the pneumoperitoneum test are reproducible from the second test on. During the first cycle, the distribution of the gas inside the cavity and an internal reshaping of the diaphragm movement provoke an abdominal response that is not presented on the following tests.

- During the pneumoperitoneum tests, tissue located on the lateral sides of the abdomen (formed by the transversal, external and internal muscle layers) shows a more compliant response than tissue of the central area (formed by the rectus abdominis and linea alba). This result contradicts most previous works presented in literature, but it can be explained considering the different stress levels evaluated on these works.

- The insertion of a *Surgipro*^{TM} provokes a severe stiffening in the abdominal wall that probably involved pain and discomfort to the patient. On the other hand, the other two meshes here tested (*Neomesh Soft*® and *Nopore*®) seem to better reproduce the natural distensibility of the healthy abdomen.

- The heterogeneity of the abdominal wall can be numerically reproduced by a unique constitutive model but a specific distribution of material parameters throughout the abdominal surface. Different values of material parameters would lead in a distinct mechanical behavior. The specific distribution that better reproduces the response of a certain specimen can be obtained by solving the inverse problem, where the unknown variables would be the material parameter in node. To solve this inverse problem the Tikhonov regularization (H^1) rather than the Total Variation Diminishing (TVD) is recommended, since it smooths the solution and provides the same accuracy but a more reliable spatial material distribution.

- The distribution of the material parameters on the abdominal surface showed

a defined zone with higher values. This zone takes the form of wide stripe located along the craneo caudal direction and can be correlated with the mechanical behavior of the rectus abdominis in conjunction with the linea alba.

- The application of the inverse analysis to a certain specimen provides the mechanical characterization of this specific specimen. Since the way of measure is completely non invasive, this technique can be used to determine the particular mechanical requirements of a specific patient. This attribute may be highly beneficial in humans were the mechanical response of the abdominal wall is strongly influenced by age, gender or physical constitution.
- A 3D mechanical model of a specific abdominal wall can also be reconstructed from the photogrammetry technique. This model can be used to perform finite element simulations that determine the mechanical implications of using a particular surgical mesh to repair an hernia defect. Mechanical properties of meshes needed to carry out this simulation can be extracted from prior biaxial mechanical tests.

Some of the main conclusions described on this section have been already presented in international conferences and researching journals detailed in Appendix B.

6.2 Future lines

The work presented in this Thesis constitutes the first but firm steps towards the *in vivo* characterization of the passive mechanical behaviour of abdominal wall. Nevertheless, some future lines should be explored in order to fully determine the *in vivo* response of the abdominal wall and transform this knowledge into a tangible improvement to the surgical hernia repair. Some of these future lines are proposed here:

- The implementation of the methodology to human tissue is the primary and main next step proposed. Since the measurement method has proved to be completely non invasive and the pneumoperitoneum tests are already performed in surgical rooms, the inverse methodology could be applied to human cases to provide mechanical information in a specific patient treatment. In relation to that, a database of mechanical properties considering different attributes, such as age, gender or body-mass index, could be built so that general assumptions based on these properties could be established.

- The process of image acquisition should be developed, improved and automatized. The current method obtains data from the anterolateral wall, but some points of the back remain missed. This could be solved by increasing the number of cameras involved in the process. Besides that, an automatization of the model reconstruction is completely required if the application to the surgical environment becomes real. An interesting way to proceed may lie in the use of magnetic resonance imaging (MRI), which could provide a more accurate reconstruction as well as relevant thickness information.

- New constitutive models should be considered during the inverse analysis to mechanically characterize the abdominal wall. Although the isotropic hyperelastic model here used was able to capture the main deformation noticed in the frontal abdomen, the response at initial stress was missed. Additional models depending on more than two material parameters or materials that include the fiber insertion would definitely help to mimetize the response of the abdominal tissue for the whole process. In such cases, the inverse analysis algorithm should be widen and completed with these new models where additional parameters, as well as the fiber direction, could constitute new variables to optimize.

- A standard database of surgical meshes, that included mesh features (density, pore size, thread size) together with the response to mechanical tests (e.g. uniaxial, biaxial or bulge tests), may help to compare the benefits and drawbacks of each prothesis and determine the optimal conditions for its implementation.

- The study of the active response for different abdominal muscles would be very interesting since it would help to define a complete view of the abdominal wall behavior. The development of a material model that allows for numerically simulating the complete response of the abdominal wall would constitute a real advance in the hernia treatment field.

- A biological modelling of the healing process present after a wound closure or mesh hernia repair would complement the information needed to assess the goodness of a determine prothesis. When a surgical mesh is inserted into the tissue, both biological and mechanical aspects must be satisfied so that the patient does not suffer any postoperative complications. A dual analysis that approach the problem from both points of view could help to reduce postoperative pain and decrease the risk of infection and recurrence.

Appendices

A

Resumen en Español

A.1 Aspectos médicos

A.1.1 Anatomía de la pared abdominal

Se conoce por abdomen a la zona del cuerpo humano que comprende desde el tórax a la pelvis y extremidades inferiores. Esta zona contiene en su interior diversos órganos vitales y está desprovista en gran parte de una estructura ósea que la proteja, por lo que es de suma importancia que la capa de músculo que la recubre esté correctamente formada y definida. Esta capa de músculo recibe el

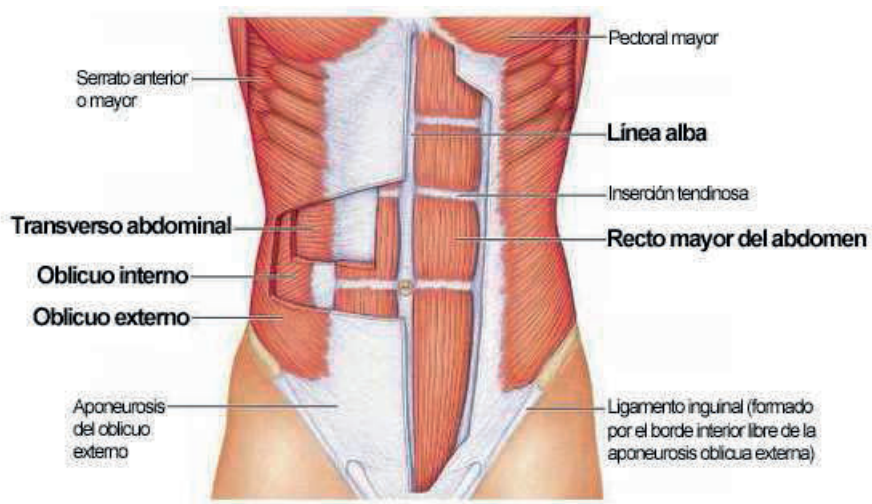

Figure A.1: Músculos principales que conforman la pared abdominal.

nombre de pared abdominal.

Este trabajo tiene como objetivo la caracterización *in vivo* de la región anterolateral de la pared abdominal, que en mamíferos está formada principalmente por cuatro músculos (Minn and Hutchings, 1982; Miller, 1993; Marieb, 2009): oblicuo interno (OI), oblicuo externo (OE), recto mayor y tranverso (TA) (ver Figura A.1). Estos músculos a su vez se distribuyen en tres capas en función de su proximidad a la cara exterior del abdomen. Anatómicamente, en la zona anterior y lateral de la capa más externa se encuentra el oblicuo externo mientras que en la zona central se sitúa el recto abdominal, atravesado longitudinalmente por la linea alba. A continuación en la capa intermedia se encuentra el oblicuo interno y ya por último, el transverso en la capa más interna. Cada uno de estos músculos desarrolla una serie de funciones claves en el movimiento y mantenimiento del cuerpo humano.

El oblicuo externo (OE) se conforma de dos partes situadas a los lados del cuerpo, cada una de las cuales es responsable de la rotación del tronco hacia el

lado contrario y su inclinación lateral. Trabajando ambas partes conjuntamente, se ocupan de la inclinación hacia delante del cuerpo y participan también en la respiración limitando la presión intra-abdominal durante el proceso de espiración (Troyer and Loring, 2011). En esta misma capa pero en la parte central, se extiende el recto mayor, comúnmente conocido como abdominales. Este músculo contribuye directamente a mantener la postura corporal erguida así como a proteger las vísceras internas. Produce flexión de la columna vertebral a través de las costillas e inclinación lateral del tronco con su contracción unilateral. También influye directamente en la evacuación de contenidos abdominales al contraerse ya que aumenta sobremanera la presión intra-abdominal.

El oblicuo interno (OI) situado en una capa más interna desarrolla principalmente dos funciones. Por un lado, ayuda a la respiración ejerciendo presión sobre la pared baja del pecho en función del movimiento del diafragma. De esta manera, contribuye dejando espacio o presionando los pulmones, que de modo reflejo provocarán la inhalación o exhalación del aire respectivamente. Por otro lado, colabora con el OE en la rotación del tronco, modulando el grado de rotación entre la caja torácica y el hueso de la pelvis.

Por último los músculos transversos (TA) denominados así por la disposición de las fibras musculares, se sitúan tras el IO en la capa más interna de la musculatura. Sus funciones primordiales son las de comprimir el abdomen actuando como prensa, ejerciendo contracción o distensión en la pared abdominal y aportando estabilidad al tórax y pelvis. Sin embargo, este músculo también interviene en muchas de las acciones cotidianas del ser humano tales como la micción, vómitos o espiración forzada, y colabora directamente durante el parto en las mujeres embarazadas.

Además de la parte muscular existen otros componentes anatómicos que colaboran en las funciones desarrolladas por el abdomen, algunas de las cuales convendría destacar para un mejor entendimiento de esta tesis. La linea alba es una banda de tejido fibroso situada entre los rectos y formada por la unión de las aponeurosis del resto de músculos comentados. Está formada principalmente de

tejido conectivo, por lo que se le atribuye un comportamiento bastante rígido. Por otro lado tenemos el peritoneo, que es una fina membrana que recubre los órganos internos y sirve como conducto de vasos sanguíneos y nervios. Otro elemento importante es el diafragma, situado en la parte más baja de la caja torácica. Este músculo influye de manera directa en la respiración de los mamíferos y está relacionado con la presión intra-abdominal que domina tantas funciones anatómicas. Por último nombrar el ligamento inguinal, que es donde tienen lugar las hernias inguinales, y el suelo pélvico que mantiene las vísceras y colabora en el control de la presión intra-abdominal.

Atendiendo a la composición del material, el tejido muscular se considera como una red de fibras musculares, de colágeno y elastina, embebidas en una matriz extracelular. La necesidad de diferenciar entre estas fibras radica en las distintas propiedades que tiene cada una de ellas, ya que su cantidad y dirección determinan directamente la respuesta del material desde el punto de vista mecánico del tejido. En el músculo las fibras de tejido conjuntivo, fundamentalmente colágeno, son las responsables de la resistencia y rigidez, lo que se conoce como comportamiento pasivo del músculo. Las fibras musculares, por otra parte, son las responsables de la contracción muscular, es decir, la generación de fuerza y movimiento conocida como respuesta activa del músculo.

La pared abdominal está sometida a diferentes fuerzas externas propias de la actividad diaria. Como se ha comentado anteriormente, actividades como flexionar el cuerpo, toser o simplemente respirar provocan un aumento de la presión intra-abdominal que el músculo ha de ser capaz de soportar con su respuesta activa y pasiva. Cuando se produce una descompensación entre dichas tensiones, pueden desarrollarse debilitamientos o incluso a pequeños desgarros en la pared abdominal, dando lugar a la aparición de hernias.

Dentro de las causas que pueden producir una hernia se encuentran, por tanto, todas aquellas que generen una esfuerzo intenso en la zona abdominal, tales como el embarazo, tos crónica, obesidad o elevación de pesos pesados entre otros.

A.1.2 Cirugía herniaria

Se entiende por hernia a la protrusión de parte de un órgano o tejido fuera de la cavidad reservada para ellos. Esta afección es debida a una debilidad en la pared muscular que debiera proteger los tejidos internos y que permite que se desplacen traspasando el músculo y provocando un abultamiento en la superficie exterior.

Si la protusión es pequeña o está en las primeras etapas suelen tratarse de hernias reducibles, que pueden ser colocadas suavemente en su posición original de un modo manual y sin el uso de la cirugía. Este tipo de hernias pueden mostrar o no un síntoma externo, de modo que mientras la protrusión no conlleve dolor el paciente no siempre es consciente de su aparición. Sin embargo, con el paso del tiempo suelen aumentar de tamaño y problemática, ya que las hernias no se curan de modo espontáneo. Cuando la protusión aumenta hasta el punto en el que interfiere en el riego sanguíneo de la zona se convierte ya en un riesgo para el paciente y por tanto, en una emergencia médica. Se hace necesario en esos casos una intervención quirúrgica.

Aunque pueden producirse en cualquier parte del cuerpo, la zona más frecuente de aparición de hernias es la zona abdominal, entre las que se engloban entre otras las hernias inguinal y umbilical, responsables de un alto porcentaje de los casos. Otras clasificaciones comunes, dentro del área de la medicina, diferencian los tipos de hernias según el contenido del saco, gravedad de la afección, criterios anatómicos o incluso personales, siendo la clasificación por zona de aparición la más general y determinante.

Atendiendo al tratamiento de esta afección, se han venido utilizando diversos métodos que pueden paliar temporalmente el dolor producido por una hernia. Sin embargo, a la larga, el único tratamiento fiable y definitivo para la reparación del músculo es la intervención quirúrgica. El procedimiento estándar consiste en unir los bordes del área debilitada, bien mediante una sutura si el orificio es pequeño o con una malla sintética si la zona es importante o está tan debilitada que no es

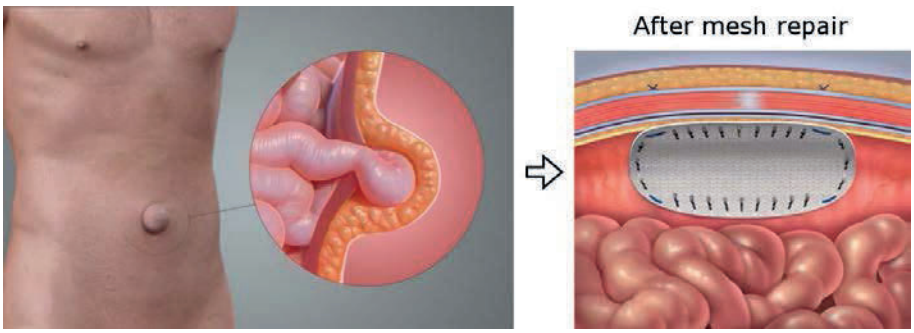

Figure A.2: Ejemplo de hernia ventral y tratamiento con malla.

capaz de soportar la tensión de la sutura. Esta malla es la encargada de estabilizar y reforzar los defectos de los tejidos blandos, sirviendo como refuerzo mecánico al músculo mientras este se regenera.

La colocación de esta malla puede realizarse tanto por laparoscopia como por cirugía abierta y ambos procedimientos son comúnmente utilizados hoy en día en los quirófanos. Sin embargo, la laparoscopia es una técnica menos invasiva que reduce y simplifica el postoperatorio del paciente, por lo que su uso se está extendiendo a muchas de las intervenciones realizadas actualmente (Reza and Blasco, 2004; Sanz et al., 2010). El procedimiento diseñado en este proyecto está pensado preferentemente para reparación de hernias mediante laparoscopia, aunque no excluye los casos que se traten con cirugía abierta.

Para evitar dolor o molestias posteriores en el paciente, así como el rechazo biológico por parte de los tejidos, estas mallas han de cumplir ciertos requisitos. El más importante, es que debe ser capaz de acompañar y reproducir el comportamiento mecánico del músculo al que refuerza, ya que si es demasiado flexible el defecto volverá a aparecer y si por el contrario sobrepasa su rigidez, puede llegar a provocar desgarros en la sutura además de molestias al paciente. El comportamiento mecánico de la malla depende de factores como el material, tamaño de poro, forma o tipo de fibra que la conforma. El comportamiento mecánico del músculo que refuerza, sin embargo, es algo más difícil de determinar ya que varía

con la persona según su constitución, edad, etc.

Para caracterizar un material, desde el punto de vista mecánico, existen diferentes ensayos experimentales. En el caso de los tejidos biológicos, y más concretamente en tejido muscular, se recurre a menudo a ensayos de tracción uniaxiales o biaxiales en los que se somete una probeta de material a un historial de carga determinado, con el fin de poder obtener la relación tensión-deformación. La limitación de este tipo de ensayos es que se tratan de ensayos *in vitro* en los cuales la probeta es extraída de su localización inicial en el ser vivo. Eso hace que pierda parte de sus propiedades mecánicas y el estado tensional al que está inicialmente sometido. Además, aunque se consiguiera caracterizar un tejido a partir de este tipo de ensayos, la información que nos aporta puede variar respecto al mismo tejido de otro espécimen, con lo que no sería de utilidad.

La solución que se propone, por tanto, es la de intentar caracterizar el tejido de interés (en este caso pared abdominal) mediante un ensayo *in vivo* y medir los resultados del ensayo de una manera no invasiva para que la medida no perturbe la respuesta mecánica de la pared. Los procedimientos y metodología propuestos son los que se explican a lo largo de esta tesis.

A.2 Motivación

La principal motivación de esta tesis reside en la necesidad de ampliar el conocimiento de la respuesta mecánica pasiva de la pared abdominal para poder aportar información en casos específicos de patologías herniarias.

Aunque la reparación de hernias es un procedimiento ampliamente utilizado en los quirófanos, lo cierto es que debido a sus índices de recurrencia y complicaciones postoperatorias esta técnica sigue llamando la atención de pacientes, cirujanos e industria médica. ÃŽltimamente, una de la técnica más aceptadas es la hernioplastia por vía laparoscópica, que consiste en la implantación por medio del laparoscopio de una malla quirúrgica que cubra parcial o totalmente el de-

fecto herniario. El propósito de esa malla es el de reemplazar mecánicamente al músculo mientras éste se regenera, reduciendo de esta manera el tiempo de espera del paciente antes de volver a su vida normal. Para evitar posibles molestias al paciente, esta malla tiene que ser biológicamente compatible con el tejido y reproducir su comportamiento mecánico la más fielmente posible ya que de otro modo la inserción de la malla puede llegar a provocar dolor, inflamación o incluso desgarro. Hoy en día hay una amplia gama de prótesis herniarias en el mercado, sin embargo, el protocolo de elección de malla no está todavía definido y los cirujanos deben basarse en su experiencia e intuición para elegir. Puesto que la malla tiene que mimetizar el comportamiento mecánico del abdomen hace falta por tanto entender el comportamiento mecánico del músculo para elegir la malla adecuada.

Sin embargo, el tejido abdominal todavía no está completamente caracterizado. En la literatura existen múltiples trabajos referentes a este tema donde se intenta caracterizar los músculos abdominales a partir de ensayos *in vitro*. Estos trabajos, si bien aportan una información muy valiosa para en entendimiento del músculo, no dejan de ser trabajos *in vitro* cuya repuesta pueden diferir de la real al ser ensayados en condiciones distintas a las fisiológicas. Debido a la complejidad del los estudios *in vivo*, el número de trabajos previos encontrados en la literature se reduce drásticamente y de acuerdo con el conocimiento de la autora de esta tesis, todavía no se han determinado las propiedades mecánicas del comportamiento *in vivo* de la pared abdominal.

Respecto a esta caracterización, hay que tener en cuenta que ese comportamiento *in vivo* no va a ser igual para todos los pacientes, sino que factores como el sexo, edad o condición física del paciente pueden alterar la respuesta específica de esa pared abdominal. Según lo expuesto anteriormente, la malla ideal es aquella que mejor reproduce el comportamiento del tejido abdominal sano. Por ello, para seleccionar la malla idónea con vistas a un paciente específico se hace indispensable determinar *in situ* el comportamiento mecánico de su pared abdominal, es decir, su caracterización *in vivo*.

Proveer a los cirujanos de la información mecánica de un paciente específico,

que facilite la correcta elección de la prótesis y mejore con ello tratamiento de patologías herniarias, constituye la principal motivación de esta Tesis.

A.3 Objetivos

Basado en la motivación expuesta en el apartado anterior, el objetivo principal de esta Tesis es el diseño de una metodología que permita caracterizar *in vivo* la respuesta mecánica pasiva de la pared abdominal. La idea futura sería poder aplicar esta metodología en un quirófano, y utilizar el neumoperitoneo previo a una cirugía laparoscópica como fuente de información mecánica para esa caracterización. Con ello, una vez automatizado el proceso, los cirujanos podrían obtener información mecánica relevante que les permitiese evaluar de una forma cuantitativa la idoneidad de cada prótesis herniaria.

Sin embargo, para poder introducir cualquier innovación en un quirófano, esta debe estar antes comprobada y verificada en un modelo animal. En este caso dados su manejabilidad, bajo coste y similitud en cuanto a anatomía del abdomen, el modelo de animal utilizado ha sido el conejo de Nueva Zelanda. Para alcanzar el objetivo general previamente expuesto se definieron diversos objetivos parciales que se han ido cumpliendo en el desarrollo de esta Tesis.

- Estudio de los procesos biológicos que tienen lugar tras el cierre con distintos materiales de una incisión en la línea alba y correlación con su resistencia mecánica a corto y largo plazo.
- Búsqueda y adaptación de una técnica de adquisición de imagen que permita obtener información de una manera no invasiva durante el neumoperitoneo.
- Realización de ensayos de inflado en el modelo animal (neumoperitoneo inducido). Entendimiento de los dispositivos médicos utilizados en el proceso así como de los procesos internos que tienen lugar dentro de la cavidad abdominal durante el desarrollo del ensayo. Ensayo realizado sobre animales

sanos y otros con un defecto inducido reparado con una malla de alta densidad (Surgipro^{TM}).

- Obtención de coordenadas y desplazamientos en la región anterolateral del abdomen. Evaluación de diferencias entre espécimen sano y herniado basado en las medidas experimentales. Reconstrucción de la cavidad abdominal y evolución de la durante el ensayo. Estudio de propiedades mecánicas en distintos puntos de la superficie abdominal.

- Creación de un modelo de elementos finitos a partir de las medidas experimentales y aproximación a la caracterización de la pared abdominal usando un mismo modelo constitutivo y parámetros de material (respuesta homogénea) aplicando la metodología de superficies de respuesta.

- Caracterización de la pared abdominal suponiendo variación de parámetros (respuesta heterogénea) por medio de análisis inverso. Comparación de resultados con dos tipos de regularización para el problema de optimización: Total Variation Diminishing (TVD) y Tikhonov (H^1).

- Ampliación de la parte experimental. Aumento de muestra de especímenes sanos y nuevos ensayos en casos reparados con dos mallas sintéticas de polipropileno: *Neomesh Soft*® y *Neopore*® (DIMA S.L.).

- Caracterización mecánica de cuatro mallas herniarias a partir de ensayos biaxiales. Comparación entre su respuesta *in vitro* y la obtenida *in vivo* una vez implantadas.

- Construcción de un modelo de elementos finitos de la pared abdominal correspondiente a un espécimen herniado y capaz de reproducir su respuesta tras reparar el defecto con distintos materiales protésicos.

A.4 Contribuciones originales

A continuación se detallan las principales contribuciones originales en las que se ha recogido gran parte del trabajo detallado en esta tesis. También se muestran

algunas publicaciones cuyo trabajo no está aquí incluido, pero que sin duda han aportado un conocimiento transversal que ha contribuido en varias secciones de la tesis.

A.4.1 Publicaciones

Los siguientes trabajos hacen referencia a artículos escritos publicados (o próximamente publicados) en revistas científicas internacionales, cuyo contenido está total o parcialmente recogido en esta tesis.

1. **Simón-Allué R.**, Pérez-López P., Sotomayor S., Peña E., Pascual G., Bellón J.M., Calvo B. Short- and long-term experimental and biomechanical study of new suture types in abdominal wall closure. *Journal of the Mechanical Behavior of Biomedical Materials* 37 (2014):1-11. **doi**:10.1016/j.jmbbm.2014.04.014.
   FI: 2.876 (Q1: 18/76 Engineering, Biomedical)

2. Bellón J.M., Pérez-López P., **Simón-Allué R.**, Sotomayor S., Pérez-Köehler B., Peña E., Pascual G., Calvo B. New suture materials for midline laparotomy closure: an experimental study. *BioMed Central Surgery* 14 (2014):1-11. **doi**: 10.1186/1471-2482-14-70.
   FI: 1.469 (Q3: 107/200 Surgery)

3. **Simón-Allué R.**, Montiel J.M.M., Bellón J.M., Calvo B. Developing a new methodology to characterize in vivo the passive mechanical behavior of abdominal wall on an animal model. *Journal of the Mechanical Behavior of Biomedical Materials* 51 (2015):40-49. **doi**:10.1016/j.jmbbm.2015.06.029.
   FI: 2.876 (Q1: 18/76 Engineering, Biomedical)

4. **Simón-Allué R.**, Calvo B., Oberai A., Barbone P. Mechanical characterization of abdominal wall by inverse analysis on an animal model. *Journal of the Mechanical Behavior of Biomedical Materials* (2016) *Under review.*

5. **Simón-Allué R.**, Ortillés A., Calvo B. Mechanical behavior of meshes for repair abdominal wall: in vivo versus biaxial characterization. *Under preparation.*

Por otro lado, también se detallan dos publicaciones adicionales que se han realizado paralelamente al desarrollo de esta tesis. Su elaboraciÃşn, si bien no está directamente relacionada con el contenido de la tesis, ha contribuido definitivamente a mejorar el contenido de la misma.

1. **Simón-Allué R.**, Cordero A., Peña E. Unraveling the effect of boundary conditions and strain monitoring on estimation of the constitutive parameters of elastic membranes by biaxial tests. *Mechanics Research Communications* 57 (2014):82-89. **doi**:10.1016/j.mechrescom.2014.01.009.
FI: 1.400 (Q2: 65/135 Mechanics)

2. **Simón-Allué R.**, Hernández-Gascón B., Lèoty L., Bellón J.M., Peña E., Calvo B. Prostheses size dependency of the mechanical response of the herniated human abdomen. *Hernia* (2016) 1-10. **doi**:10.1007/s10029-016-1525-3.
FI: 2.054 (Q2: 67/200 Surgery)

A.4.2 Congresos

Las siguientes ponencias han sido presentadas en reuniones y congresos nacionales e internacionales relacionados con el ámbito científico dentro del área de la ingeniería mecánica o la biomécanica.

1. **Simón-Allué R.**, Agudo A., Montiel J.M.M., Calvo B. Mechanical characterization of abdominal muscle by stereo images. *III Reunión del Capítulo Nacional Español de la Sociedad Europea de Biomecánica* (ESB). Barcelona (Spain), 2013.

2. **Simón-Allué R.**, Montiel J.M.M., Calvo B. Mechanical characterization of abdominal muscle using photogrammetry. *6^{th} Surgical Robotics Summer School.* Montpellier (France), 2013.

3. **Simón-Allué R.**, Agudo A., Montiel J.M.M., Calvo B. Caracterización mecánica del músculo abdominal a partir de imágenes 2D. *I Jornadas Doctorales Campus Iberus.* Jaca (Spain), 2014.

4. **Simón-Allué R.**, Montiel J.M.M., Calvo B. Caracterización mecánica del músculo abdominal mediante fotogrametría y análisis inverso. *I Jornada de Doctorandos del Programa de Doctorado en Ingenería mecánica.* Zaragoza (Spain), 2014.

5. **Simón-Allué R.**, Agudo A., Montiel J.M.M., Bellón J.M., Calvo B. Mechanical characterization of abdominal muscle using stereo imaging. *11^{th} World Congress on Computational Mechanics (WCCM XI).* Barcelona (Spain), 2014.

6. **Simón-Allué R.**, Oberai A., Montiel J.M.M., Calvo B. Mechanical characterization of abdominal muscle by inverse analysis on an animal model. *21^{st} Congress of the European Society of Biomechanics.* Prague (Czech Republic), 2015.

7. **Simón-Allué R.**, Oberai A., Calvo B. Using inverse finite element analysis to obtain passive mechanical behavior of abdominal wall. *IV Jornada Jóvenes Investigadores Instituto de Investigación en Ingeniería de Aragón.* Zaragoza (Spain), 2015.

8. **Simón-Allué R.**, Oberai A., Barbone P., Calvo B. In-vivo mechanical characterization of abdominal muscle by inverse analysis. *III Jornada de Doctorandos del Programa de Doctorado en Ingenería mecánica.* Zaragoza (Spain), 2016.

9. **Simón-Allué R.**, Oberai A., Barbone P., Montiel J.M.M., Calvo B. Towards in vivo mechanical characterization of abdominal wall. *7^{th} Summer School on Biomechanics of Soft Tissues: Multiscale Modeling, Simulation and Applications.* Graz (Austria), 2016.

A.5 Conclusiones

A lo largo de esta tesis se han tratado distintos aspectos relacionados con las caracterización mecánica de la pared abdominal. Trabajos previos encontrados en literatura coincidían en tratar de abordar el problema de dentro a fuera, es decir, tratar de caracterizar cada una de las capas de músculo y resto de componentes del abdomen para conseguir reproducir de un modo numérico la respuesta de la pared entera. Aunque está aproximación presenta muchas ventajas en cuanto al número de muestras a ensayar o la exactitud de cada ajuste experimental, lo cierto es que no pasa de ser una experimentación *in vitro*, y por tanto parte de las propiedades mecánicas reales del tejido se pierden.

En este trabajo se presenta el tipo de aproximación opuesta, es decir, desarrollar una metodología para intentar caracterizar el tejido de la pared abdominal de una manera general (sin distinguir inicialmente capas) a partir de unos ensayos experimentales realizados *in vivo* y medidos de una manera completamente no invasiva.

Para ello, se ha realizado inicialmente un estudio biológico y mecánico del cierre de una herida situada a distintas alturas de la línea alba y cerrada con 4 tipos distintos de hilos de sutura. El tejido suturado se analizó a corto y largo plazo para tener en cuenta su cambio de propiedades en función del grado de regeneración del tejido. Después, se llevaron a cabo unos ensayos mecánicos sobre el abdomen de un modelo animal *in vivo* en el que se determinó mediante fotogrametría la respuesta mecánica pasiva de la pared. Los datos experimentales obtenidos fueron analizados numéricamente, primero con la metodología de superficies de respuesta y después mediante un análisis inverso que permitió obtener la distribución de parámetros mecánicos a lo largo de la superficie abdominal. A partir de esa caracterización se reconstruyó un modelo de elementos finitos de un abdomen herniado en el que se evaluó el efecto provocado por la reparación de distintas prótesis frente a la respuesta del tejido sano.

Las conclusiones que se pueden extraer del estudio biomecánico recogido en esta tesis son las siguientes:

- Respecto al cierre de la linea alba, la sutura elástica PUe demostró ser el material óptimo en términos biológicos y mecánicos. A corto plazo, cuando el tejido todavía no ha comenzado a regenerarse y por tanto la sutura es la responsable de absorber la mayor parte de la carga, este material mostró mayor resistencia mecánica debido a un mayor contenido de colágeno I, también llamado colágeno maduro, en el tejido que regenerado a su alrededor. A largo plazo, todas las suturas mostraron un comportamiento mecánico similar, alejado del tejido sano. No se encontraron diferencias significativas entre materiales absorbibles y no absorbibles, y el nuevo modelo de sutura barbeada demostró no tener mayor ventaja que la posibilidad de evitar los nudos de sutura durante el cierre de la herida.

- El neumoperitoneo que se induce siempre al inicial una laparoscopia puede ser utilizado para obtener información mecánica de la respuesta pasiva del tejido abdominal. Para ello han de utilizarse métodos de medida no invasiva, que permita obtener dicha información sin alterar el comportamiento del tejido.

- El ensayo en el que se recrea el neumoperitoneo se considera reproducible a partir del segundo test. Durante el primero, la distribución de gas entre los órganos y un posible reasentamiento del diafragma producen una respuesta de la pared abdominal en función de la presión inducida que no se corresponde con la encontrada en los siguientes tests.

- Durante el ensayo de inflado (neumoperitoneo) el tejido localizado en los laterales del abdomen (donde están presente el oblicuo interno, externo y el músculo transverso) muestra una respuesta más elástica que la zona central, donde se encuentran los rectos y la linea alba. Este descubrimiento puede ser fácilmente explicado por el efecto rigidizante de la línea alba, sin embargo, contradice la mayor parte de los resultados encontrados en la literatura cuando se estudia el comportamiento de las distintas capas.

- El uso de la malla *Surgipro*^{TM} para reparar un defecto herniario produce una severa rigidación en pared abdominal, que seguro supondría una respuesta dolorosa en el paciente. Otras mallas estudiadas en esta tesis,*Neomesh Soft*® y *Nopore*®, parecen reproducir mejor la distensión natural del abdomen.

- La anisotropía de la pared abdominal puede ser numéricamente reproducida a partir de un único modelo constitutivo en el que los parámetros de material puedan variar de una zona a otra, determinando con ello una respuesta mecánica distinta en función de los valores alcanzados por esos parámetros. La distribución concreta de parámetros que mejor reproduzca la respuesta mecánica de un modelo experimental específico se puede calcular mediante un análisis inverso, en el cual los datos serían los obtenidos experimentalmente y el valor de los parámetros en cada nodo serían las variables a determinar. Para resolver este problema inverso la regularización de Tikhonov (H^1) es más recomendable que la de Total Variation Diminishing (TVD), ya que su tendencia a evitar cambios bruscos en las distribuciones lleva a obtener mapas más fiables sin alterar por ello la precisión.

- La distribución obtenida para el modelo animal utilizado (conejo de Nueva Zelanda) localiza un banda en la dirección cráneo caudal con una respuesta mucho más rígida que el resto del abdomen. Esos resultados confirman lo obtenido experimentalmente y pueden relacionarse anatómicamente con la posición de los rectos abdominales y la línea alba.

- La aplicación del análisis inverso, junto con un sistema de medida no invasivo, posibilita el uso de esta metodología a casos de paciente específico.

- Al conseguir recrear la geometría de un modelo específico y obtener la caracterización pasiva mecánica para la zona de la pared anterolateral, se ha podido construir un modelo de elementos finitos donde simular numéricamente la posible respuesta mecánica del abdomen herniado tras reparar el defecto con diferentes prótesis. Las propiedades mecánicas de esas prótesis se pueden obtener a partir de ensayos biaxiales, que podrían venir tabuladas directamente desde fábrica pudiendo así crear un criterio estándar para determinar su idoneidad en un paciente específico.

A.6 Líneas futuras

El trabajo presentado en esta tesis constituye los primeros pasos de una metodología que permita caracterizar la respuesta pasiva mecánica de la pared abdominal. En esta sección se proponen algunas líneas futuras por las que continuar la investigación aquí iniciada, que permitan transformar estos primeros pasos en una mejora tangible para el tratamiento quirúrgico de hernias.

- La consecución inmediata al trabajo aquí presentado es la aplicación de la metodología a tejido humano. Puesto que el sistema de medida utilizado es completamente no invasivo y el ensayo mecánico por el cual se obtiene información ya se realiza de una manera estándar en los quirófanos, la metodología de análisis inverso podría ser fácilmente implementada en modelo humano. En relación a eso, una vez conseguido ese objetivo sería interesante construir una base de datos en los que se recogiesen propiedades mecánicas de la pared abdominal en función de otros atributos, como la edad, género o índice de masa corporal de la persona. Esta información contribuiría a establecer un criterio acerca de qué prótesis usar para cada caso.
- El proceso de adquisición de imagen debería desarrollarse, mejorarse y sobre todo, automatizarse. El proceso actual, basado únicamente en imágenes provenientes de dos cámaras, aporta información de la parte anterolateral de la pared pero pierde datos de la parte posterior correspondiente a la espalda. Esto se podría mejorar añadiendo el número de cámaras que tienen lugar en el momento de grabación. Aparte de eso, se requiere automatizar la etapa de post proceso de las imágenes y reconstrucción del modelo, para que la implementación en un ambiente quirúrgico sea viable. La reconstrucción inicial de la geometría podría realizarse a partir de resonancias magnéticas, que conllevarían una posible mejorara en la precisión junto con un aporte adicional de información sobre el espesor de la capa muscular.
- Referente a la parte de análisis numérico, se deberían considerar para el problema inverso otros modelos constitutivos de material que permitiesen

reproducir la respuesta mecánica de la pared a todos los niveles de presión. Modelos dependientes de más de dos parámetros u otros que considerasen la inserción de fibras ayudarían a mimetizar la respuesta del material. En este aspecto, se podría considerar la dirección de las fibras como una variable adicional para el cálculo inverso, con lo que podría variar según la localización en el abdomen.

- Una base de datos completa y estandarizada que reúna los aspectos mecánicos de mallas herniarias sería un aporte muy útil de cara al tratamiento hernias. Esta base de datos debería incluir tanto las características generales de cada prótesis (densidad, tamaño de poro, grosor de hilo) como la respuesta de dichas prótesis ante los mismos ensayos mecánicos (uniaxiales, biaxiales, inflado). De esta manera se podrían comparar directamente la ventajas o inconvenientes de cada malla frente a un caso concreto.

- El estudio de la respuesta activa de diferentes músculos abdominales ayudaría en gran medida a mejorar el tratamiento en casos de hernias, ya que aportaría una visión global y completa del comportamiento mecánico del músculo y por tanto de los requisitos que debe cumplir una malla durante el tiempo de regeneración de tejido.

- Por último, también sería interesante diseñar un modelo numérico que simulase los procesos biológicos que tienen lugar tras la implantación de una malla herniaria, desde la integración tisular como la regeneración del tejido. De esta manera una simulación previa a la intervención podría predecir tanto los aspectos mecánicos como los biológicos de la intervención, adelantando con ello posibles inconvenientes y molestias.

B

Original Contributions

The original contributions carried out during the period of this Thesis are detailed and attached in this section. Some of them were directly related to the main theme of this Thesis, while others were indirectly linked and their attainment transversally complemented the work developed.

B.1 Publications

The following publications were directly related to the topic of this work and they were totally or partially included in this Thesis:

1. **Simón-Allué R.**, Pérez-López P., Sotomayor S., Peña E., Pascual G., Bellón J.M., Calvo B. Short- and long-term experimental and biomechanical study of new suture types in abdominal wall closure. *Journal of the Mechanical Behavior of Biomedical Materials* 37 (2014):1-11. **doi**:10.1016/j.jmbbm.2014.04.014.
   IF: 2.876 (Q1: 18/76 Engineering, Biomedical)

2. Bellón J.M., Pérez-López P., **Simón-Allué R.**, Sotomayor S., Pérez-Köehler B., Peña E., Pascual G., Calvo B. New suture materials for midline laparotomy closure: an experimental study. *BioMed Central Surgery* 14 (2014):1-11. **doi**: 10.1186/1471-2482-14-70.
   IF: 1.469 (Q3: 107/200 Surgery)

3. **Simón-Allué R.**, Montiel J.M.M., Bellón J.M., Calvo B. Developing a new methodology to characterize in vivo the passive mechanical behavior of abdominal wall on an animal model. *Journal of the Mechanical Behavior of Biomedical Materials* 51 (2015):40-49. **doi**:10.1016/j.jmbbm.2015.06.029.
   IF: 2.876 (Q1: 18/76 Engineering, Biomedical)

4. **Simón-Allué R.**, Calvo B., Oberai A., Barbone P. Mechanical characterization of abdominal wall by inverse analysis on an animal model. *Journal of the Mechanical Behavior of Biomedical Materials* (2016) *Under review.*

5. **Simón-Allué R.**, Ortillés A., Calvo B. Mechanical behavior of meshes for repair abdominal wall: in vivo versus biaxial characterization. *Under preparation.*

Furthermore, the following articles have been conducted during the development of this Thesis and the knowledge acquired through their execution have definitely contributed to the fulfilment of this work

1. **Simón-Allué R.**, Cordero A., Peña E. Unraveling the effect of boundary conditions and strain monitoring on estimation of the constitutive parameters of elastic membranes by biaxial tests. *Mechanics Research Communi-*

cations 57 (2014):82-89. **doi**:10.1016/j.mechrescom.2014.01.009.
IF: 1.400 (Q2: 65/135 Mechanics)

2. **Simón-Allué R.**, Hernández-Gascón B., Lèoty L., Bellón J.M., Peña E., Calvo B. Prostheses size dependency of the mechanical response of the herniated human abdomen. *Hernia* (2016) 1-10. **doi**:10.1007/s10029-016-1525-3.
IF: 2.054 (Q2: 67/200 Surgery)

The first page of each published work has been included in this Section in the original form of its publication.

Mechanics Research Communications 57 (2014) 82–89

Contents lists available at ScienceDirect

Mechanics Research Communications

journal homepage: www.elsevier.com/locate/mechrescom

Unraveling the effect of boundary conditions and strain monitoring on estimation of the constitutive parameters of elastic membranes by biaxial tests

Raquel Simón-Allué[a], Alberto Cordero[a,b], Estefanía Peña[a,b,*]

[a] Applied Mechanics and Bioengineering, Aragón Institute of Engineering Research (I3A), University of Zaragoza, Spain
[b] CIBER de Bioingeniería, Biomateriales y Nanomedicina (CIBER-BBN), Spain

ARTICLE INFO

Article history:
Received 18 October 2013
Received in revised form 3 January 2014
Available online 22 February 2014

Keywords:
Biaxial testing
Biomaterials
Strain measuring
Gripping method
Sample geometry

ABSTRACT

The purpose of this study is to study the effects of boundary conditions and strain monitoring on the estimation of the constitutive parameters of elastic membranes by biaxial tests. We analyze the effect of geometry, different gripping methods and strain monitoring. Experiments were conducted on membrane silicon using two samples geometries – cruciform and square – of different sizes, two gripping arrangements – clamped and sutured edges – and two strain monitoring methods – displacement between grips and Digital Image Correlation techniques. The strain maps were compared with that produced by a geometrically matched finite element model.

We report two important findings. First, as the St Venant principle pointed for medium or large samples the gripping method had no effect on the material parameters and the strain distribution at the center of the sample. However, due to size the restrictions imposed by soft biological tissues, using sutures is the commonly used technique. Secondly, biaxial strain fields measured using surface markers or DIC methodologies are suitable for clamped method and be essential when sutures are used. As conclusion, the parametric study realized can give guidelines for future researchers on biomechanics on the minimum size of samples and an interesting way to extract data from tests.

1. Introduction

The experimental study of the mechanical properties of soft biological tissues is of vital importance. Thorough research into the mechanical response of biomaterials is the basis for the creation of models which can accurately reproduce the mechanical behavior of such materials. In order to obtain their material properties, classical engineering testing techniques have been applied to biological materials (see e.g., Fung, 1993; Humphrey, 2002, and references therein). To reproduce the mechanical behavior of these kinds of material, many constitutive models have been proposed for soft tissues (Fung, 1993; Holzapfel et al., 2000; Humphrey, 2002; Weiss et al., 1996). In some cases, the validation of these models based on only uniaxial test data is inappropriate because biological and biomaterial membranes generally develop multiaxial stress states during real-life loading conditions.

Although a large number of experiments have been conducted over the years on measuring the structural and functional properties of biological tissues, the standardization of such measurements and the interpretation of results are difficult to establish. The geometry of the sample, the method of gripping the sample edges and the method used to determine the strain may have profound effects on any measured mechanical properties since they directly influence how the load is transferred to the membrane (Humphrey and Strumpf, 1989; Jacobs et al., 2013; Sacks, 2000; Waldman and Lee, 2002, 2005). Although these issues are known to be important, they have been essentially ignored for the biaxial mechanical testing of biological materials.

The purpose of this work is to study the effects of boundary conditions and strain monitoring on the estimation of the constitutive parameters of elastic membranes by biaxial tests. In spite of the anisotropy of soft planar tissues, we have developed the study using isotropic elastic membranes in order to decouple the effect of the anisotropy from those other geometrical factors (Waldman and Lee, 2002). Specifically, we analyze the effect of geometry,

* Corresponding author at: Applied Mechanics and Bioengineering, Aragón Institute of Engineering Research (I3A), University of Zaragoza, Spain.
Tel.: +34 876555233; fax: +34 976762578.
E-mail address: fany@unizar.es (E. Peña).

http://dx.doi.org/10.1016/j.mechrescom.2014.01.009
0093-6413/

JOURNAL OF THE MECHANICAL BEHAVIOR OF BIOMEDICAL MATERIALS 37 (2014) 1–11

Available online at www.sciencedirect.com

ScienceDirect

www.elsevier.com/locate/jmbbm

Research Paper

Short- and long-term biomechanical and morphological study of new suture types in abdominal wall closure

R. Simón-Allué[a,d], P. Pérez-López[c,d], S. Sotomayor[b,d], E. Peña[a,d], G. Pascual[b,d], J.M. Bellón[c,d], B. Calvo[a,d,*]

[a]Aragón Institute of Engineering Research (I3A), Universidad de Zaragoza, Spain
[b]Department of Medicine and Medical Specialities, Faculty of Medicine and Health Sciences, Universidad de Alcalá, Spain
[c]Department of Surgery, Medical and Social Sciences, Faculty of Medicine and Health Sciences, Universidad de Alcalá, Spain
[d]Centro de Investigación Biomédica en Red en Bioingeniería, Biomateriales y Nanomedicina (CIBER-BBN), Spain

ARTICLE INFO

Article history:
Received 19 February 2014
Received in revised form
18 April 2014
Accepted 27 April 2014
Available online 9 May 2014

Keywords:
Sutures
Mechanical properties
Morphological studies
Linea alba closure

ABSTRACT

To perform an abdominal-wall closure, a continuous suture is the preferred method. The suture materials that are most commonly employed in abdominal surgery are polypropylene and polydioxanone. However, in recent times, new products have been marketed, such as non-absorbable polyurethane with elastic properties (*Assuplus*®, Assut Europe, Italy) and absorbable barbed polydioxanone (*Filbloc*®, Assut Europe, Italy). The purpose of this study was to compare the ability of those against the standard polypropylene (*Surgipro*™, Covidien, USA) and polydioxanone (*Assufil*®, Assut Europe, Italy) to mimic the biomechanical behavior of the abdominal wall closure. Comparison of the sutures was made first with the materials alone and later in a laparotomy closure of a rabbit abdomen, used as an animal model. The biomechanical analysis consisted of uniaxial tensile tests of threads and sutured samples of the animal abdomen. In the latter case, results were analyzed at short- (21 days) and long- (180 days) term intervals after the surgery. The morphology studies and collagen expression of the samples were also investigated.

The results determined that polydioxanone and polypropylene sutures showed a linear elastic behavior, with barbed polydioxanone as the most compliant suture and polyurethane as the stiffest. The sutured samples showed a statistically significant loss of resistance, measured as the load needed to perform a certain stretch, when compared with the corresponding control tissue. Analysis of the stress–stretch curves showed that elastic polyurethane was the only suture able to reproduce the mechanical behavior of healthy tissue in the short term, while the rest of the sutures remained less stiff. This coincides with the expression of type I collagen observed in this group at this point in the study. In the long term, there was no difference among the sutures, and none was able to mimic control behavior.

*Corresponding author at. Applied Mechanics and Bioengineering (AMB), c/ Maria de Luna s/n 50018, Zaragoza, Spain. Tel.: +34 876555109.
E-mail address: bcalvo@unizar.es (B. Calvo).

http://dx.doi.org/10.1016/j.jmbbm.2014.04.014
1751-6161/

Bellón et al. BMC Surgery 2014, 14:70
http://www.biomedcentral.com/1471-2482/14/70

BMC Surgery

RESEARCH ARTICLE Open Access

New suture materials for midline laparotomy closure: an experimental study

Juan M Bellón[1,3*], Paloma Pérez-López[1,3], Raquel Simón-Allue[4], Sandra Sotomayor[2,3], Bárbara Pérez-Köhler[1,3], Estefanía Peña[4], Gemma Pascual[2,3] and Begoña Calvo[4]

Abstract

Background: Midline laparotomy closure carries a significant risk of incisional hernia. This study examines the behavior of two new suture materials, an elastic material, polyurethane (PUe), and a barbed polydioxanone (PDXb) suture thread in a rabbit model of midline incision closure.

Methods: Three 2-cm midline incisions were made in 68 New Zealand White rabbits. The incisions were closed by running suture using four 3/0 threads: polypropylene (PP) (Surgipro®, *Covidien*), PUe (Assuplus®, *Assut Europe*), PDX (Assufil®, *Assut Europe*) or PDXb (Filbloc®, *Assut Europe*). Animals in each suture group were euthanized 3 weeks and 6 months after surgery. Histological sections of the tissue-embedded sutures were subjected to morphological, collagen expression, macrophage response and uniaxial tensiometry studies.

Results: No signs of wound dehiscence or complications were observed. At 3 weeks, all sutures were surrounded by connective tissue composed mainly of collagen III. PUe showed greater collagen I expression than the other sutures. All sutures elicited a macrophage response that diminished from 3 weeks to 6 months ($p < 0.001$). This response was similar for the non-reabsorbable sutures (PP and PUe) yet PDXb showed a significantly greater response than the other reabsorbable suture (PDX) at 3 weeks ($p < 0.01$). At this early time point, the tensile strength of PUe was similar to that of control intact tissue ($p > 0.05$).

Conclusion: Three weeks after surgery, PUe revealed more collagen I deposition than the remaining materials and this translated to a similar biomechanical behavior to linea alba, that could avoid the appearance of short term dehiscences and thus reduce the incidence of incisional hernia. PDXb provides no additional advantages in their behavior regarding PDX suture.

Keywords: Polypropylene, Polyurethane, Polydioxanone, Abdominal wall closure, Midline closure, Laparotomy closure, Barbed sutures, Elastic sutures

Background

Although the use of laparoscopic procedures for abdominal surgery is on the rise, in routine clinical practice, open surgery involving a laparotomy is still often required. Despite several benefits of a transverse laparotomy (e.g., less pain, improved respiratory tolerance) [1-3], the midline laparotomy incision is still the most common approach for many digestive, vascular (especially aortic) and abdominal trauma surgery procedures. This type of laparotomy can be performed quickly and can be extended proximally or distally according to requirements to provide a wide surgical field. On the downside, it is more exsanguinous than the transverse approach.

A midline laparotomy requires opening of the linea alba, which is a weak, tendinous zone of the abdominal wall where fibers of the muscle fascia on each side of the linea alba intersect. The weakness of the linea alba is enhanced when its fibers are vertically sectioned to access the peritoneal cavity. Thus, when repairing or closing the linea alba using sutures, these are subjected to the tension induced by the mechanical forces that act upon it. These forces are that produced by the intraabdominal pressure and the force of the muscle complex comprised

* Correspondence: juanm.bellon@uah.es
[1]Departments of Surgery, Medical and Social Sciences, Faculty of Medicine and Health Sciences, University of Alcalá, Alcalá de Henares, Madrid, Spain
[3]Networking Research Centre on Bioengineering, Biomaterials and Nanomedicine (CIBER-BBN), Madrid, Spain
Full list of author information is available at the end of the article

JOURNAL OF THE MECHANICAL BEHAVIOR OF BIOMEDICAL MATERIALS 51 (2015) 40–49

Available online at www.sciencedirect.com

ScienceDirect

www.elsevier.com/locate/jmbbm

Research Paper

Developing a new methodology to characterize *in vivo* the passive mechanical behavior of abdominal wall on an animal model

R. Simón-Allué[a,*], *J.M.M. Montiel*[a], *J.M. Bellón*[b,c], *B. Calvo*[a,c]

[a]*Aragón Institute of Engineering Research (I3A), Universidad de Zaragoza, Mechanical Department, c/ María de Luna s/n, Zaragoza, Spain*

[b]*Department of Surgery, Medical and Social Sciences, Faculty of Medicine and Health Sciences, Universidad de Alcalá, Spain*

[c]*Centro de Investigación Biomédica en Red en Bioingeniería, Biomateriales y Nanomedicina (CIBER-BBN), Spain*

ARTICLE INFO

Article history:
Received 17 April 2015
Received in revised form
17 June 2015
Accepted 23 June 2015
Available online 9 July 2015

Keywords:
Abdominal wall
Mechanical properties
In vivo studies
Photogrammetry

ABSTRACT

The most common surgical repair of abdominal wall hernia goes through implanting a mesh that substitutes the abdominal muscle/fascia while it is healing. To reduce the risk of relapse or possible complications, this mesh needs to mimic the mechanical behavior of the muscle/fascia, which nowadays is not fully determined. The aim of this work is to develop a methodology to characterize *in vivo* the passive mechanical behavior of the abdominal wall. For that, New Zealand rabbits were subjected to pneumoperitoneum tests, taking the inner pressure from 0 mmHg to 12 mmHg, values similar to those used in human laparoscopies. Animals treated were divided into two groups: healthy and herniated animals with a surgical mesh (polypropylene *Surgipro*™ Covidien) previously implanted. All experiments were recorded by a stereo rig composed of two synchronized cameras. During the postprocessing of the images, several points over the abdominal surface were tracked and their coordinates extracted for different levels of internal pressure. Starting from that, a three dimensional model of the abdominal wall was reconstructed. Pressure–displacement curves, radii of curvature and strain fields were also analysed. During the experiments, animals tissue mostly deformed during the first levels of pressure, showing the noticeable hyperelastic passive behavior of abdominal muscles. Comparison between healthy and herniated specimen displayed a strong stiffening for herniated animals in the zone where the high density mesh was situated. Cameras were able to discern this change, so this method can be used to measure the possible effect of other meshes.

*Corresponding author. Tel.: +34 876555187.
E-mail address: rsimon@unizar.es (R. Simón-Allué).

http://dx.doi.org/10.1016/j.jmbbm.2015.06.029
1751-6161/

Hernia
DOI 10.1007/s10029-016-1525-3

ORIGINAL ARTICLE

Prostheses size dependency of the mechanical response of the herniated human abdomen

R. Simón-Allué[1,2] · B. Hernández-Gascón[1,2] · L. Lèoty[3] · J. M. Bellón[2,4] · E. Peña[1,2] · B. Calvo[1,2]

Received: 17 March 2016 / Accepted: 29 July 2016

Abstract
Background Hernia repairs still exhibit clinical complications, i.e. recurrence, discomfort and pain and mesh features are thought to be highly influent. The aim of this study is to evaluate the impact of the defect size and mesh type in an herniated abdominal wall using numerical models.
Methods To do so, we have started from a FE model based on a real human abdomen geometry obtained by MRI, where we have provoked an incisional hernia of three different sizes. The surgical procedure was simulated by covering the hernia with a prostheses, and three surgical meshes with distinct mechanical properties were used for the hernia repair: an isotropic heavy-weight mesh (*Surgipro*®), a slightly anisotropic light-weight mesh (*Optilene*®) and a highly anisotropic medium-weight mesh (*Infinit*®). The mechanical response of the wall to a high intraabdominal pressure (corresponding to a coughing motion) was analyzed here.
Results Our findings suggest that the anisotropy of the mesh becomes more relevant with the increase of the defect size. Additionally, according to our results *Optilene*® showed the closest deformation to the natural distensibility of the abdomen while *Infinit*® should be carefully used due to its excessive compliance.

Keywords Hernia · Repair · Polypropylene mesh · Failure · Finite element analysis

Introduction

Nowadays, clinical evidence recommends the use of prosthetic materials for hernia repair, being this a prime defect (primary hernia) or derived from a previous laparotomy (incisional hernia). Last years, the evolution of prosthetic materials has raised meshes with different spatial arrangement of filaments and specially pore size [1, 2]. Consequently, porosity has led to classify meshes in three distinct groups: high (HW, above 80 g/m^2), medium (MW, between 80 and 50 g/m^2) or low density (LW, below 50 g/m^2). Pore size is linked to the prosthetic weight (g/m^2): small pore size is related to the high density while large size is associated to the low density meshes [3].

After repairing an abdominal hernia defect with a surgical mesh, it is necessary to ensure that the implant can bear the abdominal mechanical loads the post-implant is going to suffer. To do so, the great variability of the intraabdominal pressure (IAP) has to be considered [4]. Moreover, once the mesh is placed into the tissue the whole has to work in the most physiological way, which is specially hard to determinate since this mechanical demand varies depending on the individual biotype. Regarding this aspect, obesity has revealed to be a very determining factor [4].

In general, high density meshes are associated to a high tensile strength, but also a profound tissue reaction and dense scarring due to the large mass of material [3]. Low density, on the contrary, attempt to produce less

✉ R. Simón-Allué
rsimon@unizar.es

[1] Applied Mechanics and Bioengineering, Aragón Institute of Engineering Research, University of Zaragoza, Saragossa, Spain

[2] CIBER de Bioingeniería, Biomateriales y Nanomedicina (CIBER-BBN), Madrid, Spain

[3] Ecole Centrale de Centrale Nantes, Nantes, France

[4] Department of Surgery, Medical and Social Sciences, Faculty of Medicine and Health Sciences, Universidad de Alcalá, Madrid, Spain

Published online: 22 August 2016

B.2 Conferences

With the view to expanding the work developed on this Thesis and encouraging the transmission of the knowledge acquired, the following communications have been presented during the project duration.

1. **Simón-Allué R.**, Agudo A., Montiel J.M.M., Calvo B. Mechanical characterization of abdominal muscle by stereo images. *III Reunión del Capítulo Nacional Español de la Sociedad Europea de Biomecánica* (ESB). Barcelona (Spain), 2013.

2. **Simón-Allué R.**, Montiel J.M.M., Calvo B. Mechanical characterization of abdominal muscle using photogrammetry. *6^{th} Surgical Robotics Summer School.* Montpellier (France), 2013.

3. **Simón-Allué R.**, Agudo A., Montiel J.M.M., Calvo B. Caracterización mecánica del músculo abdominal a partir de imágenes 2D. *I Jornadas Doctorales Campus Iberus.* Jaca (Spain), 2014.

4. **Simón-Allué R.**, Montiel J.M.M., Calvo B. Caracterización mecánica del músculo abdominal mediante fotogrametría y análisis inverso. *I Jornada de Doctorandos del Programa de Doctorado en Ingenería mecánica.* Zaragoza (Spain), 2014.

5. **Simón-Allué R.**, Agudo A., Montiel J.M.M., Bellón J.M., Calvo B. Mechanical characterization of abdominal muscle using stereo imaging. *11^{th} World Congress on Computational Mechanics (WCCM XI).* Barcelona (Spain), 2014.

6. **Simón-Allué R.**, Oberai A., Montiel J.M.M., Calvo B. Mechanical characterization of abdominal muscle by inverse analysis on an animal model. *21^{st} Congress of the European Society of Biomechanics.* Prague (Czech Republic), 2015.

7. **Simón-Allué R.**, Oberai A., Calvo B. Using inverse finite element analysis to obtain passive mechanical behavior of abdominal wall. *IV Jornada*

Jóvenes Investigadores Instituto de Investigación en Ingeniería de Aragón. Zaragoza (Spain), 2015.

8. **Simón-Allué R.**, Oberai A., Barbone P., Calvo B. In-vivo mechanical characterization of abdominal muscle by inverse analysis. *III Jornada de Doctorandos del Programa de Doctorado en Ingenería mecánica.* Zaragoza (Spain), 2016.

9. **Simón-Allué R.**, Oberai A., Barbone P., Montiel J.M.M., Calvo B. Towards in vivo mechanical characterization of abdominal wall. *7^{th} Summer School on Biomechanics of Soft Tissues: Multiscale Modeling, Simulation and Applications.* Graz (Austria), 2016.

B.3 Financial support

Financial support for this research was provided by the Spanish Ministry of Economy and Competitiveness through research projects DPI2011-27939-C02-01, DPI2012-32168 and DPI2014-54981R and the Instituto de Salud Carlos III (ISCIII) through the CIBER initiative and the Tissue Characterization Platform of the CIBER-BBN. Concurrently, the author gratefully acknowledges research support from the Spanish Ministry of Economy and Competitiveness for the specific financial support to R. Simón-Allué through the grant BES-2012-053422 and the mobility fellowships EEBB-I-14-08368 and EEBB-I-15-09811, which provided the opportunity to conduct two research stays in United States.

Bibliography

(2002). Yoganatomy. `http://www.yoganatomy.com/`. accessed May, 2016.

(2015). Teachmeanatomy. `http://teachmeanatomy.info/`. accessed May, 2016.

Acosta Santamaría, V., O. Siret, P. Badel, G. Guerin, V. Novacek, F. Turquier, and S. Avril (2015). Material model calibration from planar tension tests on porcine linea alba. *Journal of the Mechanical Behavior of Biomedical Materials 43*, 26–34.

Agency for Healthcare Research and Quality (2013, July). Surgery for an inguinal hernia. Consumer summary, U.S. Department of Health & Human Services.

Ahrens, J., B. Geveci, and C. Law (2005). *ParaView: An End-User Tool for Large Data Visualization, Visualization Handbook*. Elsevier.

Albertsmeier, M., C. M. Seiler, L. Fischer, P. Baumann, J. Hüsing, C. Seidlmayer, A. Franck, K.-W. Jauch, H.-P. Knaebel, and M. Büchler (2012). Evaluation of the safety and efficacy of MonoMax® suture material for abdominal wall closure after primary midline laparotomy-a controlled prospective multicentre trial. *Langenbeck's Archives of Surgery 397*(3), 363–371.

Alcamo, J. (1964). Surgical suture. US Patent 3,123,077.

Amid, P., A. Shulman, and I. Lichtenstein (1995). The lichtenstein open "tension-free" mesh repair of inguinal hernias. *Surgery today 7*(25), 619–625.

Amid, P., A. Shulman, and I. Lichtenstein (1996, June). Open "tension-free" repair of inguinal hernias: the lichtenstein technique. *The European journal of surgery 162*(6), 447–453.

Amid, P. K. (1997). Classification of biomaterials and their related complications in abdominal wall hernia surgery. *Hernia 1*(1), 15–21.

Arruda, E. M., K. Mundy, S. Calve, and K. Baar (2006). Denervation does not change the ratio of collagen i and collagen ii mrna in extracellular matrix of muscle. *Am J Physiol Regulatory Integrative Comp Physiol 292*, 983–987.

Askar, O. M. (1977). Surgical anatomy of the aponeurotic expansions of the anterior abdominal wall. *Annals of the Royal College of Surgeons of England 59*(4), 313–321.

Axer, H., D. G. von Keyserlingk, and A. Prescher (2001a). Collagen fibers in linea alba and rectus sheaths: I. General Scheme and Morphological Aspects. *The Journal of Surgical Research 96*(2), 239–245.

Axer, H., D. G. von Keyserlingk, and A. Prescher (2001b). Collagen fibers in linea alba and rectus sheaths: Ii. variability and biomechanical aspects. *The Journal of Surgical Research 96*(2), 239–245.

Bailey, H., R. Russell, R. Love, N. Williams, and C. Bulstrode (2000). *Bailey and Love's Short Practice of Surgery*. A Hodder Arnold Publication. Arnold.

Barbone, P. E., C. E.Rivas, I. Harari, U. Albocher, A. A. Oberai, and Y. Zhang (2009). Adjoint-weighted variational formulation for the direct solution of inverse problems of general linear elasticity with full interior data. *International Journal for Numerical Methods in Ingineering 81*(13), 1713–1736.

Beets, L., D. Dirksen, H. Go, A. Geisler, I. Baeten, and G. Kootstra (1999). Open or laparoscopic preperitoneal mesh repair for recurrent inguinal hernia? *Surgical Endoscopy 13*(4), 323–327.

Bellón, J. M. (2007). Abdominal wall hernia repair: A comparison of sepramesh and parietex composite mesh in a rabbit hernia model. *Journal of the American College of Surgeons 205*, 192–198.

Bellón, J. M. (2014). Revisión de una clasificación de materiales protésicos destinados a la reparación herniaria: correlación entre estructura y comportamiento en los tejidos receptores. *Revista Hispanoamericana de Hernia 2*(2), 49–57.

Bellón, J. M., J. Buján, A. L. Contreras, L. Carrera-San Martín, and F. Jurado (1996). Comparison of a new type of polytetrafluoroethylene patch (mycro mesh) and polypropylene prosthesis (marlex) for repair of abdominal wall defects. *Journal of the American College of Surgeons 183*, 11–18.

Bellón, J. M., P. Pérez-López, R. Simón-Allue, S. Sotomayor, B. Pérez-Köhler, E. Peña, G. Pascual, and B. Calvo (2014). New suture materials for midline laparotomy closure: an experimental study. *BMC surgery 14*, 70.

Ben Abdelounis, H., S. Nicolle, M. Otténio, P. Beillas, and D. Mitton (2013). Effect of two loading rates on the elasticity of the human anterior rectus sheath. *Journal of the Mechanical Behavior of Biomedical Materials 20*, 1–5.

Bendavid, R., J. Abrahamson, M. Arregui, J. Flament, and E. Phillips (Eds.). *Abdominal Wall Hernias: Principles and Management*.

Bezerra, M., R. Santelli, E. Oliveira, L. Villar, and L. Escaleira (2008). Response surface methodology (rsm) as a tool for optimization in analytical chemistry. *Talanta 76*(5), 965–977.

Bilsel, Y. and I. Abci (2012). The search for ideal hernia repair; mesh materials and types. *International Journal of Surgery 10*(6), 317–321.

Blázquez Hernando, L., M. García Ureña, J. López Monclús, A. Lersundi Robin del Valle, D. Melero Montes, A. Cruz Cidoncha, C. Jiménez Ceinos, and C. Castelló Pavó (2015). Roturas de malla: una causa poco frecuente de recidiva herniaria. *Revista Hispanoamericana de Hernia 3*(4), 155–159.

Bloemen, A., P. van Dooren, B. F. Huizinga, and A. G. M. Hoofwijk (2011). Randomized clinical trial comparing polypropylene or polydioxanone for midline abdominal wall closure. *British Journal of Surgery 98*(5), 633–639.

Böl, M., R. Kruse, A. E. Ehret, K. Leichsenring, and T. Siebert (2012). Compressive properties of passive skeletal muscle. The impact of precise sample geometry on parameter identification in inverse finite element analysis. *Journal of Biomechanics 45*(15), 2673–2679.

Bouguet, J. (2011). *Camera Calibration Toolbox for Matlab*. Computational Vision at the California Institute of Technology.

Box, G. E. P. and K. B. Wilson (1951). On the experimental attainment of optimum conditions. *Journal of the Royal Statistical Society. Series B (Methodological) 13*(1), 1–45.

Brown, C. N. and J. G. Finch (2010). Which mesh for hernia repair? *Annals of the Royal College of Surgeons of England 92*(4), 272–278.

Buganza Tepole, A., M. Gart, C. Purnell, A. Gosain, and E. Kuhl (2015). Multi - view stereo analysis reveals anisotropy of prestrain, deformation, and growth in living skin. *Biomechanics and Modeling in Mechanobiology 14*(5), 1007–1019.

Calvo, B., E. P. na, M. A. Martínez, and M. Doblaré (2008). Computational modeling of ligaments at non-physiological situations. *International Journal for Computational Vision and Biomechanics IJV&B 1*, 107–115.

Calvo, B., E. P. na, P. Martins, T. Mascarenhas, M. Doblare, R. Natal, and A. Ferreira (2009). On modelling damage process in vaginal tissue. *Journal of Biomechanics 42*, 642–651.

Cassar, K. and A. Munro (2002). Surgical treatment of incisional hernia. *British Journal of Surgery 89*(5), 534–545.

Ceydeli, A., J. Rucinski, and L. Wise (2005). Finding the best abdominal closure: an evidence-based review of the literature. *Current Surgery 62*(2), 220–225.

Chauvet, D., M. Imbault, L. Capelle, C. Demene, M. Mossad, C. Karachi, A.-L. Boch, J.-L. Gennisson, and M. Tanter (2015, April). In vivo measurement of brain tumor elasticity using intraoperative shear wave elastography. *Ultraschall in der Medizin*.

Cobb, W., J. Burns, R. Peindl, A. M. Carbonell, B. Matthews, K. W. Kercher, and B. Heniford (2006). Textile analysis of heavy weight, mid-weight, and light weight polypropylene mesh in a porcine ventral hernia model. *Journal of Surgical Research 136*(1), 1–7.

Coda, A., R. Lamberti, and S. Martorana (2012). Classification of prosthetics used in hernia repair based on weight and biomaterial. *Hernia 16*(1), 9–20.

Conze, J. and U. Klinge (1999). Biocompatibility of biomaterials-clinical and mechanical aspects. In V. Schumpelick and A. N. Kingsnorth (Eds.), *Incisional Hernia*, Chapter 14, pp. 169–177. Berlin, Heidelberg: Springer Berlin Heidelberg.

Cooney, G., K. Moerman, M. Takaza, D. C. Winter, and C. Simms (2015). Uniaxial and biaxial mechanical properties of porcine linea alba. *Journal of the Mechanical Behavior of Biomedical Materials 41*, 68–82.

Cordero, A., B. Hernández-Gascón, G. Pascual, J. M. Bellón, B. Calvo, and E. Peña (2015). Biaxial Mechanical Evaluation of Absorbable and Nonabsorbable Synthetic Surgical Meshes Used for Hernia Repair: Physiological Loads Modify Anisotropy Response. *Annals of Biomedical Engineering*.

Dabbas, N., K. Adams, K. Pearson, and G. Royle (2011). Frequency of abdominal wall hernias: is classical teaching out of date? *Journal of the Royal Society of Medicine, Short Reports 2*(1), 5.

Davis, J., K. R. Kaufman, and R. L. Lieber (2003). Correlation between active and passive isometric force and intramuscular pressure in the isolated rabbit tibialis anterior muscle. *Journal of Biomechanics 36*(4), 505–512.

Delalleau, A., G. Josse, J.-M. Lagarde, H. Zahouani, and J.-M. Bergheau (2006, jan). Characterization of the mechanical properties of skin by inverse analysis combined with the indentation test. *Journal of biomechanics 39*(9), 1603–10.

Demiray, H. (1972). A note on the elasticity of soft biological tissues. *Journal of biomechanics 5*, 309–311.

Demiray, H. (1981). Large Deformation Analysis of Some Soft Biological Tissues. *Journal of biomechanics 103*, 73–78.

Demiray, H., H. W. Weizsacker, K. Pascale, and H. Erbay (1988). A stress-strain relation for a rat abdominal aorta. *Journal of biomechanics 21*, 369–374.

Diener, M., S. Voss, K. Jensen, M. Büchler, and C. Seiler (2010). Elective midline laparotomy closure: the inline systematic review and meta-analysis. *Annals of Surgery 251*(5), 843–856.

Docobo-Durantez, F., C. Sacristán-Pérez, B. Flor-Civera, S. Lledó-Matoses, E. Kreisler, and S. Biondo (2006). Randomized clinical study of polydioxanone and nylon sutures for laparotomy clousure in high-risk patients. *Cirugía Española 79*(5), 305–309.

Drake, R., W. Vogl, A. Mitchell, R. Tibbitts, and P. Richardson (2012). *Gray´s Basic Anatomy*. ClinicalKey. Churchill Livingstone.

DuBay, D. A., X. Wang, B. Adamson, W. Kuzon, R. G. Dennis, and M. G. Franz (2006). Mesh incisional herniorrhaphy increases abdominal wall elastic properties: A mechanism for decreased hernia recurrences in comparison with suture repair. *Surgery 140*(1), 14–24.

Earle, D. and L. Mark (2008). Prosthetic material in inguinal hernia repair: How do I choose? *Surgical Clinics of North America 88*(1), 179–201. Advances in Abdominal Wall Hernia Repair.

Facy, O., V. Blasi, M. Goergen, L. Arru, L. Magistris, and J. S. Azagra (2013). Laparoscopic gastrointestinal anastomoses using knotless barbed sutures are safe and reproducible: a single-center experience with 201 patients. *Surgical Endoscopy 27*(10), 3841–3845.

Fitzgibbons, R. J. and R. A. Forse (2015). Groin hernias in adults. *New England Journal of Medicine 372*(8), 756–763.

Flamini, V., A. P. Creane, C. M. Kerskens, and C. Lally (2015). Imaging and finite element analysis: A methodology for non-invasive characterization of aortic tissue. *Medical engineering & physics 37*(1), 48–54.

Flory, P. J. (1961). Thermodynamic relations for high elastic materials. *Transactions of the Faraday Society 57*, 829–838.

Förstemann, T., J. Trzewik, J. Holste, B. Batke, M. a. Konerding, T. Wolloscheck, and C. Hartung (2011). Forces and deformations of the abdominal wall - A mechanical and geometrical approach to the linea alba. *Journal of biomechanics 44*(4), 600–6.

Franz, M., M. Kuhn, T. Wright, T. L. Wachtel, and M. C. Robson (2000). Use of the wound healing trajectory as an outcome determinant for acute wound healing. *Wound Repair and Regeneration 8*(6), 511–516.

Franz, M. G. (2006). The biology of hernias and the abdominal wall. *Hernia: the Journal of Hernias and Abdominal Wall Surgery 10*(6), 462–471.

Franz, M. G. (2008). The biology of hernia formation. *The Surgical Clinics of North America 88*(1), 1–15.

Gasser, T. C., R. W. Ogden, and G. A. Holzapfel (2006). Hyperelastic modelling of arterial layers with distributed collagen fibre orientations. *Journal of The Royal Society Interface 3*(6), 15–35.

Giovanni, M. (1983). Response surface methodology and product optimization. *Food technology 37*, 41–45.

Goellner, M., J. Schmitt, M. Karl, M. Wichmann, and S. Holst (2010). Photogrammetric measurement of initial tooth displacement under tensile force. *Medical Engineering & Physics 32*(8), 883–888.

Goenezen, S., P. Barbone, and A. A. Oberai (2011). Solution of the nonlinear elasticity imaging inverse problem: The incompressible case. *Computer Methods in Applied Mechanics and Engineering 200*, 1406 – 1420.

Gokhale, N. H., P. E. Barbone, and A. A. Oberai (2008, aug). Solution of the nonlinear elasticity imaging inverse problem: the compressible case. *Inverse Problems 24*(4), 045010.

Granados, P. H. (2010). Dolor crÃşnico tras cirugÃŋa de la hernia inguinal. *Cirugía Española 87*(4), 199–201.

Grant, A. (2000). Mesh compared with non-mesh methods of open groin hernia repair: systematic review of randomized controlled trials. *British Journal of Surgery 87*(7), 854–859.

Grasa, J., M. Sierra, N. Lauzeral, M. Muñoz, F. Miana-Mena, and B. Calvo (2016). Active behavior of abdominal wall muscles. Experimental results and numerical model formulation. *Journal of the Mechanical Behavior of Biomedical Materials 61*, 444–454.

Grässel, D., A. Prescher, S. Fitzek, D. G. V. Keyserlingk, and H. Axer (2005). Anisotropy of human linea alba: A biomechanical study. *Journal of Surgical Research 124*(1), 118–125.

Greca, F. H., J. B. de Paula, M. L. Biondo-Simões, F. D. da Costa, A. P. da Silva, S. Time, and A. Mansur (2001). The influence of differing pore sizes on the biocompatibility of two polypropylene meshes in the repair of abdominal defects. Experimental study in dogs. *Hernia 5*(2), 59–64.

Hernández, B., E. Peña, G. Pascual, M. Rodríguez, B. Calvo, M. Doblaré, and J. Bellón (2011). Mechanical and histological characterization of the abdominal muscle. a previous step to modelling hernia surgery. *Journal of the Mechanical Behavior of Biomedical Materials 4*(3), 392–404.

Hernández-Gascón, B., A. Mena, E. Peña, G. Pascual, J. M. Bellón, and B. Calvo (2013, feb). Understanding the passive mechanical behavior of the human abdominal wall. *Annals of biomedical engineering 41*(2), 433–44.

Hernández-Gascón, B., E. Peña, J. Grasa, G. Pascual, J. Bellón, and B. Calvo (2013, May). Mechanical response of the herniated human abdomen to the placement of different prostheses. *Journal of biomechanical engineering 135*(5), 51004.

Hernández-Gascón, B., E. Peña, H. Melero, G. Pascual, M. Doblaré, M. Ginebra, J. Bellón, and B. Calvo (2011). Mechanical behaviour of synthetic surgical meshes: Finite element simulation of the herniated abdominal wall. *Acta Biomaterialia 7*(11), 3905–3913.

Hernández-Gascón, B., E. Peña, G. Pascual, M. Rodríguez, J. Bellón, and B. Calvo (2012). Long-term anisotropic mechanical response of surgical meshes used to repair abdominal wall defects. *Journal of the Mechanical Behavior of Biomedical Materials 5*(1), 257–271.

Hodges, P., L. Pengel, R. Herbert, and S. Gandevia (2003, June). Measurement of muscle contraction with ultrasound imaging. *Muscle & nerve 27*(6), 682–92.

Höer, J., K. Junge, A. Schachtrupp, U. Klinge, and V. Schumpelick (2002). Influence of laparotomy closure technique on collagen synthesis in the incisional region. *Hernia 6*(3), 93–98.

Holzapfel, G. A. (2000). *Nonlinear Solid Mechanics*. Wiley, New York.

Holzapfel, G. A., T. C. Gasser, and R. W. Ogden (2000). A new constitutive framework for arterial wall mechanics and a comparative study of material models. *Journal of elasticity and the physical science of solids 61*(1), 1–48.

Huijing, P. A. (1999). Muscle as a collagen fiber reinforced composite: a review of force transmission in muscle and whole limb. *Journal of Biomechanics 32*(4), 329–345.

Hwang, W., J. C. Carvalho, I. Tarlovsky, and A. M. Boriek (2005). Passive mechanics of canine internal abdominal muscles. *Journal of Applied Physiology 98*(5), 1829–1835.

Ingle, N., M. King, and M. Zikry (2010). Finite element analysis of barbed sutures in skin and tendon tissues. *Journal of Biomechanics 43*(5), 879–886.

Israelsson, L. and D. Millbourn (2012). Closing midline abdominal incisions. *Langenbeck's Archives of Surgery 397*(8), 1201–1207.

Israelsson, L. A. and T. Jonsson (1994). Closure of midline laparotomy incisions with polydioxanone and nylon: The importance of suture technique. *British Journal of Surgery 81*(11), 1606–1608.

Ito, K., B. Jin, and T. T. (2011). A regularization parameter for nonsmooth tikhonov regularization. *SIAM Journal on Scientific Computing 33*, 4015–38.

Jandali, S., J. A. Nelson, M. R. Bergey, S. S. Sonnad, and J. M. Serletti (2011). Evaluating the use of a barbed suture for skin closure during autologous breast reconstruction. *Journal of Reconstructive Microsurgery 27*(05), 277–286.

Jenkyn, T. R., B. Koopman, P. Huijing, R. Lieber, and K. R. Kaufman (2002). Finite element model of intramuscular pressure during isometric contraction of skeletan muscle. *Physics in Medicine and Biology 47(22)*, 4043–61.

Jordan, P. and R. Howe (2008). Constitutive modeling of porcine liver in indentation using 3D ultrasound imaging. *Journal of the Mechanical Behavior of Biomedical Materials 2*(2), 192–201.

Junqueira, L. C. and J. Carneiro (2007). *Basic Histology, 11th ed.* McGraw-Hill.

Kabanikhin, S. I. (2008). Definitions and examples of inverse and ill-posed problems. *Journal of Inverse and Ill-Posed Problems 16*(4), 317–357.

Kauer, M., V. Vuskovic, J. Dual, G. Szekely, and M. Bajka (2002). Inverse finite element characterization of soft tissues. *Medical Image Analysis 6*(3), 275–287.

Kim, J.-C., Y.-K. Lee, B.-S. Lim, S.-H. Rhee, and H.-C. Yang (2007). Comparison of tensile and knot security properties of surgical sutures. *Journal of Materials Science. Materials in Medicine 18*(12), 2363–9.

Kingsnorth, A. and K. LeBlanc (2003). Hernias: inguinal and incisional. *The Lancet 362*, 1561–1571.

Kirilova, M., S. Stoytchev, D. Pashkouleva, and V. Kavardzhikov (2011). Experimental study of the mechanical properties of human abdominal fascia. *Medical engineering & physics 33*(1), 1–6.

Kirilova, M., S. Stoytchev, D. Pashkouleva, V. Tsenova, and R. Hristoskova (2009). Visco-elastic mechanical properties of human abdominal fascia. *Journal of Bodywork and Movement Therapies 13*(4), 336–337.

Klinge, U. (2007). Experimental comparison of monofile light and heavy polypropylene meshes: Less weight does not mean less biological response. *World Journal of Surgery 31*(4), 867–868.

Klinge, U., B. Klosterhalfen, V. Birkenhauer, K. Junge, J. Conze, and V. Schumpelick (2002). Impact of polymer pore size on the interfaces scar formation in a rat model. *Journal of Surgical Research 103*, 208–214.

Klosterhalfen, B., K. Junge, and U. Klinge (2002). The lightweight and large porous mesh concept for hernia repair. *Expert Review Medical Devices 2*(1), 103–117.

Koo, T. K., J. Guo, J. H. Cohen, and K. J. Parker (2013, aug). Relationship between shear elastic modulus and passive muscle force: an ex-vivo study. *Journal of biomechanics 46*(12), 2053–2059.

Kransdorf, M. and M. Murphey (2006). *Imaging of Soft Tissue Tumors*. LWW Doody's all reviewed collection. Lippincott Williams & Wilkins.

Kulacoglu, H. (2011). Current options in inguinal hernia repair in adult patients. *Hippokratia 15*(3), 223–231.

Kureshi, A., P. Vaiude, S. N. Nazhat, A. Petrie, and R. A. Brown (2008). Matrix mechanical properties of transversalis fascia in inguinal herniation as a model for tissue expansion. *Journal of Biomechanics 41*(16), 3462–3468.

Kybic, J. and D. Smutek (2005). Estimating elastic properties of tissues from standard 2d ultrasound images. In *Medical Imaging 2005: Ultrasonic Imaging and Signal Processing*.

LeBlanc, K., D. Bellanger, K. Rhynes, D. Baker, and R. Stout (2002). Tissue attachment strength of prosthetic meshes used in ventral and incisional hernia repair. *Surgical Endoscopy And Other Interventional Techniques 16*(11), 1542–1546.

Li, J., Z. Ji, and T. Cheng (2012). Lightweight versus heavyweight in inguinal hernia repair: a meta-analysis. *Hernia 16*(5), 529–539.

Lichtenstein, I. and A. Shulman (1986). The tension-free hernioplasty. *International surgery 1*(71), 1–4.

Liem, M., Y. van der Graaf, C. van Steensel, R. Boelhouwer, G. Clevers, W. Meijer, J. Stassen, L. Vente, W. Weidema, A. Schrijvers, and van Vroonhoven T.J. (1997). Comparison of conventional anterior surgery and laparoscopic surgery for inguinal-hernia repair. *New England Journal of Medicine 336*(22), 1541–1547.

Linden, V. D. (1998). *Mechanical modeling of skeletal muscle functioning*. Ph. D. thesis, University of Twente, The Netherlands.

Lintin, L. A. D. and A. N. Kingsnorth (2014). Mechanical failure of a lightweight polypropylene mesh. *Hernia 18*(1), 131–133.

Liu, J., L. Lin, W. Zhang, and G. Li (2013). A novel combined regularization algorithm of total variation and Tikhonov regularization for open electrical impedance tomography. *Physiological Measurement 34*(7), 823–838.

Lomanto, D., S. Iyer, A. Shabbir, and W.-K. Cheah (2006). Laparoscopic versus open ventral hernia mesh repair: a prospective study. *Surgical Endoscopy And Other Interventional Techniques 20*(7), 1030–1035.

Lophaven, S., H. Nielsen, and J. Sondergaard (2002, August). *A Matlab Kriging Toolbox* (Version 2.0 ed.). Kongens Lyngby: Technical University of Denmark. Technical Report No. IMM-TR-2002-12.

Lubowiecka, I., K. Szepietowska, C. Szymczak, and A. Tomaszewska (2016). A preliminary study on the optimal choice of an implant and its orientation in ventral hernia repair. *Journal of Theoretical and Applied Mechanics (Poland) 54*(2), 411–421.

Lubowiecka, I., A. Tomaszewska, C. Szymczak, and M. Śmietański (2012). Mechanical modelling of human hernia repair based on experimental simulation. In *6th European Congress on Computational Methods in Applied Sciences and Engineering (ECCOMAS)*.

Luhmann, T., S. Robson, S. Kyle, and J. Boehm (2014). *Close-Range Photogrammetry and 3D Imaging*. De Gruyter Textbook. De Gruyter.

Lyons, M., D. Winter, and C. Simms (2014). Mechanical characterisation of porcine rectus sheath under uniaxial and biaxial tension. *Journal of biomechanics 47*(8), 1876–84.

Marieb, E. (2009). *Essentials of Human Anatomy and Physiology Laboratory Manual* (4 ed.). Pearson Benjamin Cummings.

Marquardt, D. (1963). An algorithm for least-squares estimation of nonlinear parameters. *SIAM Journal on Applied Mathematics 11*, 431–441.

Martins, P., E. Peña, R. M. N. Jorge, A. Santos, L. Santos, T. Mascarenhas, and B. Calvo (2012). Mechanical characterization and constitutive modelling of the damage process in rectus sheath. *Journal of the Mechanical Behavior of Biomedical Materials 8*, 111–122.

McCormack, K., N. Scott, P. Go, S. Ross, and A. Grant (2003). Laparoscopic techniques versus open techniques for inguinal hernia repair. *Cochrane Database of Systematic Reviews 1*.

McKay, M., W. Conover, and R. Beckman (1979). A comparison of Three Methods for Selecting Values of Input Variables in the Analysis of Output from a Computer Code. *Technometrics 21*(2).

Mikhail, E. M., J. S. Bethel, and J. C. McGlone (2001). Introduction to modern photogrammetry. *New York*.

Miller, M. (1993). *Miller's Anatomy of the dog*. Saunders, Philadelphia: Pfizer, S.A.

Minn, R. M. H. M. and R. T. Hutchings (1982). *Atlas a color de anatomía humana*. España: Pfizer, S.A.

Mitton, D., J. Minonzio, M. Talmant, R. Ellouz, F. Rongieras, P. Laugier, and K. Bruyère-Garnier (2014, April). Non-destructive assessment of human ribs mechanical properties using quantitative ultrasound. *Journal of Biomechanics 47*(6), 1548–53.

Moore, K. and A. Dalley (1999). *Clinically Oriented Anatomy*. Clinically Oriented Anatomy. Lippincott Williams & Wilkins.

Moreno Ruiz, F. (2011). Hernia inguinal laparoscópica. In R. Lozano and M. Márquez (Eds.), *Manual de instrumentación en cirugía laparoscópica* (3rd ed.)., Chapter 15, pp. 204. Arán Ediciones, S.A.

Muysoms, F., G. Campanelli, G. Champault, A. DeBeaux, U. Dietz, J. Jeekel, U. Klinge, F. Köckerling, V. Mandala, A. Montgomery, S. Morales Conde, F. Puppe, R. Simmermacher, M. Śmietański, and M. Miserez (2012). EuraHS: the development of an international online platform for registration and outcome measurement of ventral abdominal wall hernia repair. *Hernia 16*(3), 239–250.

Nava, A., E. Mazza, M. Furrer, P. Villiger, and W. Reinhart (2008). In vivo mechanical characterization of human liver. *Medical Image Analysis 12*(2), 203–216.

Nemecek, E., L. Negrin, C. Beran, R. Nemecek, and C. Hollinsky (2013). The application of the V-Loc closure device for gastrointestinal sutures: a preliminary study. *Surgical Endoscopy 27*(10), 3830–3834.

Neumayer, L., A. Giobbie-Hurder, O. Jonasson, R. Fitzgibbons, D. Dunlop, and J. Gibbs (2004). Open mesh versus laparoscopic mesh repair of inguinal hernia. *The New England Journal of Medicine 18*(350), 1819–1827.

Nguyen, T. D. and B. L. Boyce (2011, jun). An inverse finite element method for determining the anisotropic properties of the cornea. *Biomechanics and Modeling in Mechanobiology 10*(3), 323–337.

Nieminen, M., J. Töyräs, M. Laasanen, J. Silvennoinen, H. Helminen, and J. Jurvelin (2004). Prediction of biomechanical properties of articular cartilage with quantitative magnetic resonance imaging. *Journal of Biomechanics 37*(3), 321–328.

Nilsson, T. (1982). Biomechanical studies of rabbit abdominal wall. Part I. The mechanical properties of specimens from different anatomical positions . *Journal of Biomechanics 15*(2), 123–129.

Nobile, L., L. Checchi, and G. Monaco (1997). Experimental analysis of tensile properties of some suturing materials. *Journal of Materials Science. Materials in Medicine 8*(1), 53–6.

Nozaki, K., R. Mori, K. Ryoke, and Y. Uchio (2012). Comparison of elastic versus rigid suture material for peripheral sutures in tendon repair. *Clinical Biomechanics 27*(5), 506–510.

Oberai, A. and P. Barbone (2011). Solution of inverse problems in biomechanical imaging. In G. Gladwell and A. Morassi (Eds.), *Dynamical Inverse Problems: Theory and Application*, Chapter 7. Springer Vienna.

Oberai, A. A., N. H. Gokhale, S. Goenezen, P. E. Barbone, and J. Timothy (2009). Linear and nonlinear elasticity imaging of soft tissue in vivo: demonstration of feasibility. *Physics in Medicine and Biology 54*(5), 1191–1207.

Odegard, G. M., T. L. H. Donahue, D. A. Morrow, and K. R. Kaufman (2008). Constitutive modeling of skeletal muscle tissue with an explicit strain-energy function. *Journal of Biomechanical Engineering 130*, 061017.

Odermatt, E. K., L. Funk, R. Bargon, D. P. Martin, S. Rizk, and S. F. Williams (2012). MonoMax Suture: A New Long-Term Absorbable Monofilament Suture Made from Poly-4-Hydroxybutyrate. *International Journal of Polymer Science 2012*, 1–12.

Ogden, R. W. (2001). *Nonlinear Elasticity, Anisotropy, Material Stability and Residual Stresses in Soft Tissue. Lecture Notes, CISM.* Udine: Course on Biomechanics of Soft Tissue.

Olea, R. A. (1974). Optimal contour mapping using universal kriging. *Journal of Geophysical Research 79*(5), 695–702.

Oni, G., S. A. Brown, and J. M. Kenkel (2012). A comparison between barbed and nonbarbed absorbable suture for fascial closure in a porcine model. *Plastic and Reconstructive Surgery 130*(4), 536–541.

Onofrio, L., D. Cafaro, F. Manzo, S. Cristiano, B. Sgromo, and G. Ussia (2004, August). Tension-free laparoscopic versus open inguinal hernia repair. *Minerva chirurgica 59*(4), 369–377.

Park, A., D. Birch, and P. Lovrics (1998). Laparoscopic and open incisional hernia repair: A comparison study. *Surgery 124*(4), 816–822.

Park, A., J. S. Roth, and S. M. Kavic (2006). Abdominal wall hernia. *Current Problems in Surgery 43*(5), 326–375.

Perrott, C. A. (2004, Jan). Inguinal hernias: room for a better understanding. *American Journal of Emergency Medicine 22(1)*, 48–50.

PhotoModeler (2013). *PhotoModeler Scanner.* Vancouver, Canada: Eos Systems Inc.

Podwojewski, F., M. Otténio, P. Beillas, G. Guérin, F. Turquier, and D. Mitton (2013). Mechanical response of animal abdominal walls in vitro: evaluation of

the influence of a hernia defect and a repair with a mesh implanted intraperitoneally. *Journal of biomechanics 46*(3), 561–6.

Podwojewski, F., M. Otténio, P. Beillas, G. Guérin, F. Turquier, and D. Mitton (2014). Mechanical response of human abdominal walls ex vivo: Effect of an incisional hernia and a mesh repair. *Journal of the Mechanical Behavior of Biomedical Materials 38*, 126–33.

Raghavan, K. R., a.E. Yagle, and E. Andrew (1994). Forward and Inverse Problems in Elasticity Imaging of Soft Tissues. *IEEE Transactions on Nuclear Science 41*(4), 1639–1648.

Rath, A., P. Attali, J. Dumas, D. Goldlust, J. Zhang, and J. Chevrel (1996). The abdominal linea alba: an anatomo-radiologic and biomechanical study. *Surgical and Radiologic Anatomy 18*(4), 281–288.

Reza, M. and J. Blasco (2004). *Eficacia y seguridad de la cirugÃŋa laparoscÃşpica vs cirugÃŋa abierta en el cÃąncer colorrectal*. EspaÃśa: Unidad de EvaluaciÃşn de TecnologÃŋas Sanitarias (UETS), ÃĄrea de InvestigaciÃşn y Estudios Sanitarios. Agencia LaÃŋn Entralgo.

Rhinoceros (2014). *Rhinoceros 3D*. Barcelona, Spain: McNeel Europe.

Richards, P. C., C. M. Balch, and A. J. S. (1983). A Randomized Prospective Study of 571 Patients Comparing Continuous vs. Interrupted Suture Techniques. *Annals of Surgery 197*(2), 238–243.

Rivaz, H., E. M. Boctor, M. A. Choti, and G. D. Hager (2013, December). Ultrasound elastography using multiple images. *Medical Image Analysis 18*(2), 314–329.

Rizk, N. N. (1980). A new description of the anterior abdominal wall in man and mammals. *Journal of Anatomy 131*(3), 373–385.

Röhrnbauer, B. and E. Mazza (2013). A non-biological model system to simulate the in vivo mechanical behavior of prosthetic meshes. *Journal of the Mechanical Behavior of Biomedical Materials 20*, 305–315.

Rossi, R., J. Dungan, and L. Beck (1994). Kriging in the shadows: Geostatistical interpolation for remote sensing. *Remote Sensing of Environment 49*(1), 32 – 40.

Rutkow, I. M. (2003). Demographic and socioeconomic aspects of hernia repair in the united states in 2003. *Surgical Clinics of North America 83*(5), 1045 – 1051. Hernia Repair.

Sacks, M. S. (2000). Biaxial mechanical evaluation of planar biological materials. *Journal of Elasticity 61*(1-3), 199–246.

Sakorafas, G. H., I. Halikias, C. Nissotakis, N. Kotsifopoulos, A. Stavrou, C. Antonopoulos, and G. A. Kassaras (2001). Open tension free repair of inguinal hernias; the Lichtenstein technique. *BioMed Central Surgery 1*(1), 1–3.

Sanz, C. M., M. L. H. Bogajo, M. M. Díaz, and G. T. Ruíz (2010). CirugÃŋa laparoscÃşpica con puerto Ãžnico: ampliaciÃşn del espectro de utilizaciÃşn. *CirugÃŋa espaÃśola 87*, 321–322.

Scharstein, D. and R. Szeliski (2002). A taxonomy and evaluation of dense two-frame stereo correspondence algorithms. *International journal of computer vision 47*(1-3), 7–42.

Schumpelick, V., U. Klinge, K. Junge, and M. Stumpf (2004, February). Incisional abdominal hernia: the open mesh repair. *Langenbeck's Archives of Surgery 389*(1), 1–5.

Scott, N., K. McCormack, P. Graham, P. Go, S. Ross, and A. Grant (2002). Open mesh versus non-mesh for repair of femoral and inguinal hernia. *Cochrane Database of Systematic Reviews 4*.

Simo, J. C. and R. L. Taylor (1991). Quasi-incompresible finite elasticity in principal stretches. Continuum basis and numerical algorithms. *Computer Methods in Applied Mechanics and Engineering 85*, 273–310.

Simón-Allué, R., A. Agudo, J. Montiel, J. Bellón, and B. Calvo (2014). Mechanical characterization of abdominal muscle using stereo imaging. In *11th World Congress on Computational Mechanics (WCCM XI)*.

Simón-Allué, R., A. Agudo, J. Montiel, and B. Calvo (2013). Mechanical characterization of abdominal muscle by stereo images. In *3rd Meeting of the Spanish National Chapter (ESB)*.

Simón-Allué, R., J. Montiel, J. Bellón, and B. Calvo (2015). Developing a new methodology to characterize in vivo the passive mechanical behavior of abdominal wall on an animal model. *Journal of the Mechanical Behavior of Biomedical Materials 51*, 40–49.

Simón-Allué, R., A. Oberai, J. Montiel, and B. Calvo (2015). Mechanical characterization of abdominal muscle by inverse analysis on an animal model. In *21st Congress of the European Society of Biomechanics*.

Simón-Allué, R., P. Pérez-López, S. Sotomayor, E. Peña, G. Pascual, J. Bellón, and B. Calvo (2014). Short- and long-term biomechanical and morphological study of new suture types in abdominal wall closure. *Journal of the Mechanical Behavior of Biomedical Materials 37*, 1–11.

Simulia. (2011). *Abaqus user's guide, v. 6.11*. Dassault Systemes Simulia Corp., Providence, RI, USA.

Slama, C. C., C. Theurer, and S. W. Henriksen (1980). *Manual of photogrammetry*. Number Ed. 4. American Society of photogrammetry.

Smart, N. J., M. Marshall, and I. R. Daniels (2012). Biological meshes: A review of their use in abdominal wall hernia repairs. *The Surgeon 10*(3), 159 – 171.

Śmietański, M., K. Bury, A. Tomaszewska, I. Lubowiecka, and C. Szymczak (2012). Biomechanics of the front abdominal wall as a potential factor leading to recurrence with laparoscopic ventral hernia repair. *Surgical Endoscopy and Other Interventional Techniques 26*(5), 1461–1467.

Song, C., A. Alijani, T. Frank, G. Hanna, and A. Cuschieri (2006). Mechanical properties of the human abdominal wall measured in vivo during insufflation for laparoscopic surgery. *Surgical Endoscopy 20*(6), 987–990.

Spencer, A. J. M. (1954). Theory of invariants. In *Continuum Physics*, pp. 239–253. Academic Press, New York.

Steel, R. and J. Torrie (1960). *Principles and procedures of statistics: with special reference to the biological sciences*. McGraw-Hill.

Suzuki, S. and Y. Ikada (2012). Sutures for wound closure. In *Biomaterials for Surgical Operation*, pp. 189–197. Humana Press.

Szepietowska, K. and I. Lubowiecka (2013). Mechanical behaviour of the implant used in human hernia repair under physiological loads. *Acta of Bioengineering and Biomechanics 15*(3), 89–96.

Szymczak, C., I. Lubowiecka, A. Tomaszewska, and M. Smietański (2012). Investigation of abdomen surface deformation due to life excitation: implications for implant selection and orientation in laparoscopic ventral hernia repair. *Clinical biomechanics (Bristol, Avon) 27*(2), 105–10.

Tien, C. and S. Lin (2006). Optimization of process parameters of titanium dioxide films by response surfaces methodology. *Optics Communications 266*(2), 574–581.

Todros, S., P. G. Pavan, P. Pachera, and A. N. Natali (2015). Synthetic surgical meshes used in abdominal wall surgery: Part I - Materials and structural conformation. *Journal of Biomedical Materials Research Part B: Applied Biomaterials*.

Tran, D., D. Mitton, D. Voirin, F. Turquier, and P. Beillas (2014). Contribution of the skin, rectus abdominis and their sheaths to the structural response of the abdominal wall ex vivo. *Journal of biomechanics 47*(12), 3056–63.

Tran, D., F. Podwojewski, P. Beillas, M. Ottenio, D. Voirin, F. Turquier, and D. Mitton (2016). Abdominal wall muscle elasticity and abdomen local stiffness

on healthy volunteers during various physiological activities. *Journal of the Mechanical Behavior of Biomedical Materials 60*, 451–459.

Tran, H. V., F. Charleux, M. Rachik, A. Ehrlacher, and M. C. Ho Ba Tho (2007). In vivo characterization of the mechanical properties of human skin derived from mri and indentation techniques. *Computer Methods in Biomechanics and Biomedical Engineering 10*(6), 401–407.

Troyer, A. d. and S. Loring (2011). *Action of the Respiratory Muscles*. John Wiley and Sons, Inc.

Tyrell, J., H. Silberman, P. Chandrasoma, J. Niland, and S. J. (1989, March). Absorbable versus permanent mesh in abdominal operations. *Surgery, Gynecology & Obstetrics 168*(3), 227–232.

U.S. National Cancer Institute (2016). Anatomy and physiology, muscular system, muscle types. `http://training.seer.cancer.gov/anatomy/muscular/structure.html`. accessed May, 2016.

Valanis, K. C. and R. F. Landel (1967). The strainâĂŘenergy function of a hyperelastic material in terms of the extension ratios. *Journal of Applied Physics 38*(7), 2997–3002.

Veronda, D. and R. Westmann (1970). Mechanical characterization of skin - finite deformations. *Journal of Biomechanics 3*(IN9), 111–122.

Villa, M. T., L. E. White, M. Alam, S. S. Yoo, and R. L. Walton (2008). Barbed sutures: a review of the literature. *Plastic and Reconstructive Surgery 121*(3), 102–108.

Weiland, D. E., R. C. Bay, and S. Del Sordi (1998). Choosing the best abdominal closure by meta-analysis. *American Journal of Surgery 176*(6), 666–70.

Weiss, J. A., B. N. Maker, and S.Govindjee (1996). Finite element implementation of incompressible, transversely isotropic hyperelasticity. *Computer Methods in Applied Mechanics of Engineering 135*, 107–128.

Wissing, J., T. J. M. V. van Vroonhoven, M. E. Schattenkerk, H. F. Veen, R. J. G. Ponsen, and J. Jeekel (1987). Fascia closure after midline laparotomy: Results of a randomized trial. *British Journal of Surgery 74*(8), 738–741.

Yeoh, O. H. (1993). Some forms of the strain energy function for rubber. *Rubber Chemistry and Technology 66*(5), 754–771.

Zagadou, B., P. Barbone, and D. Mountain (2014). Elastic properties of organ of Corti tissues from point-stiffness measurement and inverse analysis. *Journal of biomechanics 47*(6), 1270–1277.